

THE DECAY OF NEUTRON-ACTIVATED ERBIUM ISOTOPES

THE DECAY OF NEUTRON-ACTIVATED ERBIUM ISOTOPES

By

AGDA ARTNA, B.Sc.

A Thesis

Submitted to the Faculty of Graduate Studies

in Partial Fulfilment of the Requirements

for the Degree

Doctor of Philosophy

McMaster University

October 1961

DOCTOR OF PHILOSOPHY (1961)

McMASTER UNIVERSITY
Hamilton, Ontario

(Physics)

TITLE: The Decay of Neutron-activated Erbium Isotopes

AUTHOR: Agda Artna, B.Sc. (McMaster)

SUPERVISOR: Professor M. W. Johns

NUMBER OF PAGES: x, 166

SCOPE AND CONTENT:

The modes of disintegration of four erbium isotopes will be discussed.

The simple decays of Er^{163} , Er^{165} , and Er^{169} have been investigated experimentally using scintillation spectrometer techniques. The disintegration of the fourth isotope, Er^{171} , was analyzed using the high resolution beta-ray spectrometer. On the basis of the energy, intensity, and conversion coefficient measurements of the transitions in Tm^{171} , an energy level scheme for this nucleus is proposed and interpreted according to the unified nuclear model.

In addition, a set of experiments will be discussed which were carried out in order to calibrate the high resolution beta-ray spectrometer for gamma-ray intensity measurements. Finally, the already published results of an investigation of the decay of Pm^{149} will be included.

ACKNOWLEDGEMENTS

I wish to express my deepest gratitude to Professor M. W. Johns for his constant guidance and encouragement during my years at this university.

I should also like to thank the members of my Supervisory Committee, Dr. M. W. Johns, Dr. R. G. Summers-Gill, and Dr. R. J. Gillespie for their interest in this work. I am also indebted to Professor M. A. Preston for many informative discussions on the theoretical interpretation of the experimental results.

The association with other members of the Beta- and Gamma-ray Spectroscopy group, past and present, is gratefully acknowledged. I should like to thank them for their assistance in collecting data, for their technical advice and assistance, and also for many stimulating discussions and seminars.

The financial assistance of the National Research Council of Canada and the Shell Oil Company of Canada in the form of scholarships and research grants is gratefully acknowledged.

I should like to thank Mrs. Marion Tweedley for typing this thesis and also for providing it with a reasonable number of definite articles.

TABLE OF CONTENTS

										<u>Page No.</u>
INTRODUCTION	1
CHAPTER 1	THEORETICAL CONCEPTS OF BETA- AND GAMMA-RAY SPECTROSCOPY									3
	Introduction	3
	(A) Spin and Parity	3 ^f
	(B) Beta Decay	4
	(i) General Theory and Development	4
	(ii) Allowed Transitions	7
	(iii) Forbidden Transitions	9
	(C) Gamma Radiation	11
	(i) Nature of Gamma Radiation	11
	(ii) Interactions of Gamma Radiation with Matter	13
	(D) Internal Conversion	16
CHAPTER 2	NUCLEAR MODELS									19
	Introduction	19
	(A) Shell Model	20
	(i) Single Particle Shell Model	20
	(ii) Extended Shell Model	22
	(a) Residual Interparticle Forces	22
	(b) Independent Particle Motion in Spheroidal Well	24
	(c) Shell Model with Varying Well Depth	24

	<u>Page No.</u>
(B) Collective Motion in Nuclei	25
(i) Vibrational Model	26
(ii) Rotational Model	27
(C) Unified Model	28
(i) Spherical Nuclei	28
(ii) Strongly Deformed Nuclei	29
(a) Description of Energy Levels	30
(b) Selection Rules for Transitions between Levels	33
CHAPTER 3 INSTRUMENTS AND EXPERIMENTAL TECHNIQUES	36
Introduction	36
(A) High Resolution Beta-Ray Spectrometer	38
(i) Description of the Instrument	39
(ii) Experimental Techniques	44
(a) The Study of Beta Spectra	45
(b) The Study of Internal Conversion Spectra	47
(c) The Study of External Conversion Spectra	48
(d) Measurement of the Internal Conversion Coefficients	51
(e) Energy Measurements	53
(B) Scintillation Spectrometers	53
(i) The Study of Gamma-Ray Spectra	58
(ii) Coincidence Experiments	59
(C) Double Long Lens Coincidence Spectrometer	60
(i) Description of the Instrument	60

	<u>Page No.</u>
(ii) Experimental Techniques	63
(a) Source Preparation	63
(b) Measurement of Instrumental Transmission	64
(c) Measurement of Energy	64
(d) β -e Coincidence Experiments	65
CHAPTER 4 A STUDY OF NEUTRON-ACTIVATED ERBIUM ISOTOPES	69
Introduction	69
(A) Erbium-163	71
(i) Historical Survey	71
(ii) Experimental Study	71
(B) Erbium-165	75
(i) Historical Survey	75
(ii) Experimental Study	75
(C) Erbium-169	76
CHAPTER 5 THE STUDY OF ERBIUM-171	78
Introduction	78
(A) Description of the Experiments and Presentation of Experimental Results	81
(i) Source Material and Preparation	81
(ii) The External Conversion Spectrum	82
(iii) The Internal Conversion Spectrum	91
(iv) The Beta Spectrum	98
(v) The Direct Measurement of α_K of the 296- and 308 kev Transition	102
(vi) Summary of the Experimental Data	104

	<u>Page No.</u>
(B) Discussion of the Energy Levels in Thulium-171 ...	111
(i) The Decay Scheme	111
(ii) Coincidence Experiments of Cranston <u>et al.</u> as applied to the Present Decay Scheme ...	113
(iii) Beta- and Gamma-Ray Intensities ...	116
(iv) The Internal Conversion Coefficients ...	117
(v) Description of the Energy Levels in the Thulium-171 Nucleus.	119
SUMMARY	128
APPENDIX I GAMMA-RAY INTENSITIES FROM EXTERNAL CONVERSION MEASUREMENTS	130
Introduction	130
(A) Theoretical Expressions	131
(B) Experimental Tests of the Theory	136
(i) Test of the Expression (AI.4) for the High Energy Region	142
(ii) The Variation of the Photo-Electric Peak Height with Electron Momentum	145
(iii) The Variation of the Photo-Electric Peak Height with Radiator Thickness	146
(C) Discussion	148
APPENDIX II THE DECAY OF PROMETHIUM-149	149
Introduction	151
The Decay of Pm ¹⁴⁹ (reprint)	153
REFERENCES	162

LIST OF FIGURES

<u>Figure No.</u>	<u>Page No.</u>
1. Beta-Decay Interactions and Selection Rules	9
2. Angular Momentum Coupling Scheme in Deformed Nuclei ...	29
3. Typical rotational spectra	32
4. High Resolution Beta-Ray Spectrometer	40
5. Gamma-Ray Source Holder for the High Resolution Beta-Ray Spectrometer	43
6. Internal Conversion Calibration Lines	55
7. External Conversion Calibration Lines	56
8. Coincidence Circuit for Scintillation Spectrometer ...	59
9. Double Long Lens Coincidence Spectrometer	62
10. Coincidence Circuit for the Double Long Lens Coincidence Spectrometer	63
11. Erbium Isotopes	70
12. Scintillation Spectrometer Study of Er ¹⁶³	73
13. Decay Scheme of Er ¹⁷¹ as proposed by Cranston <u>et al.</u> ...	80
14. External Conversion Spectrum of Er ¹⁷¹ (complete) ...	83
15. External Conversion Spectrum of Er ¹⁷¹ (low energy) ...	84
16. External Conversion Spectrum of Er ¹⁷¹ (low energy) ...	85
17. External Conversion Spectrum of Er ¹⁷¹ (high energy) ...	86
18. External Conversion Spectrum of Er ¹⁷¹ (high energy) ...	87
19. External Conversion Spectrum of Er ¹⁷¹ (high energy) ...	88

<u>Figure No.</u>	<u>Page No.</u>
20. Internal Conversion Spectrum of Er ¹⁷¹	92
21. Internal Conversion Spectrum of Er ¹⁷¹	93
22. Internal Conversion Spectrum of Er ¹⁷¹	95
23. Internal Conversion Spectrum of Er ¹⁷¹	96
24. Internal Conversion Spectrum of Er ¹⁷¹	97
25. Fermi Analysis of the Er ¹⁷¹ Beta Spectrum	99
26. Internal and External Conversion Lines in the Measurement of α_K	103
27. Er ¹⁷¹ Decay Scheme	112
28. A Portion of the Nilsson Energy Level Diagram for Prolate Deformation	121
A1. Variation of $1/\zeta p\beta^3$ with Electron Momentum	137
A2a. Semi-Empirical Curves for $\sqrt{C^2 + (Rp\beta^3/t)^2}$ for gold radiators	138
A2b. Semi-Empirical Curves for $\sqrt{C^2 + (Rp\beta^3/t)^2}$ for uranium radiators	139
A3. Variation of $(n/\zeta) \sqrt{1 + (Ct/Rp\beta^3)^2}$ with radiator thickness	143

LIST OF TABLES

<u>Table No.</u>	<u>Page No.</u>
I	Standard Calibration Lines for the High Resolution Beta-Ray Spectrometer 54
II	The Endpoints and Intensities of the Er ¹⁷¹ Beta Groups...101
III	α_K for the 296- and 308 kev Transitions in Er ¹⁷¹104
IV	Internal Conversion and Gamma-Ray Data for the Low Energy Transitions in Er ¹⁷¹105
V	High Energy Gamma-Rays in Er ¹⁷¹106
VI	Comparison of the Theoretical and Experimental Conversion Coefficients and Ratios for the Er ¹⁷¹ Transitions ...109
A.I	Average Electron Densities and Mean Ionization Potentials for Gold and Uranium Radiators134
A.II	Variation of External Conversion Peak Height with Radiator width141
A.III	Radiator Thicknesses144

INTRODUCTION

The instruments and techniques of beta- and gamma-ray spectroscopy provide some of the most powerful tools for the experimental study of nuclear structure. Although other techniques have been developed which make it possible to probe into the structure of a nucleus, nuclear spectroscopy still remains one of the most important methods of studying the excited levels in nuclei. There are, however, two limitations to this method: (1) one has to excite the nucleus to an unstable state; (2) one has to wait for it to decay. Information is then gained by observing the means by which the nucleus de-excites itself. Thus, one must have an atomic nucleus which can be excited either by electromagnetic radiation or by capture of another particle, and it must be possible to observe the products of the nuclear decay.

Although any information gained from a nuclear decay study adds to the understanding of the general picture, there are groups of nuclei which, at the present, seem more interesting than others. One such interesting group includes the rare earth elements. From lanthanum ($Z=57$) to thulium ($Z=69$) the nuclei change from almost spherical shape to a highly deformed one. It is this gradual transformation, as well as the highly deformed shape of the nuclei around thulium, which make this region especially interesting.

Due to this highly deformed shape, the energy level structure of the nuclei around thulium is very complex, thus presenting an interesting problem in nuclear spectroscopy.

This thesis will describe the decay modes of the four radioactive erbium isotopes produced by neutron capture. The decays of three of these isotopes: Er^{163} , Er^{165} , and Er^{169} , will be discussed in Chapter 4. Chapter 5 will be devoted entirely to the complex decay of Er^{171} , the study of which constitutes the main part of the experimental work described in this thesis. However, before the experimental work is described, a short discussion of the theoretical and experimental concepts necessary for understanding the experiments will be presented. In addition, Appendix I will describe a set of experiments which were undertaken to investigate the reliability of the gamma-ray intensity measurements obtained with the high resolution beta-ray spectrometer. Appendix II will include the already published results of an investigation of the Pm^{149} decay.

CHAPTER 1

THEORETICAL CONCEPTS OF BETA- AND GAMMA-RAY SPECTROSCOPY

Introduction

In the study of nuclear structure by means of beta- and gamma-ray spectroscopy the object is to learn as much as possible about the nuclear levels. This involves a study of the beta spectrum of the decaying nucleus; a study of the gamma-ray and conversion electron spectra in the daughter nucleus; a measurement of the transition intensities and conversion coefficients. All these combined may provide sufficient data to permit the experimenter to put together a level scheme for the daughter nucleus and to assign spins and parities to the energy levels. This chapter will present the theoretical concepts necessary for an understanding of the nature of such measurements.

(A) Spin and Parity

The term "spin" is generally used to describe the intrinsic angular momentum of a particle. Nucleons have been found to have an intrinsic angular momentum of $\frac{1}{2} \hbar$. In describing the energy levels of a nucleus, the term spin has a different meaning. It refers to the total angular momentum of the whole nucleus in that particular state. In this case the spin is the vector sum of the spins of the individual nucleons, and their orbital angular momenta. The prediction of level spins is extremely difficult as no one nuclear model seems to fit all experimental cases. It has been

found that the shell model (Chap.2.B) gives a good representation around "magic numbers", while the Bohr-Mottelson unified model (Chap.2.D) describes the energy levels reasonably well in strongly deformed nuclei. Since angular momentum other than intrinsic spin can only occur in integral units of \hbar , it is obvious that all nuclei with an even number of particles have integral spins, and the ones with an odd number of particles have half-integral spins.

Parity is a quantum mechanical concept without a classical counterpart. The parity of a state is defined as even if the wave function of this state is invariant under an inversion of the co-ordinate system at the origin, or odd if it changes sign under this operation.

$$\text{Even parity} \quad \Psi(x,y,z) = \Psi(-x,-y,-z)$$

$$\text{Odd parity} \quad \Psi(x,y,z) = -\Psi(-x,-y,-z)$$

It is not possible to determine the parity of a single level, but it is possible to determine whether the initial and final states of a transition have the same parity or not. Although parity is a good quantum number in strong interactions and in those involving electromagnetic radiation, recent experiments (Wu et al. (1957)) have shown that it is not conserved in weak interactions, such as beta-decay.

(B) Beta-decay

(i) General Theory and Development

The process of beta-decay can take three different forms: e^- emission, e^+ emission, and orbital-electron-capture. The changes taking place in the nucleus can be described in the following equations:

for e^+ emission $Z^A \rightarrow (Z+1)^A + e^+ + \nu$

for orbital-electron-capture $Z^A + e^- \rightarrow (Z-1)^A + \nu$

where e^+ and ν refer to the beta-particle and neutrino respectively.

In beta-decay a continuous spectrum of beta-rays is emitted. In order to conserve energy, momentum, and statistics, the neutrino was "invented" by Pauli in 1927. Its existence was verified experimentally by Reines and Cowan (1953). The neutrino is a lepton with zero rest mass, no charge and half-integral spin. It carries away the energy difference between E_e and E_o , where E_e contains the rest mass of the electron. Based on the simultaneous creation of two particles, Fermi (1934) worked out a theory of beta-decay consistent with the experimental results. Because of this simultaneous creation of two particles, a nucleus will favour any other possible form of de-excitation over beta-decay.

The equations for beta-decay can be formally written down by comparison with the equations of electromagnetic radiation. The disintegration constant λ for a system with initial state i and final state f is given by

$$\lambda = \frac{2\pi}{\hbar} |H_{if}|^2 \frac{dn}{dE} \quad (1.1)$$

where $\frac{dn}{dE}$ is the density of final states and H_{if} is the matrix element of the interaction:

$$H_{if} = \int \psi_f^* H \psi_i dv. \quad (1.2)$$

ψ_f and ψ_i are the wavefunctions describing the final and initial states of the system, and H is the interaction operator. The wavefunction

describing the final state of the system can be separated into three different parts. This leads to the following form of equation (1.2).

$$H_{if} = g \int \left[U_f^* \psi_e(r) \psi_\nu(r) \right] O_x U_i dv. \quad (1.3)$$

U_i and U_f describe the nucleus before and after the interaction; $\psi_e(r)$ and $\psi_\nu(r)$ describe the electron and neutrino respectively; O_x is the interaction operator; and g is the interaction constant. It is now known that this interaction is either of vector or axial-vector form, or, more commonly, a mixture of these two interaction types.

In Fermi's original theory it was suggested that O_x may take the form of one, or a mixture of several, of five possible interactions: scalar, vector, tensor, axial-vector, and pseudoscalar. These five forms all obey the requirements of relativistic invariance. This was based, however, on the assumption that parity was conserved in all interactions, including beta-decay. In 1956 Lee and Yang (1956), in order to explain some anomalies in hyperon and meson decays, suggested the possibility of non-conservation of parity in weak interaction. This suggestion was tested by Wu et al. (1957) by observing the angular distribution of beta-particles emitted from aligned Co^{60} nuclei. The experiment proved that parity was not conserved in weak interactions. The next step was to study the polarization of electrons, an effect first detected by Frauenfelder and co-workers (1957). Electrons were found to have left-handed polarization to the degree of v/c . This result also requires non-conservation of parity.

Finally, experiments were carried out to determine whether the other particles involved in beta-decay were polarized. Goldhaber

et al.(1958) studied the correlation between the direction of nuclear recoil and the polarization of gamma-rays emitted in the decay of Eu^{152} . They concluded that the neutrino was left-handedly polarized. The fact that both electron and neutrino are left-handedly polarized leads to the conclusion that beta-decay takes place through a vector and/or axial-vector interaction. Further experiments with neutron decay by Clark et al.(1958) and by Burgy et al.(1958) have led to the conclusion that in beta-decay all particles participate through their left-handed, and all anti-particles through their right-handed, components of motion. In this context a positron is the anti-particle corresponding to the electron particle.

(ii) Allowed Transitions

Equation (1.1) with H given by equation (1.3) can be simplified by expanding ψ_e and ψ_ν and accepting only the first terms of these expansions. Making the above approximation, the partial disintegration constant $d\lambda_p$ for electron momentum between p and p+dp will be

$$d\lambda_p = K |M_{if}|^2 F(Z,E) p^2 (E_0 - E)^2 dp$$

where

$$M_{if} = \int U_f^* Q_x U_i dv. \tag{1.4}$$

The operators Q_x are approximate forms of O_x , which omit the so-called "relativistic terms" in the Dirac interaction operator, E and E_0 refer to the electron energy and the total energy released in the decay, respectively, and K is a constant proportional to the interaction strength. Thus the factor $|M_{if}|^2$ contains the properties of the nucleus, while the other factors are independent of the nuclear wavefunctions

and interaction forms. The function $F(Z,E)$ is the Coulomb correction factor (or Fermi function) describing the effect of the Coulomb field of the nucleus on the emitted beta particle. Since the number of disintegrations with momentum between p and $p+dp$ from a source of strength N_0 disintegrations/sec is $N_0 d\lambda_p = N(p)dp$, equation (1.4) can be rearranged in the form:

$$\left[N(p) / p^2 F(Z,E) \right]^{\frac{1}{2}} \propto (E_0 - E) \quad (1.5)$$

The plot of the above against E should give a straight line with an intercept at E_0 . This is very useful in determining E_0 and was first used by Kurie (1936). The method is sometimes known also as Fermi analysis.

Integrating equation (1.4) over the total energy spectrum, an expression for the comparative half-life (ft) can be found.

$$\lambda = \frac{0.693}{T_{\frac{1}{2}}} = K \left| M_{if} \right|^2 \int F(Z,E) p^2 (E_0 - E)^2 dp = K \left| M_{if} \right|^2 f(Z,E_0) \quad (1.6)$$

$$\text{or} \quad ft = \frac{0.693}{K} \left| M_{if} \right|^{-2}$$

where $T_{\frac{1}{2}}$ is the half-life. The $f(Z,E_0)$ functions have been tabulated (Feenberg (1950)) for e^{\pm} decay and for orbital electron capture for a number of Z values. Using these, ft values may be calculated and information regarding the nuclear matrix element M_{if} obtained. For allowed transitions $\log (ft)$ values range from 3.1 for the free neutron to 6 in heavy nuclei.

Of the two interaction forms, the vector operator leads to Fermi interactions with selection rules $\Delta I = 0$, and no parity change.

The axial vector operator leads to Gamow-Teller interactions with selection rules $\Delta I = 0, \pm 1, 0 \not\rightarrow 0$, no parity change. Figure 1 will show pictorially the angular relationships of the vector quantities involved in the two different weak interaction forms, and also the selection rules for the allowed case.

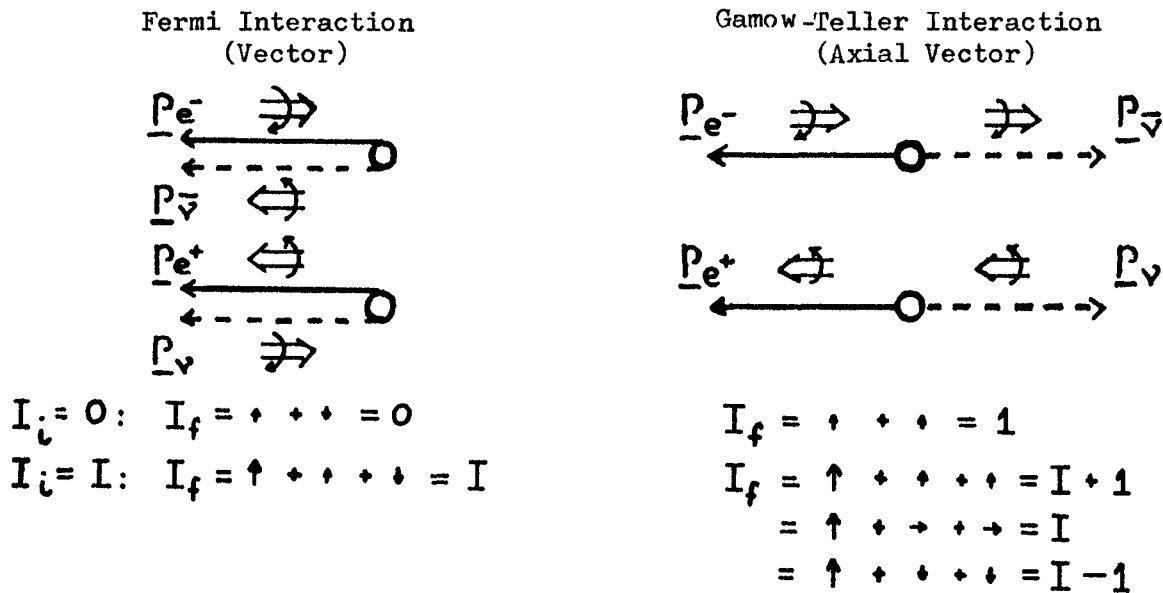


Figure 1

This diagram represents the ideal case with $v \approx c$. Since electrons are only polarized to the degree of v/c , in the general case the correlation between \underline{p}_e and \underline{p}_ν is less pronounced.

(iii) Forbidden Transitions

According to the theory of allowed beta-decay, only transitions with $\Delta I = 0, \pm 1, 0 \not\rightarrow 0$, may occur. In practice, transitions with parity change and/or $\Delta I > 1$ are found and are known as forbidden transitions. The fact that these occur means that some of the approximations made in calculating allowed transition probabilities were not justified. Two corrections

have to be made: (1) in calculating M_{if} the exact forms of Q_x must be used instead of the approximate forms Q_x and (2) in the expansions of φ_e and φ_ν higher order terms must be considered.

In the expansion of the lepton wavefunction the terms decrease in magnitude with the ratio $|r| / [(n\hbar / (p_e + p_\nu))]$ where n is the order of forbiddenness. If the first term contributes to the interaction, one is justified in neglecting the higher order terms. However, if for some reason the matrix element containing the first term vanishes, one must consider the second term, and so on. If the second term leads to a non-vanishing matrix element the transition is said to be first forbidden, the third term leads to second forbidden transitions, etc.

Making the above corrections, equation (1.4) becomes

$$d\lambda = K \left| M_{if} \right|^2 F(E, Z) p^2 (E_0 - E)^2 S_n(E) \quad (1.4a)$$

where $S_n(E)$ is the shape factor for the forbidden spectrum of degree n . In the Fermi analysis one now has to plot $[N(p) / F(Z, E) p^2 S_n(E)]^{1/2}$ against E in order to obtain a linear plot. It has been found that in the case of first forbidden spectra $S_1(E)$ is generally constant and therefore does not affect the Fermi analysis. An exception to this is the first forbidden unique case, for which $S_1(E) \approx p_e^2 + p_\nu^2$. This particular transition has $\Delta I = 2$ and a parity change. From the selection rules it can be seen that this is a first forbidden case only allowed by Gamow-Teller interaction. Similarly, there are unique 2nd forbidden (Be^{10} , $\Delta I = 3$, no) and unique 3rd forbidden (K^{40} , $\Delta I = 4$, yes) transitions. Since in these cases the interaction is of pure

vector type it has been possible to calculate the shape factors involved exactly. In the more general cases of the higher order forbidden, non-unique transitions, the shape factors cannot be calculated without a knowledge of the exact interaction form.

The product $\left| M_{if} \right|^2 S_n(E)$ is usually very sensitive to the degree of forbiddenness, thus showing that the ft values could be expected to increase in groups according to $n=0, 1, 2$ etc. The selection rules in the general case of an n th degree forbidden transition can be summarized as follows. For the Fermi interaction $\Delta I \leq n$, for Gamow-Teller interaction $\Delta I \leq n + 1$. The parity rule $\Delta \pi = (-1)^n$ applies in both cases.

(C) Gamma Radiation

(i) Nature of Gamma Radiation

A nucleus in an excited state may lose its excitation energy by emitting electromagnetic radiation. This radiation is described as electric (EL) or magnetic (ML) of multipole order L where L is the angular momentum carried away by the gamma radiation (in units of \hbar). According to the laws of conservation of angular momentum and parity there are certain selection rules governing the transitions between states with specified angular momentum (I_i, I_f) and parity (π_i, π_f). The rule for multipole order L is given by the following relationship:

$$\left| I_i - I_f \right| \leq L \leq \left| I_i + I_f \right|$$

The selection rules for parity are

$$\begin{aligned} \Delta \pi &= (-)^L && \text{for EL radiation} \\ \Delta \pi &= (-)^{L-1} && \text{for ML radiation} \end{aligned} \tag{1.7}$$

where $\Delta\pi = +1$ denotes no parity change, and $\Delta\pi = -1$ denotes a parity change. As a consequence of the transverse nature of the electromagnetic radiation, an additional rule states that no transition with $L = 0$ may occur.

The probability of a gamma-transition between two nuclear states depends on three factors: (1) the multipolarity of the transition; (2) the energy of the transition; and (3) the wavefunctions of the states involved. The single particle transition probability per second (Blatt and Weisskopf (1952)) is given by

$$T_{(i \rightarrow f)}^{\sigma}(L, M) = \frac{8\pi(L+1)}{L [(2L+1)!!]^2} \frac{k^{2L+1}}{\hbar} \left| \langle f | \mathcal{M}^{\sigma}(L, M) | i \rangle \right|^2 \quad (1.8)$$

where σ denotes the multipolarity, M is the z -component of L , and k is the wavenumber of the emitted quantum. $\left| \langle f | \mathcal{M}^{\sigma}(L, M) | i \rangle \right|^2$ is known as reduced transition probability. Blatt and Weisskopf (1952) have shown that using the independent-particle model for the nucleus a rough estimate can be derived for the single particle transition probabilities as follows:

$$T^E(L) \approx \frac{2(L+1)}{L [(2L+1)!!]^2} \left(\frac{3}{L+3} \right)^2 \frac{e^2}{\hbar c} (kR)^{2L} ck \quad (1.9)$$

and

$$T^M(L) \approx \frac{20(L+1)}{L [(2L+1)!!]^2} \left(\frac{3}{L+3} \right)^2 \frac{e^2}{\hbar c} \left(\frac{\hbar}{mcR} \right)^2 (kR)^{2L} ck$$

where m and R are the mass and the radius of the nucleon, respectively. For a single particle transition, therefore, the probability decreases rapidly with increasing multiple order, with the magnetic transition having a lower probability than the electric transition of the same

multipolarity. Thus these transitions occur with the lowest order possible, i.e., $L = |I_i - I_f|$, or with a mixture of the two lowest orders. In the latter case these are of opposite class because of parity considerations. Experimentally, however, gamma-transitions have been found which do not obey the transition probability rules stated above. A large number of cases have been found where E2 transitions are several orders of magnitude faster than expected from equation (1.8). Thus there are transitions which, although from the selection rules are expected to be M1 with possibly a small admixture of E2, turn out to be almost pure E2 with very little M1 admixture. These enhanced E2 transitions are now associated with transitions in the collective motion in nuclei.

(ii) Interaction of Gamma Radiation with Matter

The detection of gamma radiation depends on its interaction with matter. The absorption of gamma rays in passing through matter is described by the following equation $I = I_0 e^{-\mu \rho x}$, where I is the intensity of the beam of initial intensity I_0 after passing through x cm of matter with density ρ and total absorption coefficient μ cm²/gm. The total absorption coefficient can be separated into three components:

$$\mu = \mu_{P.E.} + \mu_{C.S.} + \mu_{P.P.}$$

These partial absorption coefficients refer to the three main processes by which gamma rays are absorbed in matter: photo-electric effect, Compton scattering, and pair production. (This ignores certain very improbable reactions such as nuclear interactions, double Compton effect, etc.)

The photoelectric effect is the dominant mode of absorption with gamma energies of the order of the electron binding energies in the atom. In this case the photon interacts with the whole atom, its energy being transferred to one of the bound orbital electrons. This electron is ejected from the atom with energy $E_e = h\nu - E_s$, E_s being the binding energy of that particular shell. A free electron cannot absorb this energy because a third body is needed for momentum conservation. Thus, in the photoelectric effect, a number of monoenergetic electron groups are observed corresponding to the electrons ejected from the different shells in the electron configuration. This provides an accurate method of measuring the gamma energies, provided the binding energy of the shell involved is accurately known. One is also interested in the gamma intensities. In order to measure these, it is necessary to know the photoelectric cross-section, or the absorption coefficient, $\mu_{P.E.}$. This factor increases very rapidly at the absorption edges, i.e., at energies equal to the binding energies of electron shells. Between these edges it decreases with increasing gamma energy. At energies considerably larger than E_s it varies approximately as $(E_\gamma)^{-3.5}$. The cross-section also depends on the nuclear charge, increasing approximately as Z^5 with relatively large gamma energies. The exact calculation of this cross-section is very difficult, since the Dirac relativistic equation for bound electrons must be used. A survey of the theory of this calculation has been given by Hall (1936) and Heitler (1944). The different methods of calculating

these factors have been reviewed by Davisson and Evans (1952). These authors have tabulated the values which agree best with experiment. This problem will be discussed further in Appendix I.

The second effect, Compton scattering, becomes important at gamma energies much larger than the binding energies of the electrons. Under these conditions all electrons become virtually free. In this process the gamma-ray interacts with only one electron at a time. Some of its energy is transferred to the electron during this interaction. This effect results in a continuous distribution of electrons with energies up to E_{max} .

$$E_{\text{max.}} = \frac{h\nu}{1 + (m_0 c^2)/(2h\nu)}$$

In the study of gamma radiation energies and intensities with magnetic spectrometers this mode of absorption does not usually render useful information. Instead, it provides a high background on which the photoelectric peaks are found.

At energies above $2m_0 c^2$, pair production may occur. In this case the energy of the electromagnetic radiation creates a positron-electron pair with total kinetic energy $E_K = h\nu - 2m_0 c^2$. The spectra of both particles will be continuous with maximum energy E_K . The cross-section for this effect is again a function of the energy of the gamma-ray and of the atomic number of the absorber. It increases rapidly with both increasing E_γ and Z . This effect is strictly a high energy effect. It provides a useful method for measuring gamma-ray energies in the energy range where photoelectric absorption is negligible.

As secondary effects, the Auger electrons and the X-rays should be mentioned. When an electron is ejected from one of the inner shells, a vacancy is left behind. This vacancy is then filled with an electron from an outer orbit. The energy difference between these two shells may be released in the form of an X-ray with energy $E_x = (E_i - E_f)$, where E_i and E_f are the binding energies of the electron in its initial and final states, respectively. Or it may be transferred to an electron in an outer orbit which is ejected as an Auger electron. The Auger electrons have kinetic energy $E = E_i - E_f - E_A$. E_A is the binding energy of the shell from which the Auger electron is ejected. In general with light elements the ejection of Auger electrons is favoured over the emission of X-rays; with heavy elements the reverse is true. In the rare earth region both X-ray and Auger lines can be seen in external and internal conversion spectra, respectively.

(D) Internal Conversion

The process of internal conversion is in competition with gamma emission as a mode of de-excitation for the nucleus. In this process the excitation energy of the nucleus is transferred to an orbital electron. The electron then leaves the atom with kinetic energy $E_e = E_\gamma - E_s$. E_γ is the energy lost by the nucleus, i.e., the energy of the competing gamma radiation, and E_s is the binding energy of the shell from which the electron is ejected. This was originally thought to be an internal photoelectric effect.

It is now clear that this is not the case. Positive proof of this lies in the fact that internal conversion may occur in cases where gamma transitions are completely forbidden. An example of this is the electric monopole transition between two levels with spin 0, i.e., $0 \rightarrow 0$ transitions (Fowler (1930)).

The calculation of the absolute conversion probability is very difficult because it involves the knowledge of the nuclear wavefunction. On the other hand, the ratio of the internal conversion probability from shell S to the gamma transition probability has been theoretically calculated for a number of shells. This ratio $\alpha_s = N_{es}/N_\gamma$ is called the internal conversion coefficient for shell S. It depends on five factors: (1) the transition energy; (2) the atomic number Z of the emitter; (3) the shell from which the electron is ejected; (4) the multipolarity of the competing radiation; and (5) the parity change. The total conversion coefficient is defined $\alpha = \sum_s \alpha_s$. Ratios of conversion coefficients, such as the K/L and L_1/L_2 ratios, are also very useful. These are defined: $K/L = N_{eK}/N_{eL} = \alpha_K / (\alpha_{L_1} + \alpha_{L_2} + \alpha_{L_3})$, $L_1/L_2 = \alpha_{L_1} / \alpha_{L_2}$ etc. All these ratios depend on the multipolarity of the radiation and the parity change. By comparing the experimental values with the theoretical ones, the multipolarities of the transitions and the parity changes can be determined.

It had been assumed that the conversion coefficients were independent of nuclear matrix elements. Now it is known that the transition probabilities for internal conversion involve different

nuclear matrix elements from those involved in gamma-ray transition probabilities. These new matrix elements are directly related to the finite size of the nucleus. The first tables of conversion coefficients, prepared by Rose, assumed the nucleus to be a point charge. At this limit the nuclear matrix elements do not enter into the calculations. However, these calculations have now been revised by Sliv (1956) and also by Rose (1958). Both authors assume the nucleus to be a uniformly-charged sphere with radius $1.20 \times 10^{-13} A^{1/3}$ cm. The finite size of the nucleus introduces two corrections to the conversion coefficient calculations:

(1) The electron wave function will be different from that due to a point nucleus; (2) the electron (especially the K-shell electron) spends part of its time inside the nucleus and thus the positions and motions of nuclear charges are important. Both Sliv and Rose have corrected for the first effect, but only Sliv has considered the second correction. Sliv has assumed that the nuclear currents responsible for the transitions are surface currents. In the rare earth region the agreement between the calculations of the two authors is very good, except in the case of α_L for M3 and M4. In these cases the values calculated by Sliv are considerably lower than those calculated by Rose.

CHAPTER 2

NUCLEAR MODELS

Introduction

The aim of nuclear physics is to achieve a self-consistent description of nuclei. Such a description, or model, should be capable of explaining, and predicting, the behaviour of all nuclei under all circumstances. Although a vast amount of knowledge has been gained in this direction during the last few decades, one is still far from being able to describe the behaviour of all nuclei with a single model. Instead, a number of nuclear models have developed, each being useful in a different region of the periodic table and under different circumstances. In low energy nuclear physics, such as radioactive decay, the useful models are the shell model of Mayer and Jensen and the unified model of Bohr and Mottelson. In nuclear reactions which involve higher energies these models are no longer suitable. Here one has to resort to the compound-nucleus model, the optical model, or to the statistical model.

Since this work is concerned with nuclear decay, only the two important low energy nuclear models -- the shell model and the unified model will be described in more detail.

(A) Shell Model

A nuclear shell structure was first suggested by the appearance of "magic numbers." In the early 1930's, when experimental evidence about nuclear stability and abundances started to accumulate, it was observed that certain numbers of nucleons carried with them greater stability than others. These were labelled the "magic" numbers. This suggested a nuclear structure similar to the electronic structure of atoms with magic numbers marking the closing of shells. A review of this early work is given by Bethe and Backer (1932). However, it was not until 1948 that a shell model emerged which was capable of describing a large number of nuclear properties known at that time. Such a model was proposed independently by Mayer (1948) and by Haxel, Jensen, and Suess (1948). Both authors developed their models further (Mayer (1949), Haxel et al. (1950)) and later combined these to present one Shell Model which has been amazingly successful despite its phenomenological nature. A detailed account of this model is given by Mayer and Jensen (1955) and by E. Feenberg (1955).

(i) Single Particle Shell Model

Since this model was fashioned after the atomic structure, it is based on the motion of individual particles in a central potential. The basic assumptions of the model are as follows:

- (1) Each nucleon moves independently in a spherically symmetric potential provided by all the other nucleons. The potential contains a strong spin-orbit interaction term.

- (2) The nuclear ground state corresponds to the lowest single particle energy level the neutrons and protons can occupy and still obey the Pauli exclusion principle.
- (3) An even number of protons (neutrons) in a state of lowest energy couple to zero angular momentum and even parity.
- (4) For an odd A nucleus with an odd number of protons (neutrons) the nuclear angular momentum is usually equal to that of the last proton (neutron).

The potential in which the single particles move has the form

$$V_i = V_A(r_i) - f_A(r_i) \underline{l}_i \cdot \underline{s}_i \quad (2.1)$$

$V_A(r_i)$ and $f_A(r_i)$, which are functions of the radial distance r , also depend on the size of the nucleus. $\underline{l} \cdot \underline{s}$, the spin-orbit coupling term, denotes the coupling of the nucleon spin \underline{s} and its orbital angular momentum \underline{l} . The sign of the spin-orbit coupling term is such that the level having angular momentum $j = l + \frac{1}{2}$ always lies lower than the level with $j = l - \frac{1}{2}$. The essential requirement of this potential is that it should predict a shell structure which agrees with experiments.

The simple shell model will thus explain the magic numbers - 2, 8, 20, 50, 82, 126. Each magic number denotes the closing of a major shell in the model. It is also successful in explaining the number of isomeric states at certain regions of the periodic table. These occur at places where the model predicts two single particle

energy levels with approximately equal energy and with widely different angular momenta. (This occurs at N or $Z = 38$ to 50 where the $2p_{1/2}$ and $1g_{9/2}$ states have almost equal energy, and also at Z or $N = 68$ to 82 where the $3s_{1/2}$ or $2d_{5/2}$ states are very close to the $1h_{11/2}$ state.) The model is thus quite useful in considering nuclear properties related to ground state angular momentum and parity.

However, there are nuclear properties where this single particle model only leads to a qualitative agreement with experiment. For example, the magnitudes of the beta-decay transition probabilities and nuclear magnetic moments can be explained, but their exact values cannot be predicted. In addition there are other nuclear properties, such as the nuclear quadrupole moments and the fast E2 transitions, where the experimentally-measured values and those predicted by the model can in no way be reconciled. These disagreements have pointed out the need for certain refinements of this simple shell model. Three of the more important refinements will be considered under the heading of Extended Shell Model.

(ii) Extended Shell Model

(a) Residual Interparticle Forces

In this model the residual two-body interaction between particles outside a closed shell is considered. In the single particle model the only interaction between particles is by means of the central potential. However, if there is more than one particle outside a closed shell, one should consider the possibility of internucleon forces. This force is supposed to be of short range

and of the form

$$W + MP_{12}^r + H P_{12}^r P_{12}^\sigma + B P_{12}^\sigma$$

where P_{12}^r is the radial -, and P_{12}^σ the spin-exchange operator. W , M , H and B are constants determining the relative strengths of the different interactions and are named after Wigner, Majorana, Heisenberg, and Bartlett. The interaction resulting from this force is considered as a perturbation on the shell model potential given by Equation (2.1).

The model makes the assumption that the closed shell has little effect on the interaction between the particles outside the closed shell. This is supported by two features of the shell model: (1) the energy difference between the particles in closed shells and the outer particles; (2) the spherical symmetry of a closed shell of nucleons which will lead to nearly uniform effects on the different energy levels of extra nucleons.

One result of this refinement is the negative pairing energy which will increase with increasing l . Due to the pairing energy, for example, the configuration $(3s_{\frac{1}{2}})^1(1h_{\frac{11}{2}})^2$ is lower in energy than the one with $(3s_{\frac{1}{2}})^2(1h_{\frac{11}{2}})^1$. When, in addition, the possibility of configuration mixing is considered, one achieves a reasonably good description of low-lying excited states of nuclei near closed shells. A review of the theoretical work in this direction with a number of references is given by R. J. Eden (1957).

(b) Independent Particle Motion in Spheroidal Well

A major area of disagreement between the shell model and the experiment is found in the magnitudes of the quadrupole moments of nuclei with partly filled shells. The use of a spheroidal potential instead of a spherical one has succeeded in removing this disagreement. The idea of a spheroidal potential was first suggested by Rainwater (1951), and later expanded by Nilsson (1955).

Nilsson suggests a single particle potential

$$V_i = V_0 \left[\left(1 + \frac{2}{3} \delta\right) (x_i^2 + y_i^2) + \left(1 - \frac{4}{3} \delta\right) z_i^2 \right] + C l_i \cdot s_i + D l^2 \quad (2.2)$$

The ratios of C and D to V_0 are chosen to make the level order agree with that of the spherical shell model when the distortion, δ , is zero. The distortion is determined by minimizing the value for total energy

$$E = \sum_{i=1}^A T_i + \frac{1}{2} \sum_{i=1}^A V_i$$

This model has had a great deal of success with nuclei midway between the closed shells, i.e., nuclei with a large distortion parameter. A further discussion of this model will be given in section C of this chapter.

(c) Shell Model with Varying Well Depth

The third major refinement of the shell model tackles the problem of total energy of the nucleus. If one tries to calculate the binding energies of nucleons using the potential of equation (2.1), one cannot make both the total nuclear energy and the binding energy of the

last nucleon agree with experiment. In order to achieve this agreement, it is necessary that the nucleons in different shells move in potentials of different depths.

A potential of varying well depth is achieved if the potential is assumed to be a function of the particle momentum k . The potential could then be expanded in a power series

$$V(k_i) = V_0 + bk_i^2 + \dots$$

and the energy of the particle is then given by

$$\begin{aligned} E_i &= T_i + V(k_i) = \frac{1}{2m_i} k_i^2 + V_0 + bk_i^2 + \dots \\ &= \frac{1}{2m_i^*} k_i^2 + V_0 \end{aligned}$$

where m_i^* is the effective mass of the nucleon and can be determined empirically. A great deal of the theoretical work on the effective mass theory has been done by Brueckner (1955).

(B) Collective Motion in Nuclei

The first nuclear model based on collective motion was the liquid drop model of N. Bohr (1936). This was used to describe nuclear phenomena where shell model failed and thus was considered contradictory to the single particle model. The idea of collective motion was taken up again by A. Bohr and B.R. Mottelson (1953, 1955) and, from a different viewpoint, by D.L. Hill and J.A. Wheeler (1953). It has now been shown to be supplementary rather than contradictory to the single particle models.

There are two main types of collective motion in nuclei:

(1) the nucleus may oscillate in shape while keeping the total nuclear volume constant, and (2) the nucleus may rotate. The rotation of nuclear matter plays an important part in the behaviour of strongly deformed nuclei, while the vibrations are important in nuclei with small deformations.

(i) Vibrational Model

In the vibrational model the nucleus is assumed to have a well defined surface which can be described in polar co-ordinates by

$$R(\delta, \theta) = R_0 \left[1 + \sum_{\lambda\mu} \alpha_{\lambda\mu} Y_{\lambda\mu}(\delta, \theta) \right].$$

R_0 is the nuclear radius in its spherical form, $Y_{\lambda\mu}(\delta, \theta)$ are the spherical harmonics of order λ, μ , and $\alpha_{\lambda\mu}$ are the deformation parameters. A deformation with $\lambda = 1$ corresponds to translation of the centre of mass and thus need not be considered. $\lambda = 2$ is the quadrupole vibration and the most common one. Some nuclear energy levels due to octupole vibrations with $\lambda = 3$ have also been found. The vibrational energy is given by

$$E_n = \left(n + \frac{5}{2} \right) \hbar\omega_\lambda$$

with n representing the number of "phonons," each with angular momentum λ and parity $(-)^{\lambda}$.

It has been found that for $\lambda = 2$ it is easier to describe the nucleus with two new parameters, β and γ , which bear a simple

relationship to the $\alpha_{2\mu}$'s. These two parameters distinguish between the two types of symmetry around the different nuclear axes. β -vibrations are oscillations in the eccentricity of the nucleus while preserving the symmetry around the nuclear z-axis. γ -vibrations are vibrations of shape while conserving the eccentricity of the nucleus along the z-axis.

(ii) Rotational Model

A spheroidal nucleus may also rotate around an axis of symmetry. The energy of rotation, in analogy with a rigid rotator, is given by

$$E = \frac{1}{2} \mathcal{J} \omega^2$$

where \mathcal{J} is the effective moment of inertia. Such a model will lead to nuclear excited states

$$E_{\text{rot}} = \frac{\hbar^2}{2\mathcal{J}} I(I + 1). \quad (2.3)$$

A great deal of effort has been spent to determine \mathcal{J} theoretically. The moment of inertia determined from a rigid rotator model has been found to be too large, while the one determined from the irrotational flow model is considerably smaller than the experimentally observed one. A review of this problem, with appropriate references, is given by D. M. Brink (1960).

One major success of this model is the prediction of the electric quadrupole transition probabilities between the rotational

levels which are a factor of 100 larger than those predicted by the single particle model (see page 12).

(C) Unified Model

All of the above discussed models have a place in the over-all picture of nuclei, but none of them is successful in describing any one nucleus completely. It is now clear that a full description of the nucleus will contain features of all the different kinds of nuclear behaviour. The relative importance of the different models, however, will vary from nucleus to nucleus across the periodic table. It is usual to divide the nuclei into three groups: the spherical nuclei, the strongly deformed nuclei, and, between these two regions, the transitional nuclei. The shell model is important in the region of spherical nuclei, while the collective motion models describe the deformed nuclei better.

This combination of different nuclear models is achieved in the Unified Model. A great deal of the work on this unified picture has been done by A. Bohr (1952, 1953) and B. R. Mottelson and S. G. Nilsson (1955).

(i) Spherical Nuclei

In this group belong the nuclei with closed shells, and those only a few particles removed from closed shells. These nuclei are quite well described by the shell model with a spherical potential. However, they will have an additional degree of freedom in which small oscillations in nuclear shape may occur. The collective motion here can

be considered as a perturbation on the single particle picture. The excited levels in these nuclei will exhibit single particle excitation levels and also vibrational levels with spin λ , parity $(-1)^\lambda$ and energy $\hbar\omega_\lambda$. Since the vibrational levels are levels of collective motion, the electric quadrupole transitions between these levels will be enhanced.

(ii) Strongly Deformed Nuclei

In the region of strongly deformed nuclei the collective motion is the predominant feature. Because of the large deformation, the nucleus has a certain stability of shape. This makes it possible to separate the intrinsic motion of the nucleons from the collective motion of nuclear matter. The intrinsic motion is that of single-particle motion in a spheroidal well. The collective motion in turn can be separated into its rotational and vibrational parts.

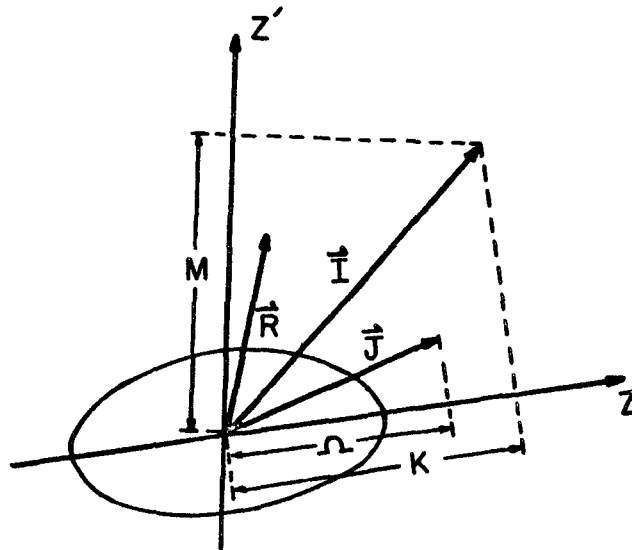


Figure 2.

The nuclear spin \underline{I} in such nuclei is made up of two components \underline{R} and \underline{J} . \underline{R} is the angular momentum of the collective motion while \underline{J} is the angular momentum of the intrinsic particle motion (Figure 2). The particle angular momentum \underline{J} ($\underline{J} = \sum \underline{j}_i$) is not a good quantum number. However, in axial symmetry its component Ω along the nuclear symmetry axis is a constant of motion. The assumption that the nucleus has axial symmetry is a valid one for most configurations. K and M are the components of \underline{I} along the nuclear symmetry axis, and along a space fixed axis, respectively. These quantum numbers describe the rotational motion.

The ground state of these nuclei will be the lowest single particle level. It is obtained by filling the levels with pairs of particles with $\pm \Omega_p$. Thus for even-even nuclei the ground state has $\Omega = 0$. For odd A nuclei the ground state has Ω equal to the Ω_p for the last particle. For odd-odd nuclei Ω will be equal to either the sum or difference of the Ω 's for the last proton and neutron. Also, for the ground state $K = \Omega$, which means that the axis of rotation is perpendicular to the nuclear symmetry axis.

(a) Description of Energy Levels

The strongly deformed nuclei will exhibit three different types of excitation.

(1) Change in Particle Motion. Nuclear levels due to this type of excitation have been calculated by Nilsson (1955) as a function of nuclear deformation. These levels can be described by quantum numbers Ω , N , n_z , Λ , ξ , and parity.

The quantum numbers are defined as follows: N is the principal quantum number with n_z being its component along the nuclear symmetry axis. For positive deformation n_z takes the values $n_z = N, N-1, N-2 \dots 0$ with increasing energy; Λ and Σ are the projections of l (the orbital angular momentum of the nucleon) and s (nuclear spin), respectively, along the nuclear symmetry axis. It is customary to denote a level with $\Omega \pi [N, n_z, \Lambda]$ (Σ need not be given since $\Omega = \Lambda + \Sigma$).

A complete theoretical description of these levels with methods for calculating transition probabilities etc. is given by Nilsson (1955).

(2) The Rotational Levels. Built on every single particle level there is a rotational band. The rotational levels are described by I, M, K (see Figure 2). The energy of a rotational state is given by Equation (2.3). The excitation energy of a rotational level is then

$$E_{\text{rot}} = \frac{\hbar^2}{2\mathcal{I}} \left[I(I+1) - I_0(I_0+1) \right] \quad (2.4)$$

with $I = I_0, I_0 + 1, I_0 + 2 \dots$ etc., and ground state parity. There are two exceptions to this. If $I_0 = 0$, symmetry considerations allow only even spins, i.e., the spin sequence becomes $0+, 2+, 4+ \dots$.

The other exception is the case with $\Omega = \frac{1}{2}$ *. In this case the particle motion is partly decoupled from the rotational motion. The modified rotational spectrum now becomes

$$E_{\text{rot}} = \frac{\hbar^2}{2\mathcal{I}} \left[I(I+1) + a(-)^{I+\frac{1}{2}}(I + \frac{1}{2}) \right] \quad (2.5)$$

with $a = \sum (-)^{j-\frac{1}{2}} (j + \frac{1}{2}) |c_j|^2$

where $|c_j|^2$ is the probability that the last odd particle has an

* In this case I_0 is usually, but not always, equal to Ω .

angular momentum j . a is known as the decoupling parameter. This modification in energy may even result in a ground state spin $I_0 \neq \Omega$. Figure 3 shows the three different types of rotational spectra

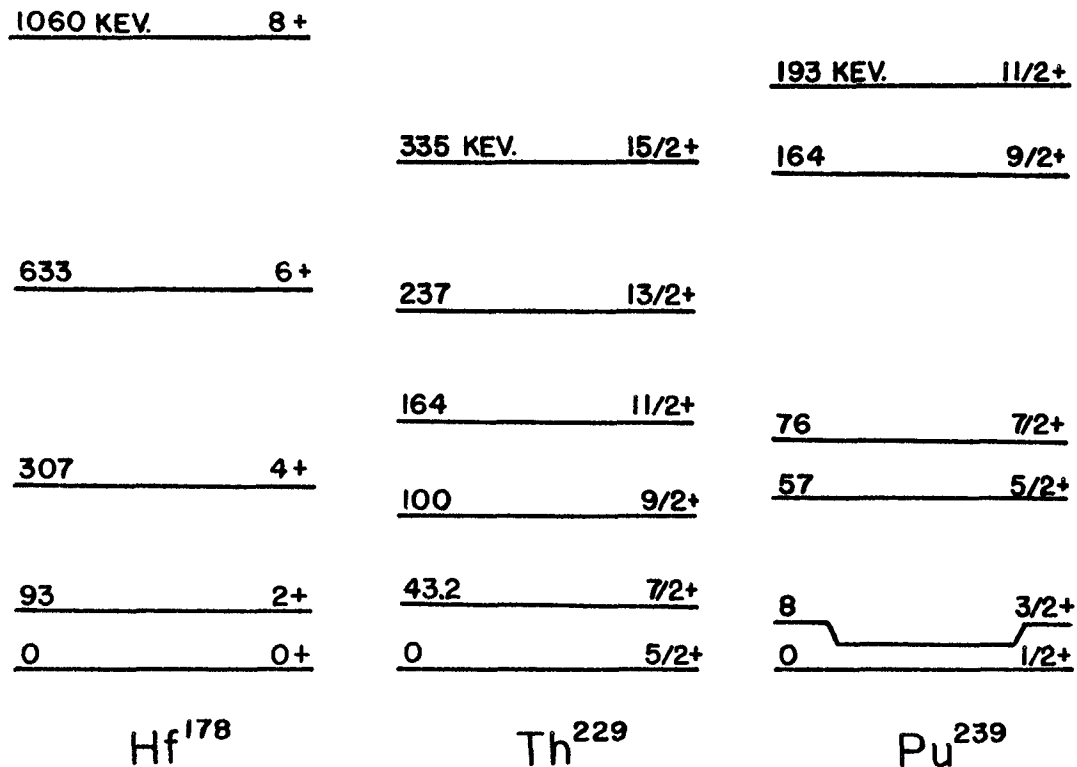


Figure 3

The energies of rotational levels may be further modified by a rotation-vibration interaction term. This term will be given to the first order by

$$\Delta E_{\text{vib}} = -2 \left[\frac{3}{(\hbar \omega_{\beta})^2} + \frac{1}{(\hbar \omega_{\gamma})^2} \right] \frac{\hbar^2}{J} (E_{\text{rot}})^2 \quad (2.6)$$

(3) Vibrational Levels. The third type of levels is due to the oscillations in nuclear shape. These can be characterized by n_β and n_γ . However, the excitation quanta of this type of excitation are considerably higher in energy than the rotational and particle excitations. For this reason they are not important in these nuclei. No vibrational levels have been uniquely identified in strongly deformed nuclei, but there seems to be no reason why this type of collective motion should not be present.

(b) Selection Rules for Transitions between Levels

With the formation of specific nuclear models several new quantum numbers have been introduced to describe nuclear states. One would expect the transitions between these states to obey, in addition to the ones stated in Chapter 1, selection rules involving these quantum numbers. Since these quantum numbers are often only approximate ones, the selection rules will not be rigorous, but will depend on how well the wavefunction used describes the nuclear state.

In strongly deformed nuclei where K is a good quantum number, one has the K selection rule:

$$\left| K_i - K_f \right| \equiv \Delta K \leq L \quad (2.7)$$

The transitions violating this selection rule are referred to as K forbidden. The degree of forbiddenness is denoted by ν

$$\nu = \Delta K - L$$

In addition to the K selection rule there are a number of additional selection rules dealing with particle quantum numbers N , n_z , Λ , and Ω . A complete list of the selection rules for beta-transitions (allowed, first-forbidden and second-forbidden) and for gamma transitions ($E1$, $E2$, $E3$, $M1$, $M2$ and $M3$) is given by G. Alaga (1957). Transitions obeying all selection rules are called unhindered (u). Those which obey $\Delta\Omega$ and ΔI selection rules, but not one or more of the others, are referred to as hindered (h).

(iii) The Transition Nuclei

In the region between the spherical nuclei and the strongly deformed nuclei, however, the different types of nuclear behaviour can no longer be separated. The predominant method of excitation in these nuclei is the vibrational mode. In even A nuclei one observes the level sequence 0, 2, 0, 2, 4, 0, 2, 3, 4, 6 etc. In odd A nuclei there is a competition between the single particle excitation and the vibrational excitation. This makes it difficult to observe the vibrational levels. In addition, the interaction between the particle motion and the collective motion is stronger here, which makes it much more difficult to recognize the vibrational levels. In general, the vibrational model seems to fit reasonably well the even A nuclei, while the description of odd A nuclei is considerably more difficult.

The transition from vibrational to rotational behaviour at $A \approx 150$ is quite sudden. Nuclei with $N = 88$ behave according to the vibrational model, while nuclei with $N = 90$ show definite

rotational behaviour. At the next transition region, however, at $A \approx 190$, the change is not so sudden. One finds there a group of nuclei which cannot be interpreted with either of these collective models. Davidov and Fillipov (1958) have proposed a model to describe this region. Their model would also reinterpret the vibrational behaviour. According to this model, a nucleus can be considered as an asymmetric rotator with a moment of inertia corresponding to that of an irrotational flow model. In this model deformations with no axial symmetry are also included. In the limit of maximum asymmetry this model leads to predictions which correspond closely to those of the vibrational model.

CHAPTER 3

INSTRUMENTS AND EXPERIMENTAL TECHNIQUES

Introduction

A great variety of instruments and experimental techniques may be used in the study of beta- and gamma-ray spectra. In general, the instruments can be divided into two groups, magnetic spectrometers and scintillation spectrometers. Under the classification of magnetic spectrometers belong all the instruments where the energy selection is achieved by means of a magnetic field, although quite often such instruments use a scintillator-photomultiplier assembly as a detector. In these spectrometers, therefore, only charged particle spectra can be studied directly. In scintillation spectrometers, on the other hand, the energy selection is obtained by measuring the amount of energy lost by a photon (or particle) when it passes through the scintillator, by means of pulse height analysis. A very important use of the scintillation spectrometers is thus found in the study of gamma-rays.

The two most important properties of any spectrometer are the resolution and transmission. In general, the magnetic instruments are capable of very high resolution while the scintillation spectrometers possess a much superior transmission (determined by the solid angle extended by the source at the detector). Because of these opposing properties, the magnetic spectrometers are used for exact measurements, or where it is necessary to separate the components

of a complicated spectrum, while the scintillation spectrometers have been extremely useful in coincidence work where the number of events is small and a large solid angle is desired.

Recently a third type of spectrometer, the solid state detector, has been introduced to the field of nuclear spectroscopy. This instrument depends on solid state effects to achieve an energy selection of incoming particles. These detectors have not been found to be very useful in the study of electrons and gamma-rays and will not, therefore, be discussed further.

In the work described in this thesis three different instruments were used. The basic instrument was a double-focusing high resolution beta-ray spectrometer, with which the beta spectra, the internal conversion spectra, and the gamma-ray spectra (by means of external conversion techniques) were studied. Two scintillation spectrometers were used; one to study gamma-spectra and the other to carry out some gamma-gamma coincidence experiments. Finally, a double long lens coincidence spectrometer was used for $e - \beta$ coincidence experiments in Pm^{149} .

In this chapter these instruments, and the experimental techniques involved, will be discussed. Emphasis will be on the high resolution double-focusing beta-ray spectrometer, since about 90% of the work was done with this instrument.

(A) High Resolution Beta-Ray Spectrometer

The high resolution spectrometer used in this work is a flat double-focusing spectrometer of the type proposed by Siegbahn and Svartholm (1946). The construction and performance of this instrument has been previously described by Johns et al. (1953). Therefore, only a short general description of the instrument will be given here, with some attention given to the modification and improvements added during the course of this work.

This type of instrument is called a "flat" spectrometer because the electrons travel in a plane perpendicular to the magnetic lines of force. The motion of the electrons is defined by the equation

$$Bev = mv^2/\rho \quad \text{or} \quad B\rho_e = mv \quad (3.1)$$

where ρ is the radius of the electron path, and the other symbols have their classical meaning. Thus the value of B will determine the momentum of electrons being focused at any one time, since ρ is defined by the instrument. In this spectrometer, as in all magnetic spectrometers, the measured magnetic field will therefore be proportional to the electron momentum and not the energy.

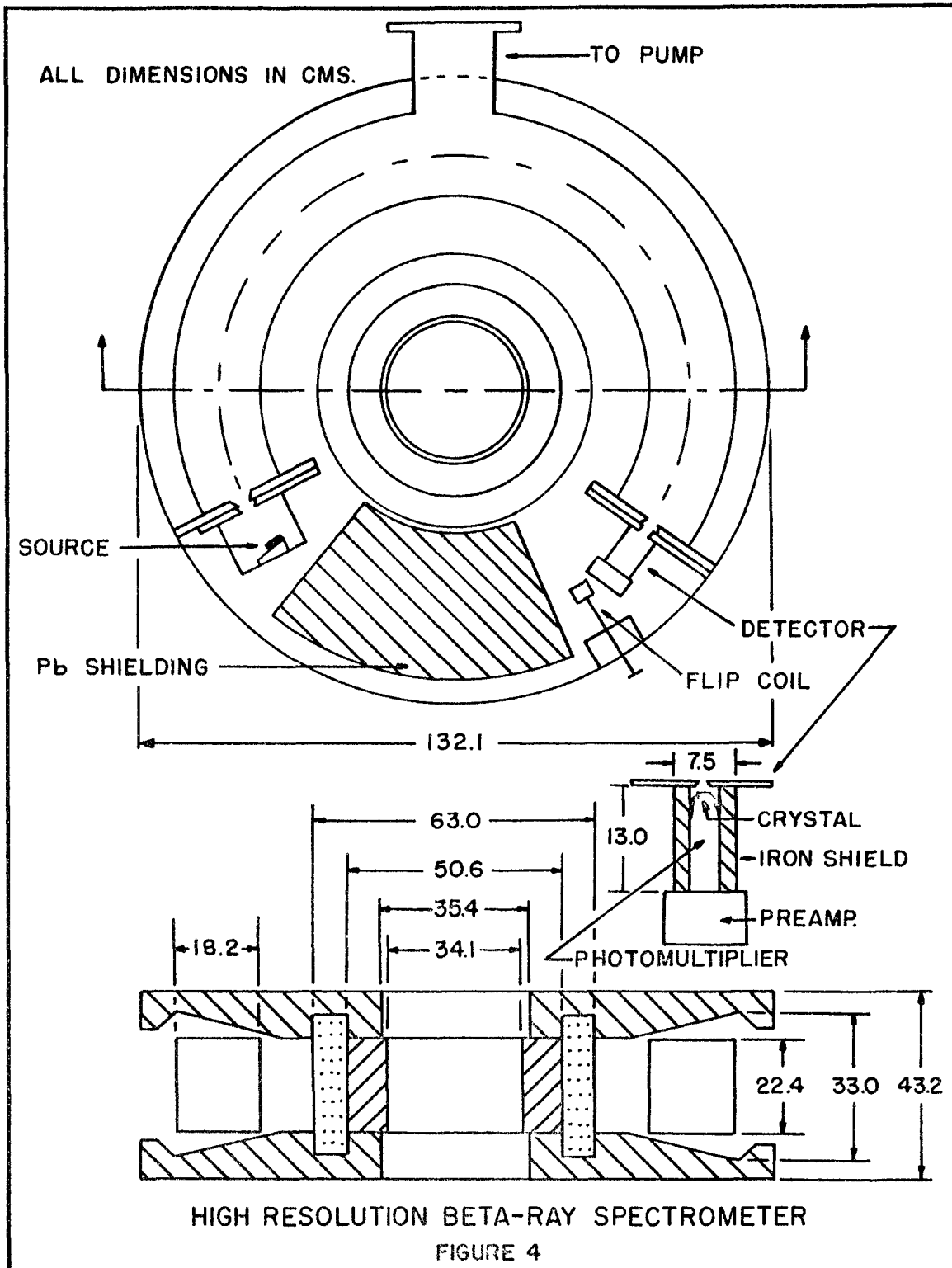
In a uniform magnetic field there will be a certain degree of one-dimensional focusing at $\phi = \pi$. However, if the magnetic field is not uniform, but a function of (r,z), some two-dimensional focusing can be obtained. The z-component of the magnetic field in a double-focusing instrument is given by

$$H_z(r, z) = H_0 \left[1 - \left(\frac{r-a}{a}\right) + \beta \left(\frac{r-a}{a}\right)^2 - \left(\frac{4\beta-1}{4a}\right) z^2 + \dots \right] \quad (3.2)$$

where H_0 refers to the axial field on the $r = a$, $z = 0$ circle, and β is the second-order focusing parameter. In such a magnetic field the electron trajectories inside a certain solid angle Ω will all cross at approximately $\phi = \pi\sqrt{2}(254^\circ)$. A thorough theoretical study of the focusing properties of the double-focusing instruments has been carried out by Lee-Whiting (1957). He has shown that for a rectangular aperture the best choices for β are $1/8$ and $3/8$. Only for these values is it possible to improve the transmission further by employing even higher-order focusing. However, he points out that the higher order focusing requires a very accurate control of the field shape which may not be possible with an iron-cored instrument. In the instrument described here $\beta = 5/8$. Due to the difficulties connected with the shaping of the magnet pole faces, no improvement was attempted on this figure, since the focusing properties of the instrument proved to be adequate.

(i) Description of the Instrument

A sketch of this instrument is shown in Fig. 4. The magnet pole faces are of Armco iron with the magnet coil consisting of 10,000 turns of No.18 formex wire wound in 8 pies. The vacuum chamber at 50 cm radius is of 1/4-inch aluminium sheet and is closed at both ends with sliding brass gates. Both the detector and the source assemblies are attached to these sliding plates, and can, therefore, be easily removed from the vacuum chamber. The electron beam is



defined by a set of six permanent baffles in the vacuum chamber (at 30° , 60° , 118° , 155° , 194° , and 224°). In addition to these, there is a set of horizontal and vertical baffles at $\sim 40^\circ$ which can be adjusted for maximum resolution. These variable baffles are used only if one is interested in resolution and can afford to sacrifice some transmission.

The chamber is evacuated by means of a water-cooled oil diffusion pump of capacity 100 liters per second, and a Cenco Megavac forepump. In normal operation, the pressure is maintained at a value somewhat below 0.1 microns.

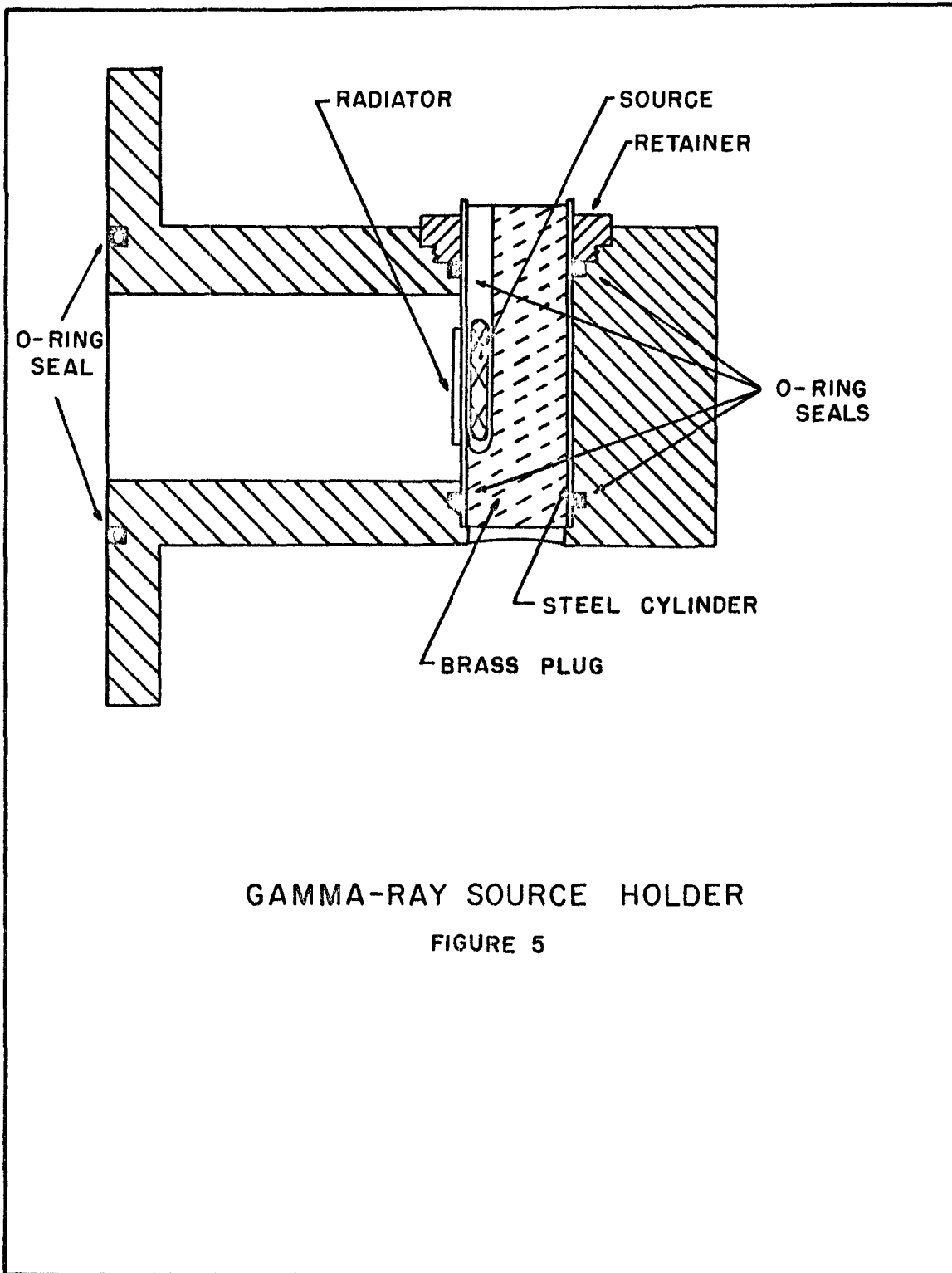
The current is provided by a stabilized power supply (Miller (1942)), supplying 850 ma at 750 v with a current stability of about 0.01%. The current is varied by means of a 10-position selector switch with the fine adjustment being made with a 10-turn helipot. In addition to this, another 10-turn helipot in series with selected resistances (with values 0, 50K, 150K, 200K), and parallel to the variable resistance of the original helipot, has been introduced during the course of this work. This makes it possible to vary the current by very small steps and thus scan over a small region of a spectrum extremely carefully. This has been found useful when working with optimum resolution of 0.2 - 0.3%.

The magnetic field is measured by means of a flip-coil with a variable number of turns (100, 70, 45, 25, 10), and a Leeds and Northrup type R galvanometer. The deflection of the galvanometer is

measured on a 100 cm scale situated at a distance of 2 meters from the galvanometer mirror.

The source is introduced into the spectrometer in the assembly attached to the sliding brass plate. For a beta source this procedure usually takes 10-15 minutes since the source assembly has to be pumped out before it can be connected with the vacuum chamber. During the course of this work, a source assembly for gamma-ray measurements was built in which the gamma-ray source itself was situated outside the vacuum chamber. In this arrangement, the radiator, which is the source of electrons inside the spectrometer, is attached to a 0.8 mm thick steel cylinder. Vacuum seals are provided by two O-rings, one at each end of the cylinder. The source is then mounted behind the radiator in a brass plug which slips into the steel cylinder in a predetermined way and has a hole or a slot at the appropriate place to accommodate the gamma source. The position of the source with respect to the radiator and the amount of material between the source and radiator can thus be varied, as desired. In this assembly no time is lost in achieving a vacuum. Figure 5 shows a drawing of this assembly.

at the other end of the vacuum chamber the detector is attached to a similar sliding gate. The detector consists of an anthracene crystal on either a 6291 DuMond or a 9524S EMI Cossor photomultiplier tube. The EMI Cossor photomultiplier has a somewhat lower dark current, giving a better signal to noise ratio at very low electron energies. With the particular tube used it was possible to detect



GAMMA-RAY SOURCE HOLDER

FIGURE 5

electrons of 25 keV energy with a photomultiplier noise background of 40 counts per minute. The anthracene crystals used were of two dimensions, $2.5 \times 1.0 \times 0.4 \text{ cm}^3$ and $2.5 \times 1.0 \times 0.2 \text{ cm}^3$. The thicker ones, which were used for work above $\sim 100 \text{ keV } E_e$, were coated with 0.1 mg/cm^2 thick lucite coating in order to reduce the evaporation of anthracene in vacuum. Since the photomultiplier is situated in the magnetic field, it is shielded by means of a cylinder of Armco iron. Although the iron is in the spectrometer gap, it does not seem to cause any significant distortion of the electron orbits. In front of the detector there is an additional set of slits which can be varied from 1 mm to 10 mm in width. For a very narrow source, these slits determine the resolution; for a wide source, they very strongly affect the transmission. The transmission of the instrument was measured with a Cs^{137} source of known strength. With this round source 2 mm in diameter, and the detector slits opened to a width of 7 mm, the measured transmission was 0.14%.

(ii) Experimental Techniques

With this instrument, experiments were carried out to study three different types of spectra: beta spectra, internal conversion spectra, and external conversion spectra. In addition, some absolute internal conversion coefficients were measured. Since each of these studies involves some special experimental techniques, a short description of the experiments carried out in each case will be given, together with the methods used in interpreting the experimental results.

(a) The Study of Beta Spectra

For the investigation of beta spectra thin beta sources were prepared. In the study of these slowly varying spectra, transmission, rather than high resolution, is important. These sources were therefore made reasonably wide and were studied with the spectrometer set at maximum transmission (detector slits at 7mm; variable baffles open). The beta spectra were scanned from a minimum energy, which was defined by source thickness, to past the end point of the total spectrum.

The material used for the preparation of beta sources was irradiated in sealed quartz capsules. After irradiation, the capsules were broken under concentrated acid and the radioactive material, always in the form of an oxide, converted to the chemical form desired for source preparation. The sources were prepared on a backing of thin aluminium-coated mylar. Two different methods of source preparation have been used. In the first method the active material dissolved in an acid solution was deposited on the backing in the form of droplets which were evaporated to dryness under a heat lamp. Although the drops were made 1-2 mm in diameter in order to obtain a source uniform in both width and thickness, even the best sources still showed source thickness effects at $E_e \approx 200$ kev. During the latter part of this study a different method of source preparation was accepted. This technique follows the ion ejection method described by Parker et al. (1960). The radioactive material was now dissolved in acetone and then sprayed out of a fine capillary onto

the source backing. The spraying was brought on by a high potential difference (≈ 3000 volts) between the anode (a fine wire inserted into the capillary), and the grounded cathode (the source backing). In order to obtain a well defined source, the source backing and holder were covered with a thin aluminium foil into which an opening, defining the size of the source, was cut. The uniformity of the source could be controlled by the distance between the capillary and the source backing. At a distance of 1-1.5 cm very even sources could be obtained, but, at the same time, a great deal of the material was lost, due to the spreading out of the ion beam. With this technique, sources could be prepared which did not show any source thickness effects at $E_e = 50$ kev.

The experimental data thus obtained were corrected for the presence of the spectra of active impurities and then subjected to a Fermi analysis. The combined Fermi functions published by the National Bureau of Standards (1952) were used in the analysis. In addition, a correction factor of $1/B\rho$ had to be applied since, in a magnetic spectrometer, the counting rate, n , is the product of the "true" number of counts at the momentum setting $B\rho$ times the spectrometer window Δp . The Fermi plot is, therefore, a plot of $\sqrt{n/B\rho f}$ against E , where $f(Z,E) = p^2 F(Z,E)$ (cf. Eq. 1.5). From this analysis the number of beta groups was then obtained by the usual "peeling off" process. Once the different groups were separated, the branching ratios could be obtained simply by replotting the various straight lines of the Fermi analysis in the form of $n/B\rho$

against B_p and comparing the areas under these curves. From the branching ratios, the $\log ft$ values (Eq. 1.6) could be calculated.

(b) The Study of Internal Conversion Spectra

In the investigation of a spectrum of internal conversion lines, the requirements as to the resolution and transmission may vary from line to line. In general, however, one desires reasonably good resolution. During the study of conversion lines, the detector slits were set at 4 mm for most of the experiments. The corresponding source width was 5 mm, providing an instrumental resolution of 0.5%. If the resolution was of importance, an improvement was attempted by narrowing the detector slits to 2 mm and making the source also 2 mm wide. It should be pointed out, however, that although in the ideal case these settings could give a resolution of 0.2%, in practice, in the low energy region, the source thickness usually sets a limit to the obtainable resolution. The peak shape and the resolution could sometimes be improved further by baffling off parts of the electron beam with the variable baffles at the 40° position.

From the internal conversion studies both the energies and intensities of the conversion lines were measured. The calibration of the instrument for energy measurements will be described in Section (e). Since the instrument has to be calibrated with known energies, these energy measurements are not absolute in nature. For internal conversion studies, the centre of the peak is chosen to denote the peak position. The intensity of a conversion line is

calculated from the area under the photopeak. Again, as in the case of the beta groups, one should plot n/B_p against B_p and then obtain the number of conversion electrons from the area of such a plot. In practice, however, the change of B_p across the peak is negligible, and therefore the intensity is calculated by dividing the measured peak area on a plot of n against B_p by the position of the peak in units of B_p . In some cases, where the low energy peaks were especially broad, the longer, but more accurate, procedure was followed. From the intensities thus obtained, various conversion ratios, such as K/L, L/M etc., were evaluated.

(c) The Study of External Conversion Spectra

The external conversion process permits one to study gamma-ray spectra in a magnetic spectrometer. A radiator consisting of some material with reasonably high photo-electric cross-section (i.e., high Z value) is inserted in front of a beam of gamma-rays. The photo-electrons which are ejected from this material are then studied. For every gamma-ray one thus observes a number of photo-peaks corresponding to the electrons ejected from the K, L_1 , L_2 , L_3 , $M_1 - M_5$ etc. shells. The energies of these lines will, of course, be a function of the gamma-ray energy, material of the radiator, and the shell from which the electrons are ejected. Since in the external conversion studies the radiator is the source of electrons in the spectrometer, its dimensions affect the instrumental resolution obtained.

Experience in this laboratory has shown that gold and uranium

can most conveniently be used for radiator materials. In this study three gold and four uranium radiators of varying thicknesses were used. The gold radiators were prepared from 0.2 mg/cm^2 gold leaf. The uranium radiators were prepared by the zapon spreading process described by Dodson et al. (1952). In this process a solution of uranium nitrate dissolved in a minimum amount of alcohol was added to a lacquer solution in acetone (lacquer was used instead of zapon). The concentrations used were as follows: $1.25 \text{ gm UO}_2(\text{NO}_3)_2 \cdot 6\text{H}_2\text{O}$ and 5 ml lacquer in 50 ml of solution. The amount of uranium on a radiator was built up layer by layer by painting the liquid on the aluminium foil and then heating the foil to burn off the organic materials and to oxidize the uranium. Each layer constituted approximately 0.08 mg/cm^2 uranium. The uranium radiators thus prepared contained uranium in the form of U_3O_8 with some UO_3 admixture. In addition to uranium and oxygen, the radiators also contained some carbon. The estimated composition of these radiators was 79% uranium, 16% oxygen, and 5% carbon. The radiators used in the external conversion work were of the following dimensions and thicknesses: gold $0.9 \times 3.0 \text{ cm}^2$ and 0.40- , 1.55- , and 4.20 mg/cm^2 thick; and uranium $0.55 \times 3.0 \text{ cm}^2$ and 1.30 mg/cm^2 thick, and $0.75 \times 3.0 \text{ cm}^2$ and 2.60- , 4.40- , and 6.60 mg/cm^2 thick.

The sources used for this work were sealed in quartz capsules. Since these capsules remained sealed during the experiment, they could be re-irradiated as many times as desired.

During the external conversion experiments the detector slits were set at 4 mm and the variable baffles were open. If improved

resolution was desired, this could be achieved in the same manner as during the internal conversion studies. During most of the work 0.5-0.6% resolution was obtained. Since a study of the lines externally converted in the L and M-shells does not give any additional information, only K-lines were studied in detail. The conversion spectra were studied with the two different radiator types. From a comparison of the spectra obtained with the gold and uranium radiators, it could be decided whether the line in question was a K, L or M-shell conversion line. Also, a check on the energy and intensity measurements could thus be obtained.

From the external conversion data the energies and relative intensities of the gamma-rays were determined. In the energy measurements the point of inflection on the high energy side of the peak was used for the peak position, since the centre of the peak is a function of the radiator thickness. The calibration of the instrument for this purpose is described in Section (e). The relative gamma-ray intensities were measured from this data by means of a semi-empirical expression:

$$I_{\gamma} = k \frac{n}{\sigma_p \beta^3} \sqrt{C^2 + (Rp\beta^3/t)^2} \quad (3.3)$$

where n is the peak height, σ is the photo-electric cross-section of the radiator material, p is the electron momentum, $\beta = v/c$ for the electron, R gives the instrumental resolution, t is the radiator thickness, and C is a slowly varying function of β and t related to the stopping power of electrons in the radiator material. k is an

instrumental constant which cancels in relative measurements. A set of semi-empirical curves of $1/\rho\beta^3$ and $\sqrt{C^2 + (R\rho\beta^3/t)^2}$ versus $B\rho$ have been prepared for the various gold and uranium radiators. The experiments performed in the preparation of these curves are described in Appendix I. In order to calculate the relative intensities, the peak heights are multiplied with the proper coefficients obtained from these curves.

(d) Measurement of the Internal Conversion Coefficients

The internal conversion intensities and the gamma-ray intensities were combined to give the transition intensities by means of a measured internal conversion coefficient. Since $\alpha_K = N_{eK}/N_\gamma$, a separately measured α_K will normalize the internal and external conversion measurement, making it also possible to calculate internal conversion coefficients for the gamma-rays where direct measurement is impractical.

This experiment was based on the following arguments. The number of internal conversion electrons N_{eK} emitted by the source is

given by
$$N_{eK} = k' A_K \tag{3.4}$$

where A_K is the number of conversion electrons obtained by the method described in Section (b), and k' is an instrumental geometry factor.

The number of gamma-rays is given by

$$\begin{aligned} N_\gamma &= n \frac{1}{\rho\beta^3} \sqrt{C^2 + (R\rho\beta^3/t)^2} k'' \\ &= I_\gamma k'' \end{aligned} \tag{3.5}$$

where I_{γ} is the relative gamma-ray intensity as calculated from external conversion studies, and k'' contains the instrumental geometry and the source-radiator geometry factors. α_K is then given by the ratio of Equations (3.4) and (3.5):

$$\alpha_K = \frac{k' A_K}{k'' I_{\gamma}} = k (A_K / I_{\gamma}) \quad (3.6)$$

with $k'/k'' = k$. Now, if A_K and I_{γ} can be measured for the same source, and k determined experimentally, α_K can be calculated.

For this experiment, an extremely strong beta source was prepared with dimensions $0.5 \times 2.5 \text{ cm}^2$ and an approximate thickness of $500 \mu\text{gm/cm}^2$. The number of internal conversion electrons was measured using this source as a beta source. The gamma-ray intensity of the same transition was obtained by covering the source with a radiator and then measuring the external conversion peak height. The factor k was obtained by repeating this experiment with a gold source of exactly the same dimensions and in the same geometry. The 411.77 keV transition of Au^{198} , with an internal coefficient $\alpha_K = 0.028$ (Wapstra et al. (1958))¹ was used to measure the factor k . In order to check the reproducibility of the geometry, the external conversion measurements were carried out with two different radiators, both when measuring k and when measuring α_K . The general procedure was to do the experiment with gold, then with the material under study, and finally with gold again. This also helped to check on the reproducibility of the geometry.

¹ This measurement has recently been confirmed by Wolfson (1961).

(e) Energy Measurements

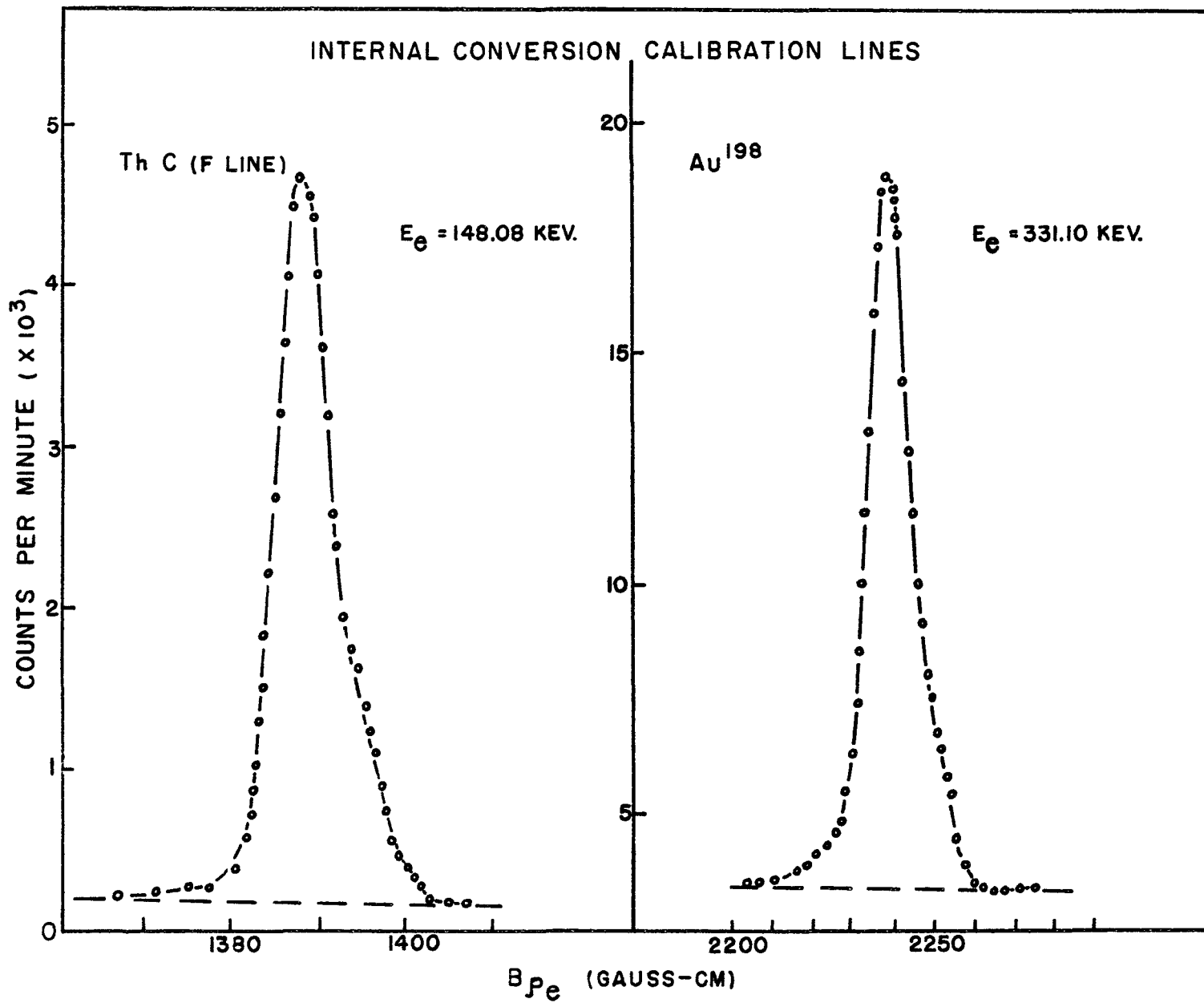
In a magnetic spectrometer containing a large amount of iron it is not possible to calculate the electron energy directly from the current producing the field. As mentioned above, the magnetic field was measured by means of a flip-coil. The galvanometer deflection was calibrated using electron lines with known energies. Over most of the range of the instrument the galvanometer deflection is directly proportional to the electron momentum. At the low momentum end, however, at $B\rho \approx 1200$, the factor $B\rho/\text{Flip Rdg.}$ starts to decrease, and at $B\rho = 600$ it is approximately 0.05% lower than at $B\rho = 1200$. Table I gives the energies and $B\rho$'s of the calibration lines used. Figures 6 and 7 show some typical calibration lines for both internal (Fig.6) and external (Fig.7) conversion.

(B) Scintillation Spectrometers

As mentioned in the Introduction, a scintillation spectrometer is very useful for the study of gamma-rays. It consists of three main parts: a crystal (or a scintillator), a photo-multiplier, and a pulse-height analyzer. A gamma-ray which enters the crystal will lose all or part of its energy to the crystal, with the energy lost appearing in the form of a light-pulse of characteristic wavelength. In the photo-cathode this light pulse is converted into an electrical pulse, with a pulse-height proportional to the energy lost in the crystal, and this pulse is subsequently amplified in the dynode system of the photo-multiplier tube. The electric pulses from the

TABLE I
Standard Calibration Lines

Calibration Line	Energy (kev)	Electron Momentum (gauss-cm)	Reference	
Internal Conversion				
Thorium C	A	24.509	534.20 \pm 0.06	Siegbahn (1955)
	B	36.150	652.38 \pm 0.07	" "
	F	148.08	1388.44 \pm 0.10	" "
	I	222.22	1753.91 \pm 0.14	" "
	L	422.84	2607.18 \pm 0.35	Lindstrom (1951)
Au ¹⁹⁸	411.770	2232.58 \pm 0.14	Muller <u>et al.</u> (1952)	
External Conversion				
Ir ¹⁹²	316.462	Au: 1816.54 \pm 0.18	Muller <u>et al.</u> (1952)	
		U: 1653.08 \pm 0.29		
	467.984	Au: 2466.82 \pm 0.24		" " " "
		U: 2321.32 \pm 0.33		
	612.87	Au: 3033.7 \pm 2.3		" " " "
		U: 2899.3 \pm 2.4		
Au ¹⁹⁸	411.770	Au: 2232.58 \pm 0.14	" " " "	
		U: 2084.18 \pm 0.14		
Co ⁶⁰	1172.8	Au: 5068.3 \pm 1.8	Lindstrom <u>et al.</u> (1953)	
		U: 4945.4 \pm 1.8		
	1332.5	Au: 5627.5 \pm 1.1		" " " "
		U: 5505.8 \pm 1.1		



B_{pe} (GAUSS-CM)

FIGURE 6

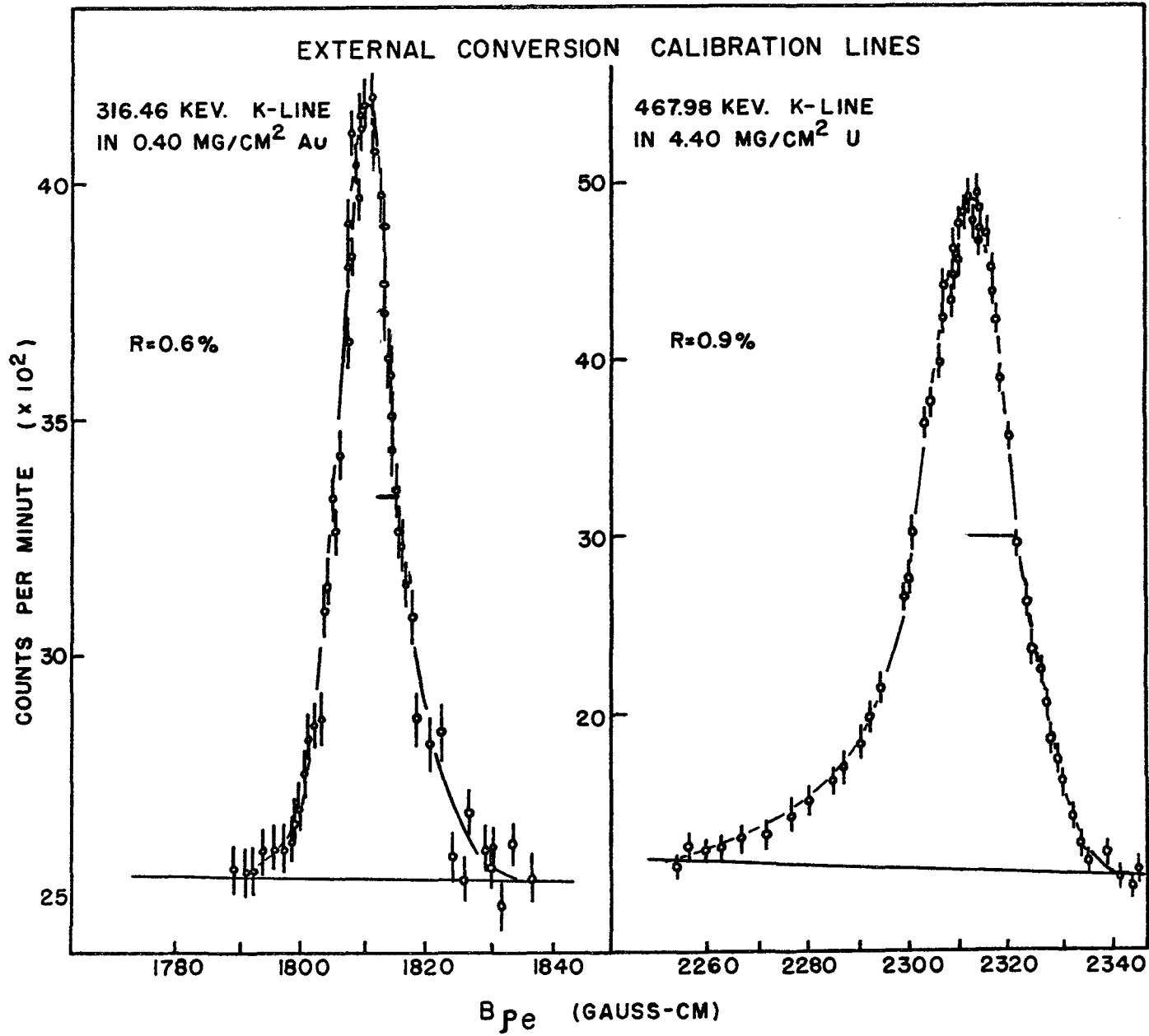


FIGURE 7

anode are then analyzed according to their pulse-heights in the pulse-height analyzer. For every gamma-ray, therefore, the pulse height spectrum will consist of two parts: the Compton distribution due to photons which have undergone Compton scattering in the crystal and then escaped, and a photo-peak where all the gamma-ray energy was lost to the crystal. In addition, when gamma-rays with energy $E_{\gamma} > 2m_0 c^2$ are present, peaks due to pair production may appear. These peaks will correspond to energies $E_{\gamma} - 2m_0 c^2$, $E_{\gamma} - m_0 c^2$, E_{γ} , depending on whether both, one, or neither of the annihilation photons escapes. NaI(Tl) crystals are favoured as gamma-ray scintillation detectors since they possess high efficiency for photo-electric absorption, linear variation of pulse height with the energy absorbed by the crystal, a high density, and a reasonably short decay time.

This type of spectrometer is superior to the magnetic instruments in that it is possible to obtain a much higher detection efficiency, which is mainly determined by the solid angle of the source viewed by the crystal. On the other hand, the resolution of such instruments is seldom better than 8%, making it impossible to unravel a complicated spectrum of gamma-rays by means of one scintillation spectrometer alone. However, by virtue of its high detection efficiency, and also because, with the help of a multi-channel analyzer, one can "look at" the whole spectrum simultaneously, these spectrometers are extremely useful when it is necessary to accumulate a large number of counts in a short time interval. Thus these instruments can be used to great advantage for a preliminary

study, since the overall spectrum can be obtained very quickly, and also for gamma-gamma coincidence study.

(i) The Study of Gamma-Ray Spectra.

In this work a commercial scintillation spectrometer unit was used for a study of simple gamma-ray spectra. This unit consisted of a DuMond 6363 photo-multiplier tube with a 3-inch NaI(Tl) crystal. The energy selection was done with a R.C.L. 256 channel analyzer. The timing was done throughout with a timer measuring the live-time of the analyser, rather than the clock-time. In this way, allowance was made automatically for the decrease in the instrumental dead-time due to the decay in source strength.

During these experiments, both the lower level discriminator (limiting the minimum size of the pulses admitted to the pulse height analyzer) and the window width (limiting the range of the pulse heights stored in any one channel) were varied to suit the particular experimental needs. At each setting the channel numbers were calibrated for energy with gamma-rays of known energies: In¹¹⁴ (192 kev), Hg²⁰³ (279 kev), Au¹⁹⁸ (412 kev), Na²² (511 kev), Cs¹³⁷ (661 kev), and Co⁶⁰ (1173 kev, and 1333 kev).

Since this spectrometer is situated on the beamport floor of the reactor building, there was always a certain amount of background radiation present. In most cases, the background was "complemented off" at the time of the experiment. Sometimes, however, especially when looking for extremely weak gamma-rays, a separate spectrum of the

background was taken and compared with the spectrum obtained from the source.

(ii) Coincidence Experiments

A second scintillation spectrometer set-up was used for some gamma-gamma coincidence experiments. Here, two 56 AVP Phillip's photo-multipliers with 2" x 1.5" NaI(Tl) crystals constituted the gamma-ray counters. A bell, Graham and Petch (1952) coincidence circuit, modified as shown in Figure 8, was used to select the coincidences. The slow coincidences, with the energy selection carried out in one side-channel, were used to gate the multichannel analyzer, which then analyzed the coincident gamma-ray spectrum. The fast coincidence circuit was 90% efficient at $E_{\gamma} = 50$ kev, and had a resolving time of 1.5×10^{-8} sec.

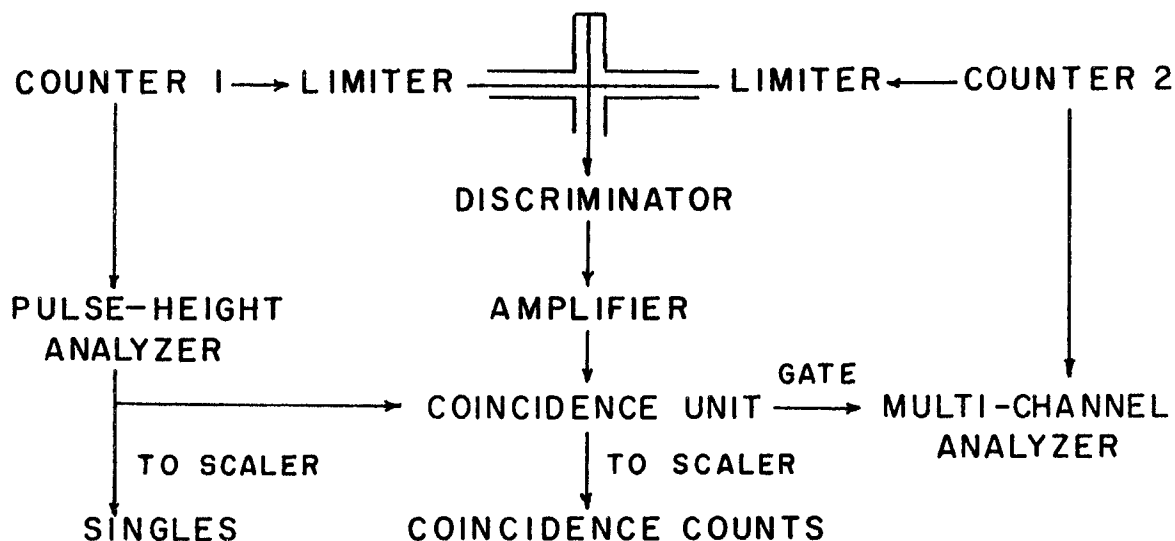


Figure 8.

(C) Double Long Lens Coincidence Spectrometer

The third instrument which was used is a double long lens coincidence spectrometer. This is also a magnetic instrument, but of the lens, or helical, type as opposed to the flat spectrometer described in Section (A). In this type of spectrometer, the electrons travel in helical paths in the direction of the magnetic field. Both the source and the detector are situated on the axis of the instrument. All electrons leaving the source, if allowed to travel freely under the action of the magnetic field, will eventually return to the axis. It follows, therefore, that all electrons leaving the source at a certain angle and with a certain momentum will return to the axis at the same time.

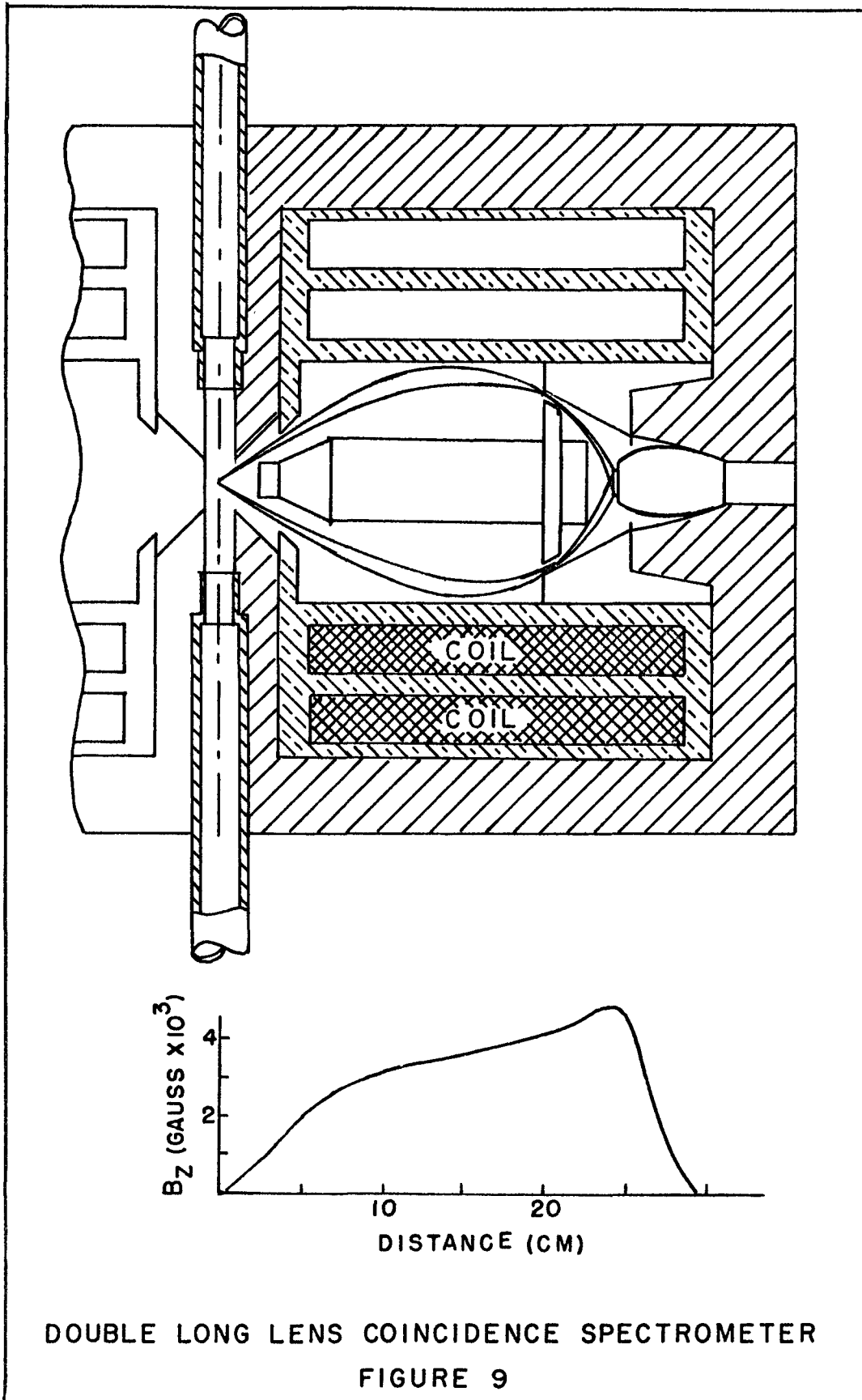
The particular instrument to be described has been built following the design of Gerholm (1955). A full description of the theory of the instrument, its construction and performance has recently been given by Habib (1961). In this section a short description of the instrument will be given, together with a discussion of some details of the experiments done in Pm^{149} .

(i) Description of the Instrument

This coincidence spectrometer consists of two beta-ray spectrometers, variously called "long lens" or "thick lens" spectrometers, placed end to end. The source and the two detectors are all placed on the axis of the instrument, with the source midway between the two spectrometers and a detector at each end. An iron shield around the

instrument provides a low reluctance path for the magnetic flux outside the field producing solenoids, thus making the two halves of the instrument magnetically independent. The solenoids and the pole pieces are designed to produce an approximately triangular field, zero at the source, rising slowly to a maximum and then falling sharply to zero again. Figure 9 shows a sketch of one half of this instrument, together with the electron trajectories and the approximate field shape. Each spectrometer contains two sets of baffles, the entrance baffles which control the maximum solid angle accepted by the instrument, and the exit baffles at the ring focus which determine both the resolution and effective transmission. The gamma-rays and the electrons travelling along the axis are prevented from reaching the detector by a lead stopper. With a point source one can achieve a resolution $\sim 0.4\%$ with a transmission of 0.4% . With a source 2mm in diameter 1% resolution can be obtained with 1% transmission.

The detector used consists of an anthracene crystal connected by means of a lucite lightpipe to a RCA 6810 photo-multiplier outside the iron yoke of the spectrometer. From the detector circuit the pulses are fed into a standard Bell, Graham and Petch (1952) fast-slow coincidence circuit. A schematic diagram of this circuit is shown on Figure 10. One is thus able to count the number of single events reaching each detector, and also the number of coincident events.



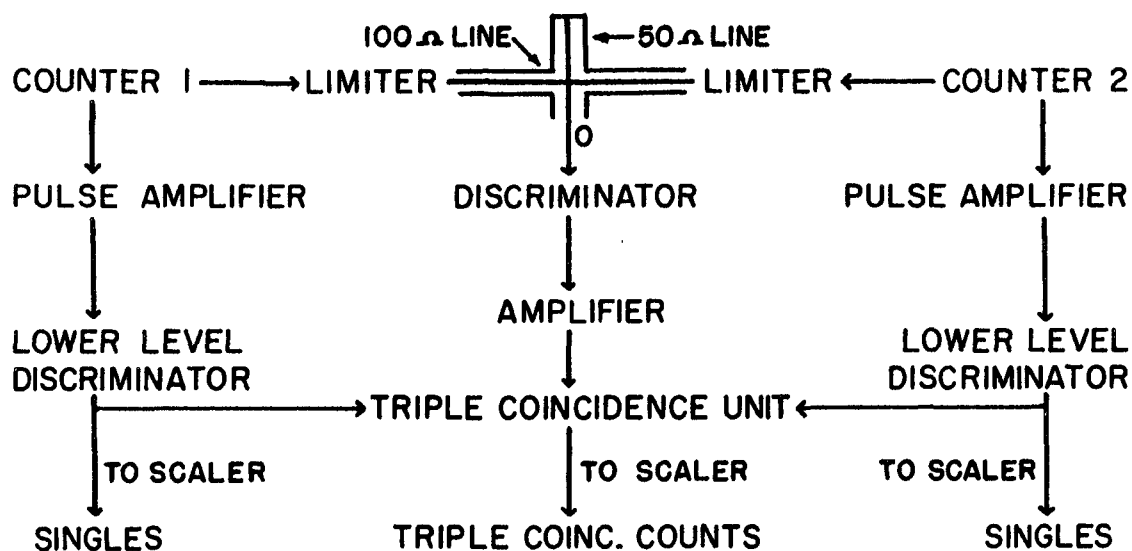


Figure 10.

During the experiments described in this thesis the instrument was operated with a transmission of 1.4% and with the resolving time of the coincidence circuit set at 8 μ -sec.

(ii) Experimental Techniques

As stated above, this instrument was used for the study of β -e coincidence work in Pm^{149} . However, in order to interpret the results of these experiments, it was necessary to know the solid angle (the transmission) of one of the spectrometers. In addition, in order to measure the endpoints of the beta spectra, the instrument had to be calibrated for energy. In this section all these techniques, together with the method of source preparation, will be described.

(a) Source Preparation

The sources used for this instrument were prepared following

the same procedure previously described in connection with the high resolution beta-ray spectrometer. In this case, however, a round source approximately 2 mm in diameter was prepared on a source backing of thin V.Y.N.S. film. The sources made were approximately $300 \mu\text{g}/\text{cm}^2$ thick.

(b) Measurement of Instrumental Transmission

In this instrument two properties strongly affect the instrumental transmission: it can be a function of the ring focus aperture, or a function of the size of the source, or a function of both these variables. With the baffles at the ring focus wide open, maximum transmission is obtained which is a constant of the instrument and does not depend on source size. With the baffles partly closed, it is strongly dependent on the source diameter, and must be determined for each source. The procedure is, therefore, to measure the number of conversion electrons in a conversion line, first, with the baffles wide open and, after the baffles have been adjusted to give the desired resolution, again, with the appropriate baffle setting. If the maximum transmission of the instrument is known, the transmission with the particular source and baffle opening can be calculated. The maximum transmission of the instrument was measured by E. Habib (1961) with a Cs^{137} source of known strength and has been found to be 5%.

(c) Measurement of Energy

It has been found that in this instrument the electron

momentum can be calculated directly from the current setting. Although the instrument is not iron-free, the hysteresis effects are negligible, since the reluctance of the iron constitutes only a small fraction of the total reluctance of the magnetic circuit. The magnetic field at any current setting has been found to be reproducible to about 0.25%. Since the instrument is generally operated at a resolution of 1 - 2%, the current setting can be accepted as a measure of the magnetic field. The instrument was calibrated for energy with the internal conversion lines of Th C (F line) and Cs¹³⁷, and these calibration factors used to calculate the B_p values from the current settings.

(d) β -e Coincidence Experiments

In the study of β -e coincidences, one spectrometer (No.1) is set on the conversion line, while the beta continuum is scanned with the second spectrometer (No.2). Two pieces of information can be obtained from such an experiment: the endpoints of the beta-group, or -groups, in coincidence with the conversion line, and, in the case of a simple decay of a beta group followed by one gamma-ray, the product of the branching ratio of the partial beta spectrum and the conversion probability of the gamma-ray can be found. The first piece of information is obtained from a Fermi analysis (described in Section A(ii)) of the coincidence spectra. The method of obtaining the second piece of information will be described below.

The counting rate in spectrometer No.1 will give the number of conversion electrons plus the number of beta particles having the same momentum as the conversion electrons:

$$N_1 = N_0 \phi(p_1) \omega_1 \eta_1 p_1 + N_0 \delta K \omega_1 \quad (3.7)$$

where N_0 is the source strength, $\phi(p)$ is the shape factor giving the probability that the beta particle will have momentum p , ω is the transmission of the spectrometer, η is the resolution, δ , is the branching ratio of the partial beta spectrum in coincidence with the conversion line, and K is the conversion probability defined by

$$K = \frac{\alpha_K}{1 + \alpha_K + \alpha_L + \dots} \quad (3.8)$$

The counting rate in spectrometer No.2 is given by

$$N_2 = N_0 \phi(p_2) \omega_2 \eta_2 p_2 \quad (3.9)$$

Of these, some will belong to the beta-spectrum in coincidence with the conversion line. A certain fraction $\omega_1 K$ of this coincidence spectrum will be registered by the coincidence circuit. The coincidence counting rate is then

$$N_c = \omega_1 K \delta N_0 \phi_1(p_2) \omega_2 \eta_2 p_2 \quad (3.10)$$

where $\phi_1(p_2)$ is the probability of a beta particle belonging to the coincident beta spectrum having a momentum p_2 . If one now compares the area under the singles beta spectrum with the area under the coincidence beta spectrum, the following relationship can be obtained

$$\int_{C_0} \frac{N_c(p)}{p} dp \bigg/ \int_S \frac{N_2(p)}{p} dp = \frac{\omega_1 K \delta N_0 \omega_2 \eta_2}{N_0 \omega_2 \eta_2} = \omega_1 K \delta$$

Thus

$$\frac{A_{\text{coinc.}}}{A_{\text{singles}}} = \omega_1 K \delta \quad (3.11)$$

Since ω_1 can easily be measured (Section (b)), a knowledge of either K or δ will allow one to calculate the other.

Before any analysis of the coincidence data can be carried out, however, the experimentally obtained coincidence counting rate has to be corrected for chance and scattered coincidences. The chance coincidences are those arising from two particles accidentally arriving at the two detectors inside the instrumental resolving time. This type of coincidence can be calculated from the singles counting rates

$$N_{cc} = 2\tau N_1 N_2, \quad (3.12)$$

N_1 and N_2 are the singles counting rates and τ is the resolving time of the coincidence circuit, or it can be measured experimentally.

In these experiments the chance rate was occasionally checked experimentally by inserting a delay line in one arm of the fast coincidence circuit, thus destroying all the true coincidences. It was found that τ calculated from experimentally-measured chance rate by means of Equation (3.12) checked well with the value expected from the stubbing cable. The second type of undesired coincidences was determined by setting spectrometer No.1 off the conversion line and scanning the beta spectrum with spectrometer No.2. These coincidences are caused by particles which have been scattered into the detector and thus do not belong in the focused electron beam. The origin of these scattered electrons has since been investigated by Mr. D. Burke of this laboratory. He found that these electrons

could be almost completely eliminated by means of a set of shallow baffles mounted on the central lead gamma stopper in front of the exit baffles.

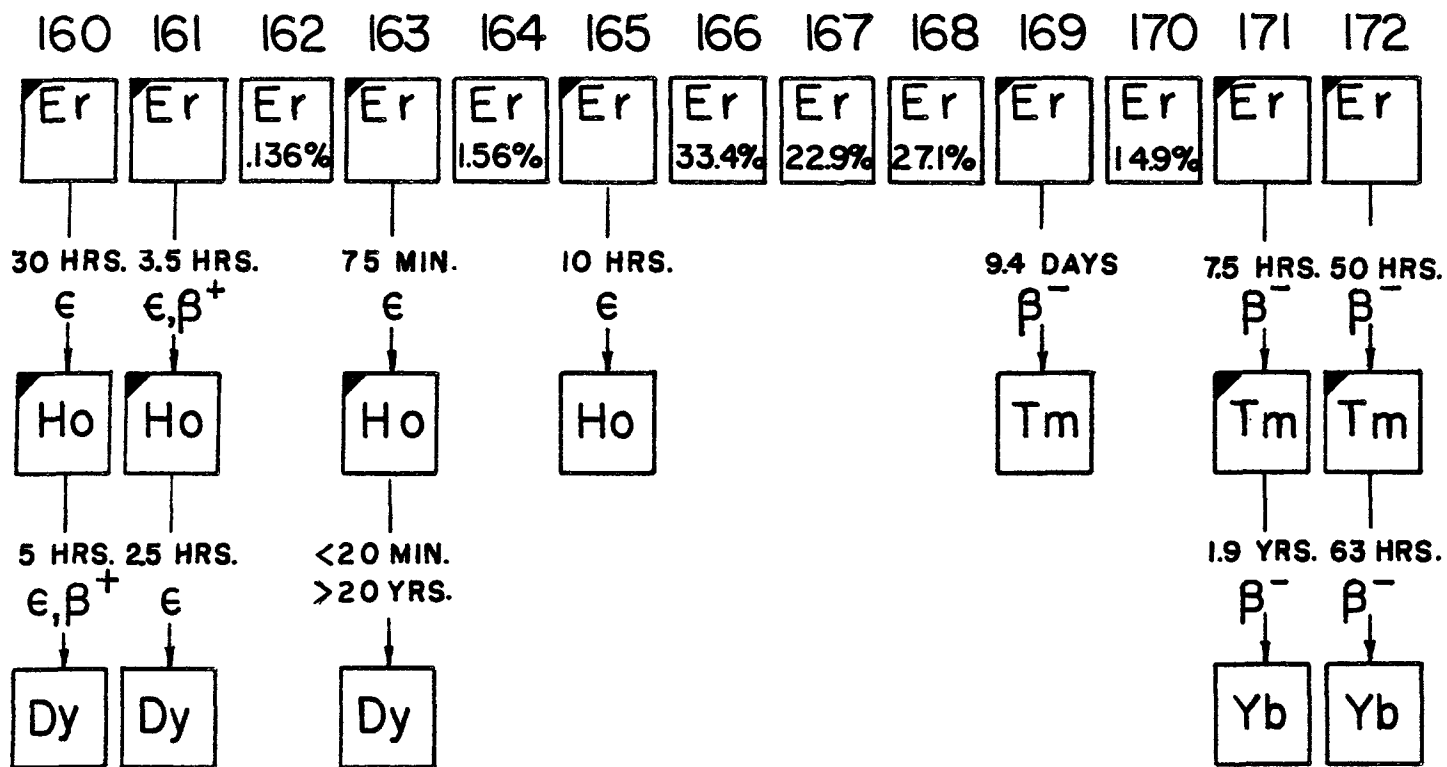
CHAPTER 4

A STUDY OF NEUTRON-ACTIVATED ERBIUM ISOTOPES

Introduction

Erbium is one of the rare earth metals with $Z=68$ and N varying from 92 to 104. Figure 11 shows the various erbium isotopes, their abundances and decay chains. An observation of this figure reveals that four erbium isotopes can be produced by means of neutron bombardment: Er^{163} , Er^{165} , Er^{169} and Er^{171} . Although at the time this study was planned some information existed about the decays of all of these isotopes, it was felt that a further investigation with the instrumental techniques available in this laboratory might yield a considerable amount of interesting information.

An investigation of the decay of the four neutron-activated erbium isotopes was thus planned, and in this thesis the results of this study will be reported. Since these experiments extend over a period of three years, additional information about the decay of some of these nuclei has meanwhile appeared in the literature. The results of the present study will, therefore, in some areas only confirm the results of other workers. In other areas, again, the results reported suggest further experiments using facilities which were not available during this investigation.



$\epsilon, \beta^-, \beta^+$ - MODE OF DECAY

ERBIUM ISOTOPES

FIGURE II

In this chapter the isotopes Er^{163} , Er^{165} , and Er^{169} will be discussed, while the next chapter will be devoted to the complex decay of Er^{171} .

(A) Erbium-163

(i) Historical Survey

Very little has been reported about the 75-minute decay of Er^{163} . Although a complicated decay would be expected for this nucleus, a complete study of this decay presents experimental difficulties because of the short half-life and the low abundance of the erbium isotopes with low atomic number.

The half-life of 75 minutes was associated with this decay by Handley and Olson (1953). They found two gamma-rays of energies 430- and 1100 keV by studying the decay of Ho^{165} activated by proton bombardment (p, $3n$ reaction). In addition they also found 50 keV X-rays and looked for but did not find 511 keV annihilation radiations. Somewhat later Harmatz et al. (1959) investigated a number of decays in this region with a permanent magnet spectrograph and assigned a 432.5 keV internal conversion line to this decay.

Since so little is known about the decay of this nucleus, a further study was attempted.

(ii) Experimental Study

During this study three different types of experiment were carried out. The scintillation spectrometer (Section 3.B.(i)) was used to obtain a gamma-ray spectrum; the coincidence spectrometer (Section 3.B.(ii)) was used to investigate gamma-gamma coincidences; and the

high resolution beta-ray spectrometer (Section 3.A) was used in an attempt to obtain energy and intensity measurements for the radiations known to exist. In all these experiments Er_2O_3 enriched in Er^{162} was used as the source material. The spectroscopic report gives the following composition for this enriched material: Er^{162} 6.1%, Er^{164} 11.6%, Er^{166} 44.2%, Er^{167} 18.2%, Er^{168} 15.1%, Er^{170} 4.8%.

The samples were irradiated in the McMaster reactor pneumatic rabbit system for 2-3 minutes at a neutron flux of 1×10^{12} and then studied with the R.C.L. multichannel analyzer. Although only 4.8% Er^{170} was present in the source material, the Er^{171} gamma-rays were prominent in the spectrum. However, it was found that in addition to the Er^{171} peaks, well known at this time, there were two additional gamma-rays which could be attributed to the 75-minute activity. These were found at 430 kev and at 1120 kev, as shown on Figure 12. The X-ray peak at 50 kev was definitely found to decay with 75-minute half-life during the first few hours of the experiment.

Since the presence of a comparatively large amount of Er^{171} activity made it impossible to be certain that no other shortlived peaks appeared, some gamma-gamma coincidence experiments were attempted. Gating over the 430 kev gamma-ray, low energy lines were observed at 50 kev and at 112 kev. These were found to decay with the half-life of Er^{171} and were attributed to coincidences between the Compton scattered photons of the Er^{171} high energy gamma-rays and the Tm X-rays and low energy gamma-rays of Er^{171} . No peaks belonging to the 75-minute activity were observed. A coincidence spectrum was also taken while

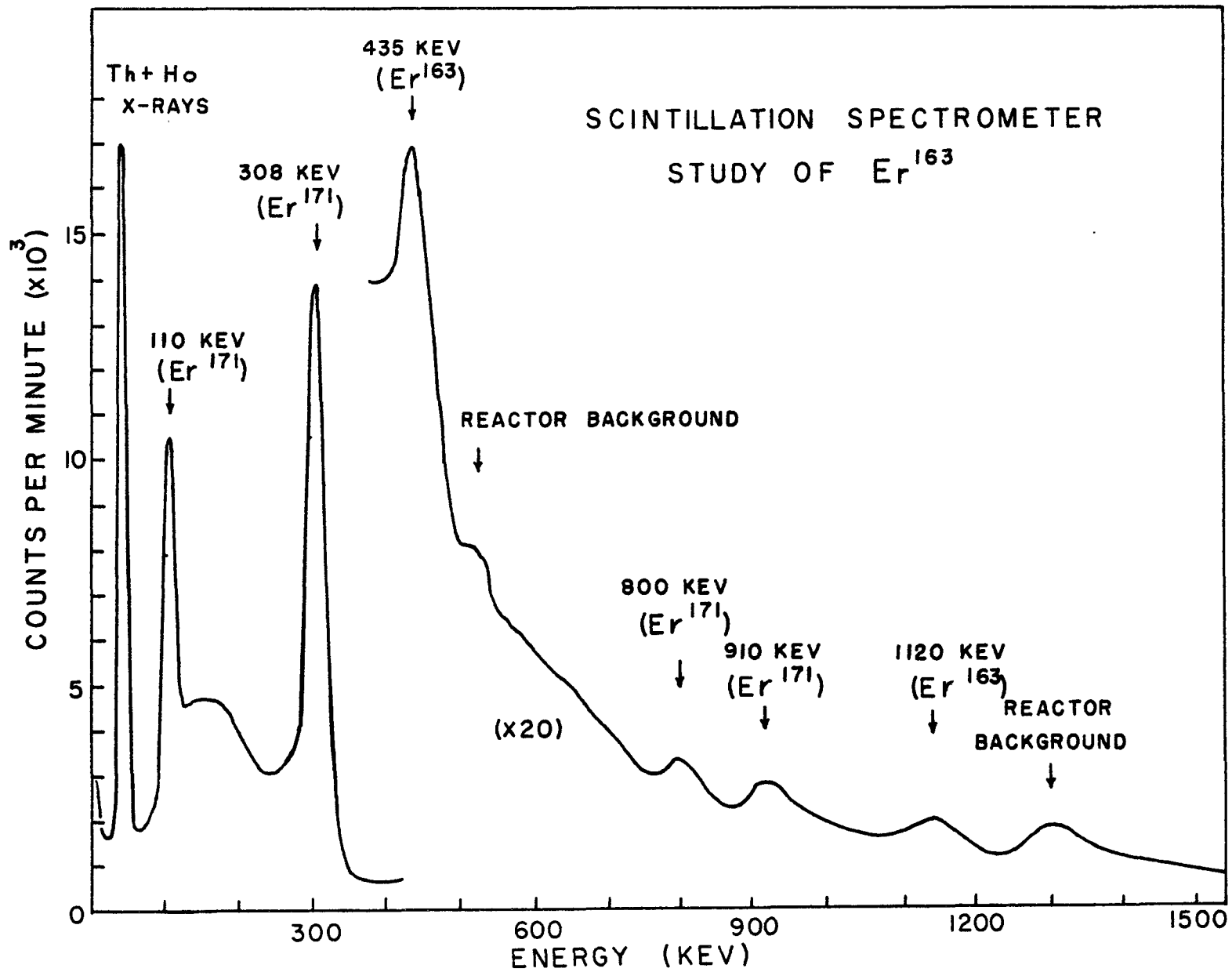


FIGURE 12

gating over the X-ray peak at 50 kev. Again, the spectrum associated with the 7.5 hour activity appeared but no short lived gamma-rays were found. In this case the source strength was limited by the very strong X-ray peak.

An attempt was then made to look for the 430 kev gamma-ray in the high resolution beta-ray spectrometer, using external conversion techniques. No experimental results can as yet be reported. The sources used in this work were irradiated in the reactor core and thus the experiments could not be started before at least 45 minutes had elapsed from the time the irradiation was ended. It was found that the gamma-ray sources used were too weak to obtain meaningful information with the high resolution spectrometer. It was decided that these experiments would be postponed until the pneumatic sample transfer system connecting the laboratories in which the magnetic spectrometers are situated with the reactor core are approved for irradiations lasting at least two half-lives of this isotope.

From these experiments it can be concluded that either the neutron capture cross section for Er^{162} is very small, considerably less than 1 barn, or, more likely, that most of the Er^{163} decay is electron capture to the ground state of Ho^{163} . From the existence of a 1120 kev gamma-ray and, at the same time, the absence of annihilation radiation, it can further be concluded that the decay energy available is probably between 1200 and 1500 kev. The existence of the previously reported 430- and 1120 kev gamma-rays was also confirmed.

(B) Erbium-165

(i) Historical Survey

The activity of Er^{165} was first found by Butement (1950,1951) who reported the production of a new 10-hour radioactive isotope by nuclear photo-disintegration. Soon afterward Kundu et al. (1952) measured the half-life to be 9.9 ± 0.1 hours and reported the existence of internal conversion electrons with energies 220- and 1100 kev. In addition, K-X-rays and gamma-rays were also detected. However, during the years 1957-1959 three groups of authors reported that no gamma-rays exist in this decay (Harmatz et al. (1959), Gorodinskii et al. (1957), and Grigorev et al. (1958)). In addition, Grigorev et al. measured the I/K capture ratio and deduced from this that the total decay energy available is 82 kev. This measurement is believed to be too low by the Nuclear Data Project Group who estimate from the log ft value that the total energy available for the decay should be $\gg 200$ kev.

(ii) Experimental Study

During the course of this study of the erbium isotopes some experiments were also carried out on Er^{165} . Using Er_2O_3 enriched in Er^{164} , the gamma-ray spectrum was obtained with the scintillation spectrometer. In addition, the gamma-gamma coincidence spectrometer was used to look for gamma-rays in coincidence with the X-rays, and also to identify an activity not found in the spectra of other erbium isotopes.

The sources used for the scintillation spectrometer study were irradiated for several hours and then left to decay for about 48 hours.

The experiment consisted of comparing the spectra obtained from two sources, one of Er_2O_3 enriched in Er^{164} , the other of natural erbium. The half-lives of the various lines in the spectrum were followed for 72 hours. The only difference between the two sources appeared in the X-ray peak at 50 kev. For the coincidence experiment the Er^{165} source was again irradiated for a longer period and then left to decay for several days in order to improve on the $\text{Er}^{165}/\text{Er}^{171}$ activity ratio. No lines other than the ones belonging to the Er^{171} activity appeared in the coincidence spectrum. However, when the spectrum was obtained right after the irradiation, it was found that a much shorter-lived activity was present with a strong gamma-ray at approximately 100 kev. In order to identify this activity, the spectrum in coincidence with the 100 kev gamma-ray was obtained. Since this showed that the 2-hour 100 kev gamma-ray was in coincidence with X-rays and gamma-rays with energies 110-, 280- and 600 kev, it was identified as the 94.8 kev transition in Ho^{165} following the decay of 2.3 hour Dy^{165} .

It can thus be concluded that the decay of Er^{165} goes by electron capture to the ground state of Ho^{165} , as reported by previous workers.

(C) Erbium-169

Er^{169} has the longest half-life of all the erbium isotopes, 9.5 days. Because of this long half-life and the comparative large abundance of Er^{168} (27.1%), the decay of this nucleus has been observed by numerous workers. It is found to consist of two beta groups of energy

332- and 340 keV and a gamma-ray of 8.4 keV. The endpoint of the total beta spectrum was measured by Bisi et al. (1956), and by Hatch and Boehm (1956). The conversion electrons and the gamma-ray of the 8.4 keV transition were studied by Charpak and Suzor (1959) with two proportional counters in coincidence. These authors measured the branching ratio of this decay to the ground state and to the first excited state of Tm^{169} to be 58% and 42%, respectively. The conversion coefficients were found to have the following values: $\alpha_M = 69$; $\alpha_N = 37$, and $M_1:M_2:M_3:M_{45} = 3:1:1:0.05$, and the multipolarity ratio $M1/E2 = 1000$.

Since no improvement could be attempted on this work, the study of the decay of Er^{169} was discontinued at an early stage.

CHAPTER 5

THE STUDY OF ERBIUM-171

Introduction

The decay of 7.5-hour Erbium-171 has been previously studied by a number of workers: by Ketelle and Peacock (1948), Keller and Cork (1951), Johansson (1957), Hatch and Boehm (1957), and Cranston, Bunker and Starner (1958). The early workers (Ketelle et al. and Keller et al.) agreed on the strong transitions in the spectrum and established the low-lying levels at 115 kev and 425 kev, but found very little else. Johansson and Hatch et al. established the ground-state rotational band based on spin $\frac{1}{2}$ with energies: 0, 5.1, 111.7, 129.1, and 339.7 kev; and a metastable level at 428 kev. Beta-decay was found to be mainly to the 425 kev level, with an endpoint of 1000 kev. Johansson investigated this decay with coincidence methods using a scintillation spectrometer, while Hatch and Boehm made a study of the conversion electron spectrum with a two-meter curved crystal spectrometer and a semicircular beta-ray spectrometer. The very accurate energy measurements obtained with the curved crystal spectrometer allowed Hatch et al. to calculate a number of nuclear parameters for the Tm^{171} nucleus from the energies of the ground state rotational band.

A much more thorough investigation of this decay was carried out by Granston et al. (1958). The decay scheme proposed by these workers is shown on Figure 13. This decay scheme is based on a series of scintillation spectrometer coincidence experiments. In addition, they carried out some beta-gamma coincidence experiments with a lens spectrometer, and also observed some low energy conversion lines in a permanent magnet spectrograph. Although they proposed a complicated decay scheme of 9 excited levels being supported by 26 gamma-rays, they were unable to resolve a number of gamma-rays. The doublet structure of all the high energy transitions was postulated by these workers on the basis of the characteristic $K = \frac{1}{2}$ ground state rotational band. In addition, the energies of these radiations as measured with a scintillation spectrometer, leave a large amount of uncertainty as to the positions of the higher excited levels. It was, therefore, felt that a further study of this decay with a high resolution beta-ray spectrometer might prove rewarding.

In this work four sets of experiments were carried out. The gamma-ray spectrum was studied with external conversion techniques using both gold and uranium radiators; the internal conversion spectrum was studied with a resolution of 0.4 - 0.6% up to $E_p = 2400$ gauss-cm; the beta-ray spectrum was measured and analyzed and the relative conversion intensities related to the total number of disintegrations through this analysis; and finally the internal conversion coefficients of the 296- and 306 kev transitions were measured directly, thus relating the relative gamma-ray intensities

CRANSTON, BUNKER, AND STARNER

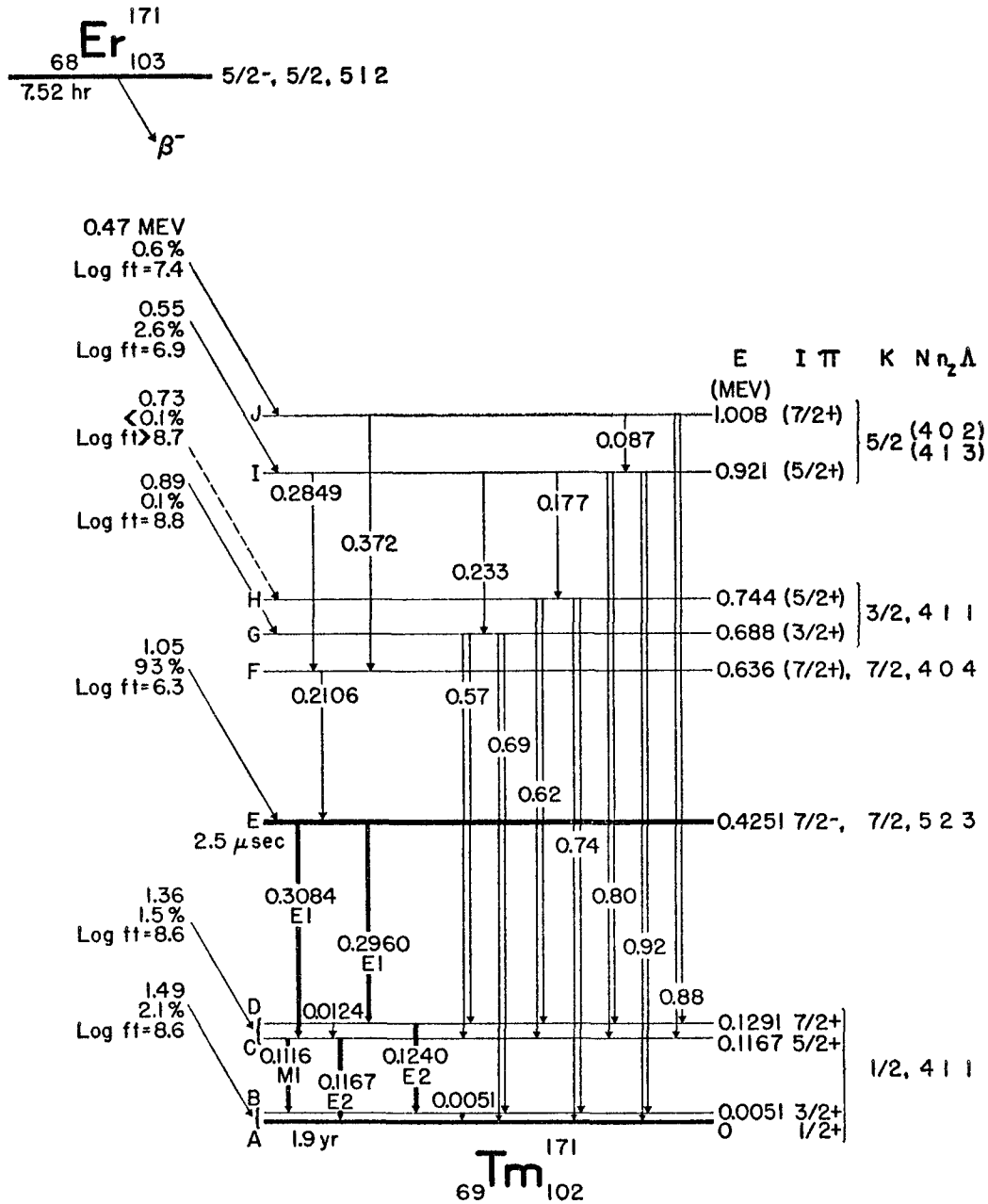


Figure 13.

to the conversion electron intensities (Section 3.A.(ii)).

(A) Description of the Experiments
and Presentation of Experimental Results

(i) Source Material and Preparation

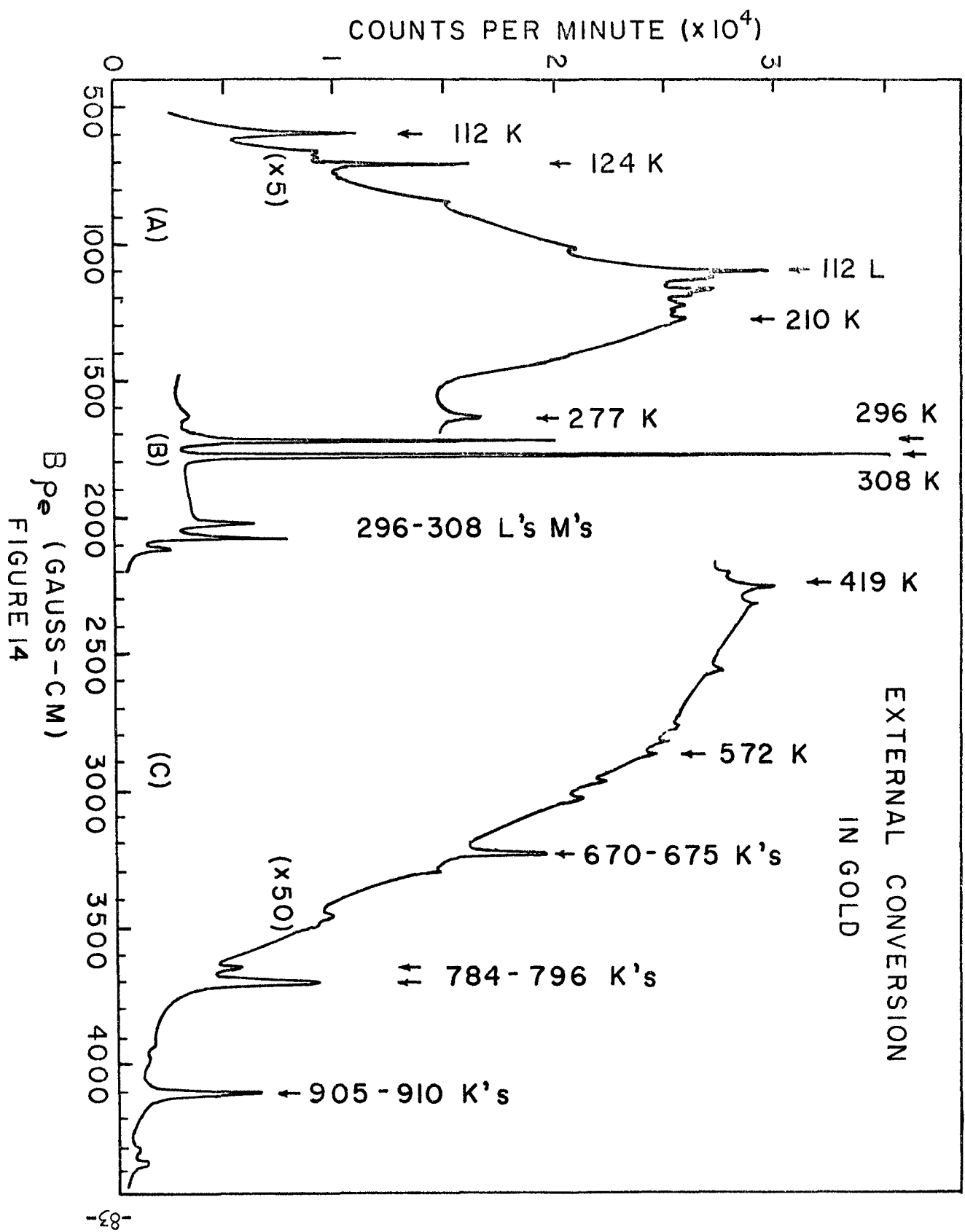
During this study both natural Er_2O_3 and Er_2O_3 enriched in Er^{170} were used. For the gamma-ray sources three quartz capsules, each containing ~ 450 mg of natural Er_2O_3 , were used as three separate sources. These were irradiated in turn in the McMaster Reactor at a neutron flux of 1.5×10^{13} neutrons $\text{sec}^{-1} \text{cm}^{-2}$. Since the prominent activity in the natural erbium oxide is the Er^{171} activity, large sources of natural Er_2O_3 , rather than smaller samples of enriched material, were found to be more economical.

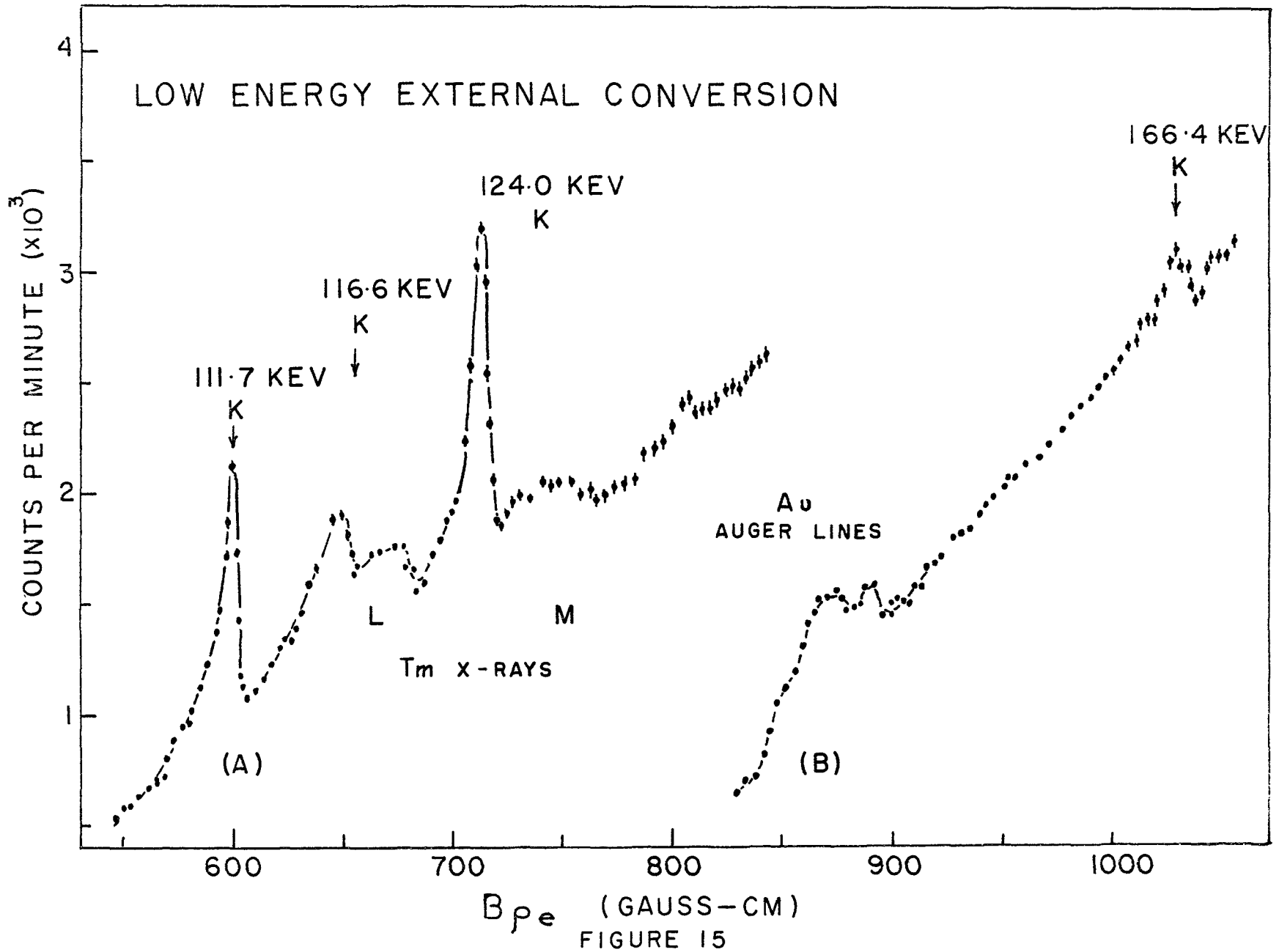
The beta sources were prepared from enriched Er_2O_3 . This material contained $< 0.05\%$ Er^{162} , $< 0.05\%$ Er^{164} , $1.68 \pm 0.05\%$ Er^{166} , $2.1 \pm 0.1\%$ Er^{167} , $9.0 \pm 0.1\%$ Er^{168} , and $87.3 \pm 0.2\%$ Er^{170} . The source material was irradiated under the same conditions as the gamma-ray sources. The radioactive oxide was dissolved in concentrated HNO_3 under a heat lamp. The solution was then evaporated to dryness, leaving a deposit of erbium nitrate. When making sources by the "droplet" technique, the nitrate was dissolved in distilled water and deposited as droplets on the backing film in the manner described in 3.A.(ii). For sources prepared by the ion ejection technique, the nitrate was "dissolved" in acetone and sprayed on the backing as described in 3.A.(ii). This technique produced much more uniform sources than the "droplet" method.

(ii) The External Conversion Spectrum

The external conversion spectrum was first scanned in sections, with each source covering a certain momentum interval of the spectrum twice. This was done to measure the half-lives of the various conversion lines. All the photo-peaks found seemed to decay with a half-life of 7.5 hours. Once the positions of the various lines were established, the interesting sections of the spectrum were studied carefully in order to obtain reliable energy and intensity measurements, especially for the weak high energy gamma-rays. Since a careful study meant a very slow scanning rate, only a small section of the spectrum could be covered with any one source. In order to normalize all the different sources, the peak height of the 303.2 keV K-conversion line was measured carefully in every source. The whole spectrum from $B_p = 500$ to 4500 gauss-cm was covered, using both gold and uranium radiators and about 45 different gamma-ray sources. Figure 14 shows a sketch of the complete external conversion spectrum converted in gold. It should be noted that the various parts of this spectrum have been obtained with radiators of varying thicknesses. Section (A) was obtained with the 0.40 mg/cm² and 1.55 mg/cm² thick radiators; section (B) with 1.55 mg/cm², and section (C) with 4.20 mg/cm² thick radiators.

The next five figures (Figs. 15 - 19) show the details of this external conversion spectrum. In Figure 15 the momentum range $B_p = 500$ to 1050 gauss-cm is covered. Spectrum (A) on that figure shows the low energy photo-peaks converted in a 0.40 mg/cm² gold





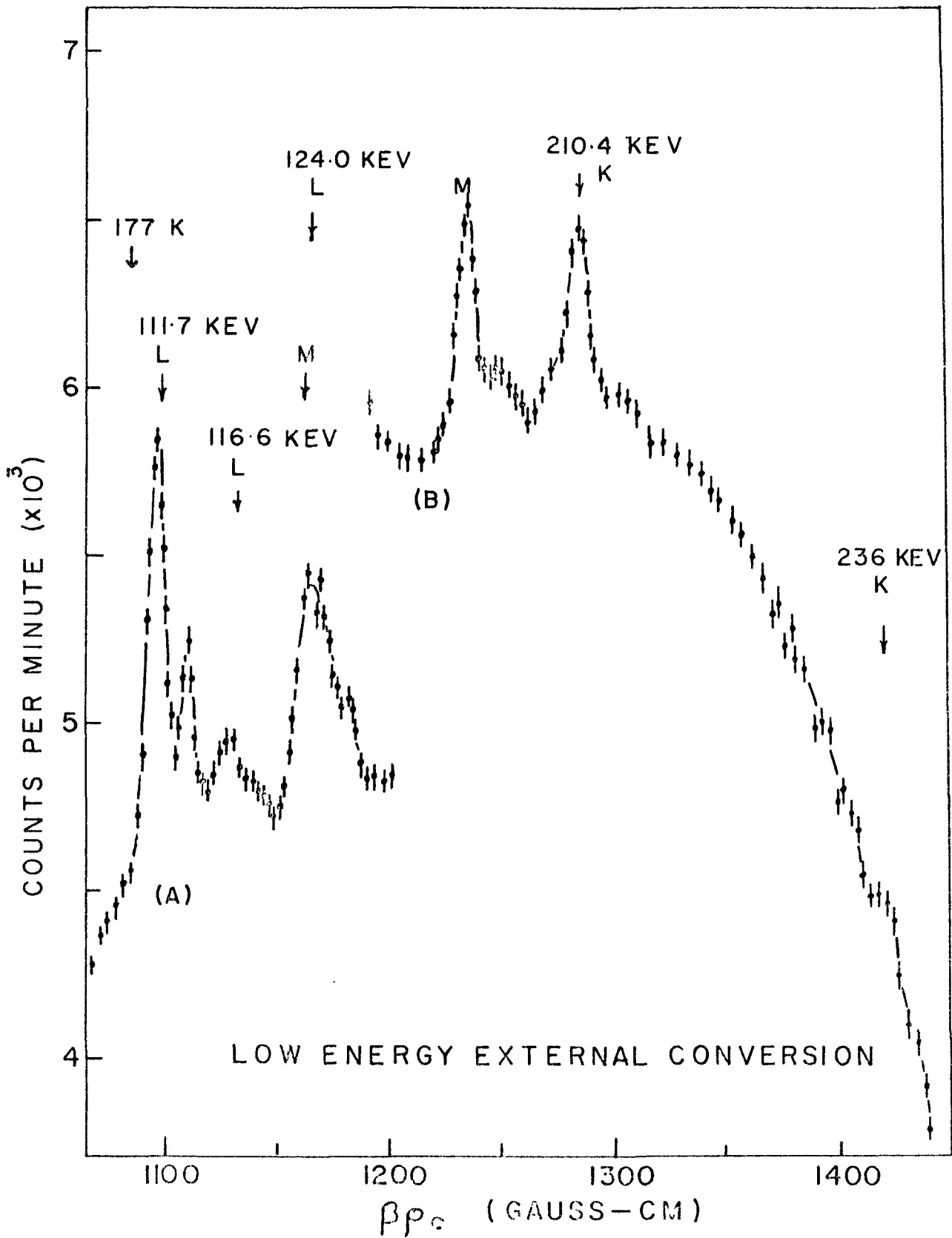


FIGURE 16

HIGH ENERGY EXTERNAL CONVERSION

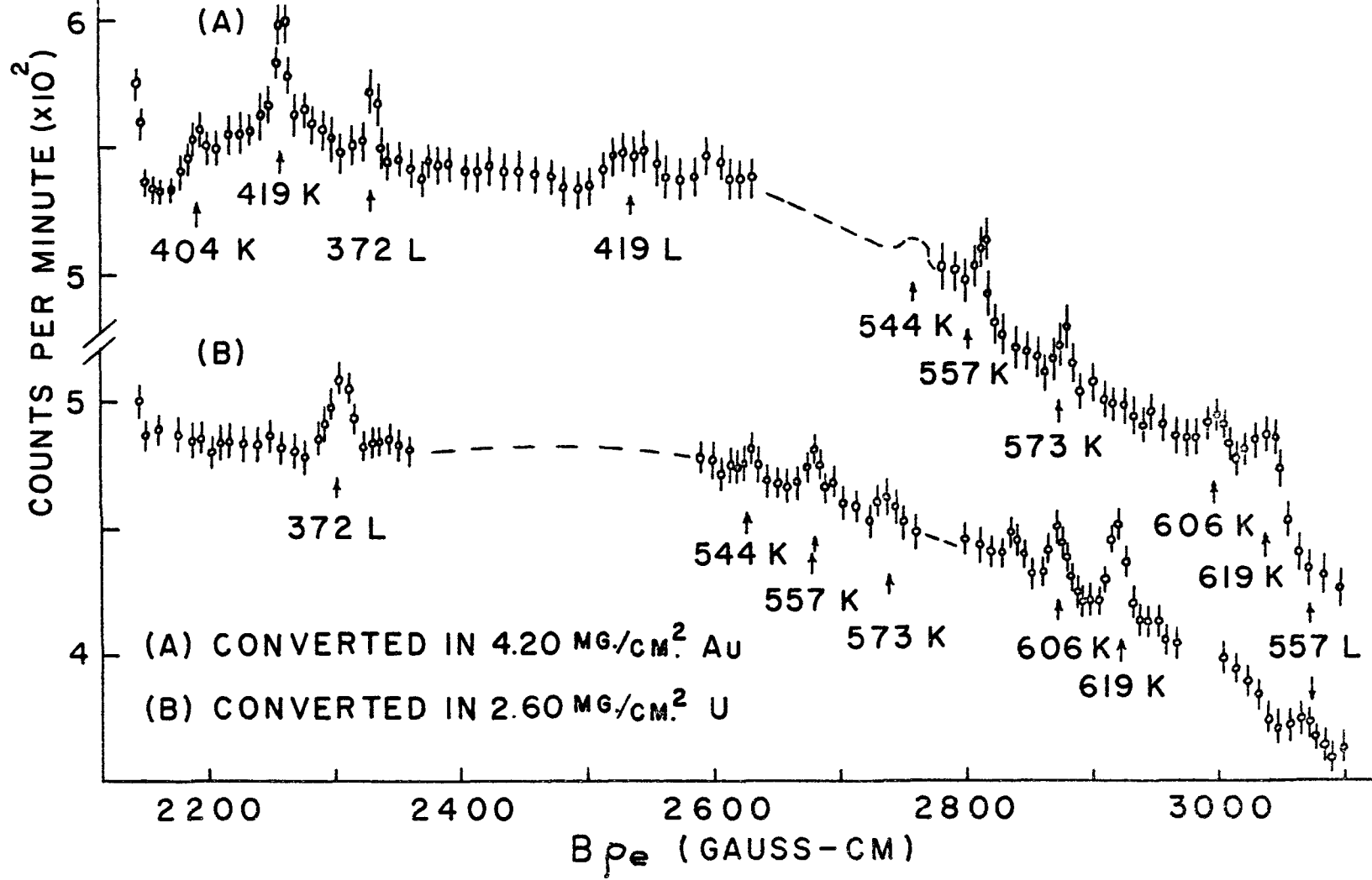


FIGURE 17

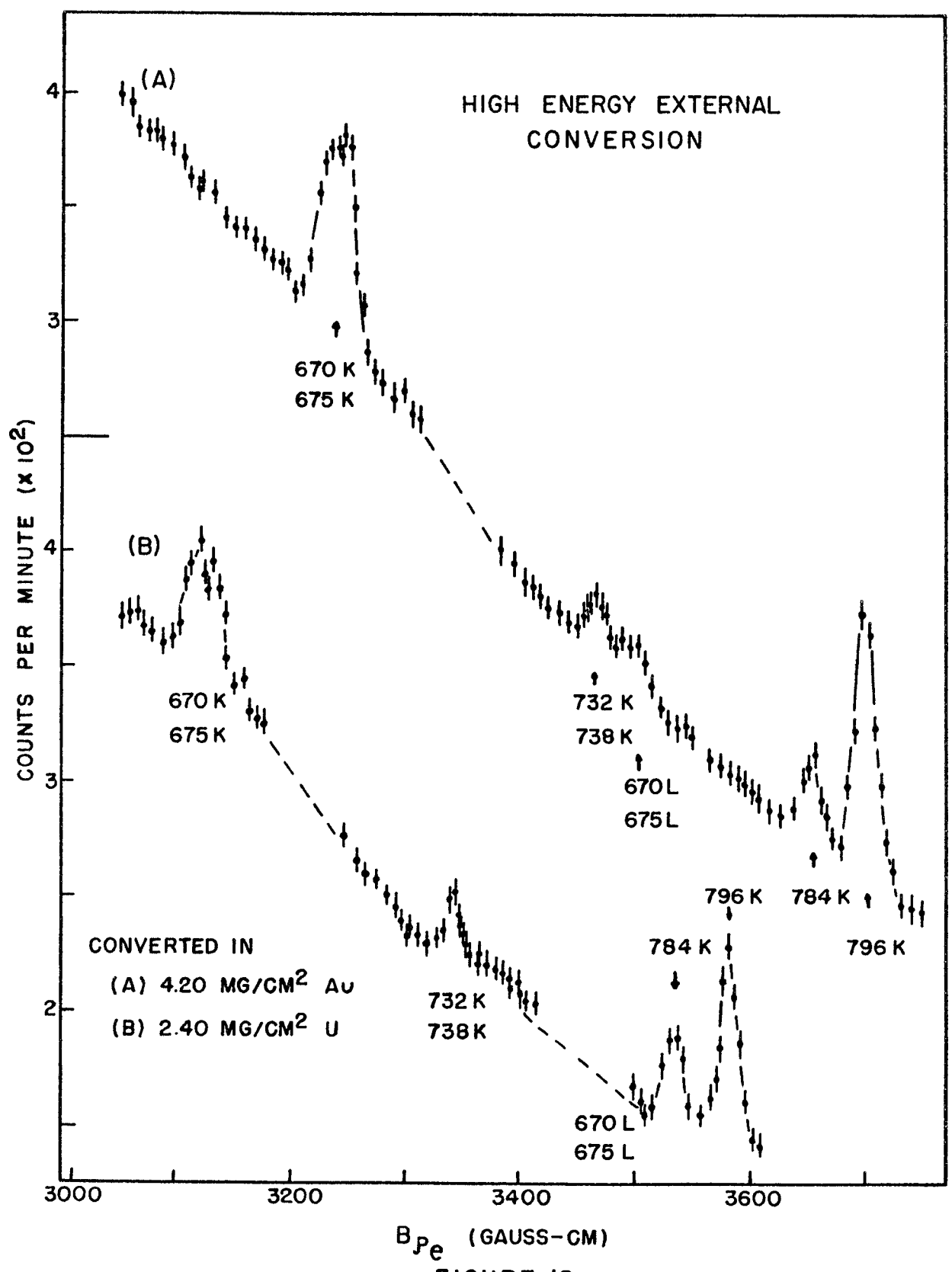


FIGURE 18

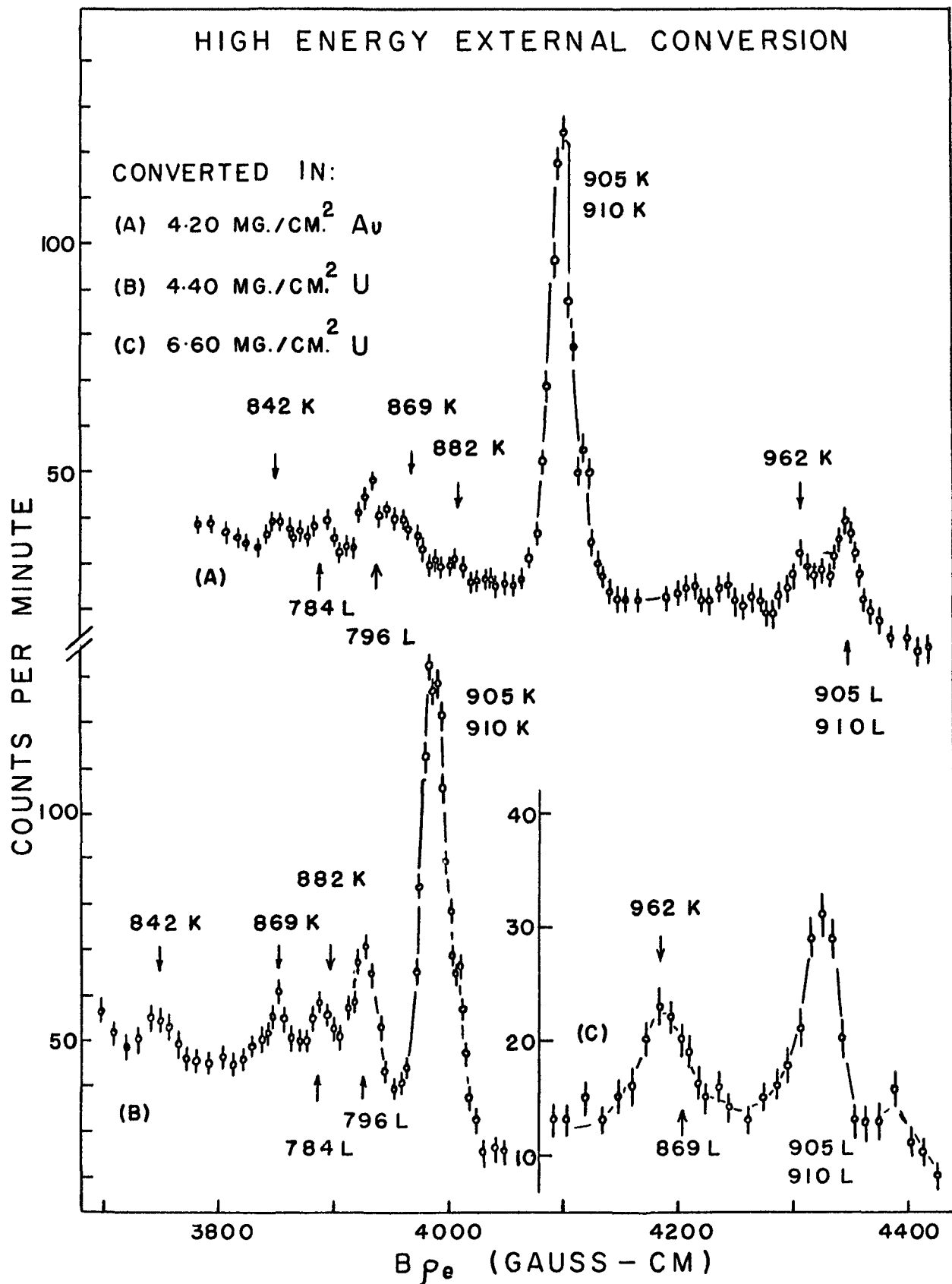


FIGURE 19

radiator. In addition to the strong photo-peaks at 603- and 714 gauss-cm due to the 111.7- and 124.0 kev gamma-rays, a number of weaker lines appear in this region. These are believed to be due to thulium X-rays converted in gold and gold Auger lines, as marked on the figure.

Although the K-peak of the relatively weak 116.6 kev transition at $B_p = 642$ gauss-cm is masked by the L-conversion lines of thulium K-shell X-rays, it was possible to make an estimate of its height. Section (B) on Figure 15 shows the almost smooth part of the spectrum from $B_p = 850$ - to 1050 gauss-cm. The photo-peak at 1030 gauss-cm is attributed to a 166 kev gamma-ray. The lines found at 860-900 gauss-cm are believed to be gold Auger lines. Although these lines are not resolved on the scale of this figure, a more detailed study showed the complicated structure characteristic of the Auger spectrum. They cannot be due to L-conversion of a thulium gamma-ray, since no photo-peaks were observed in the corresponding position in a spectrum obtained with a uranium radiator; similarly, they cannot be attributed to a K-conversion peak because the corresponding K-conversion line was absent from the internal conversion spectrum.

In Figure 16 Section (A) was obtained with a 0.40 mg/cm^2 gold and Section (B) with an 1.55 mg/cm^2 gold radiator. This figure shows the L- and M-shell photo-peaks of the low energy transitions (111.7- and 124.0 kev), and the K-conversion lines of the 210.4- and 236.4 kev gamma-rays. It should be noted that there is no evidence of the K-conversion line of a 177 kev gamma-ray reported by other workers.

Section (b) of Figure 14 is not presented as a separate figure.

This part of the external conversion spectrum shows the K-, L-, and M-lines of two very strong gamma-rays of energy 295.6- and 308.2 kev, and a K-conversion line of a somewhat weaker gamma-ray of energy 277.0 kev which has not been previously reported. This line was observed many times and found to decay with the half-life of Er^{171} .

Figures 17, 18, and 19 show details of Section (C) of Figure 14. In this part of the spectrum various radiators were used as indicated on the figures. A number of doublets are observed, some with an energy difference of 5 kev, and others with an energy difference of 12 kev. These experiments thus confirm the doublet structure of the high energy gamma-rays previously postulated by Cranston et al. (1958). Two separate spectra are plotted on each of these figures, one above the other. In each case the upper one represents conversion in gold and the lower one conversion in uranium. A comparison of the two spectra immediately differentiates between K- and L-shell photo-peaks, since their relative positions in gold and uranium are different. Figure 17 shows the previously unobserved 404 kev K-line, and also the K-shell conversion line of a 419.0 kev gamma-ray reported by Keller et al. (1951) but not observed by Cranston et al. (1958). In addition, it is found that the 0.57 Mev transition reported by Cranston et al. is really a triplet consisting of a 544-557 kev doublet and a 572 kev gamma-ray. Figures 18 and 19 show the spectra from B_p 3100 to 3650 gauss-cm, and from B_p 3700 to 4450 gauss-cm, respectively. The results presented in Figure 19 were obtained with three different radiators: 4.20 mg/cm² gold, 4.40 mg/cm² uranium and 6.60 mg/cm² uranium. This

section shows peaks associated with two previously reported gamma-rays; these are found to be doublets with energies of 869-882 keV and 905-910 keV, respectively. In addition, K-shell conversion lines associated with two new transitions appear, corresponding to gamma-ray energies of 842- and 962 keV. Both these lines may very well be members of either one of the doublets characteristic of this spectrum. However, since these peaks are very weak, it is difficult to make a definite decision concerning them.

The energies and relative intensities of the radiations associated with these observed conversion lines were determined by methods described in Chapter 3. The results are tabulated in Tables IV and V.

(iii) The Internal Conversion Spectrum

The internal conversion spectrum from $B_p = 550$ to 2400 gauss-cm was also studied in sections. Since the beta spectrum forms a very high background on which the conversion lines are superimposed, it was not possible to obtain the peaks of the weakly converted transitions above 400 keV. During this work the 111.7 keV K-line was used as a standard when dealing with thin and relatively weak beta sources, and the 308.2 keV K-line was used when dealing with stronger and thicker sources. The relative intensities of these two lines were measured in two separate sources; one of these was thin, prepared for low energy study, and the other somewhat thicker and considerably stronger.

Figures 20 and 21 show the K- and L-lines of the three low energy transitions of 111.7-, 116.6-, and 124.0 keV. In addition the positions of two other K-lines are marked on Figure 21. The

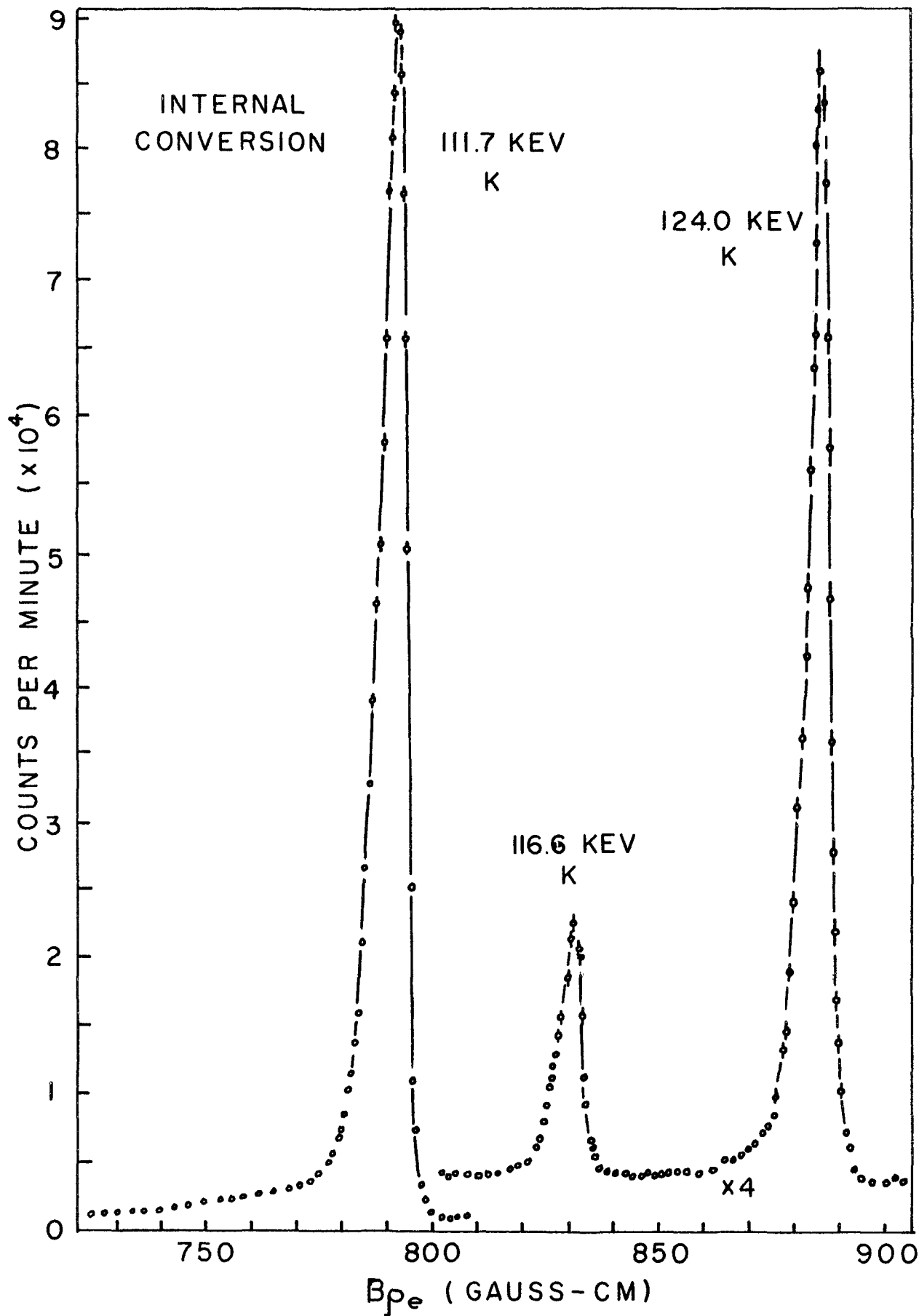


FIGURE 20

first of these, associated with the 166 keV transition clearly evident in the external conversion spectrum, falls under the 116.6 keV L-lines. It is believed that it is responsible for making the $(L_1 + L_2)/L_3$ ratio for the 116.6 keV transition slightly smaller than it is for the 124.0 keV transition. Since both the 116.6 keV and 124.0 keV transitions are believed to be pure E2, normalization of the $(L_1 + L_2)$ -peaks of the 124.0 keV transition to that of the 116.6 keV transition provides an estimate of the number of conversion electrons belonging to the 166 keV K-conversion photo-peak. The second of these positions is associated with a 177 keV K-line reported previously. From the absence of a K-conversion peak at this position, one would deduce that the intensity of the 177 keV transition reported by Cranston et al (1958) is somewhat less than their figure of 0.2%.

Figure 22 shows two weak K-lines, with an insert showing a very weak photo-peak at $B_p = 963$ gauss-cm. This low energy line is attributed to the L-conversion of a 86 keV transition, although the K-line was not observed. It is possible that the K-line was missed because the photomultiplier noise background was fairly high for electrons at 26 keV. This is believed to correspond to the previously reported 87 keV transition.

Figures 23 and 24 show the conversion lines of the 277-, 295.6-, and 308.2 keV transitions. The K-conversion peaks associated with the 277 keV transition are prominent both in external conversion in gold and uranium and in internal conversion. Despite this fact, this transition has not been previously reported. However, Hatch and Boehm

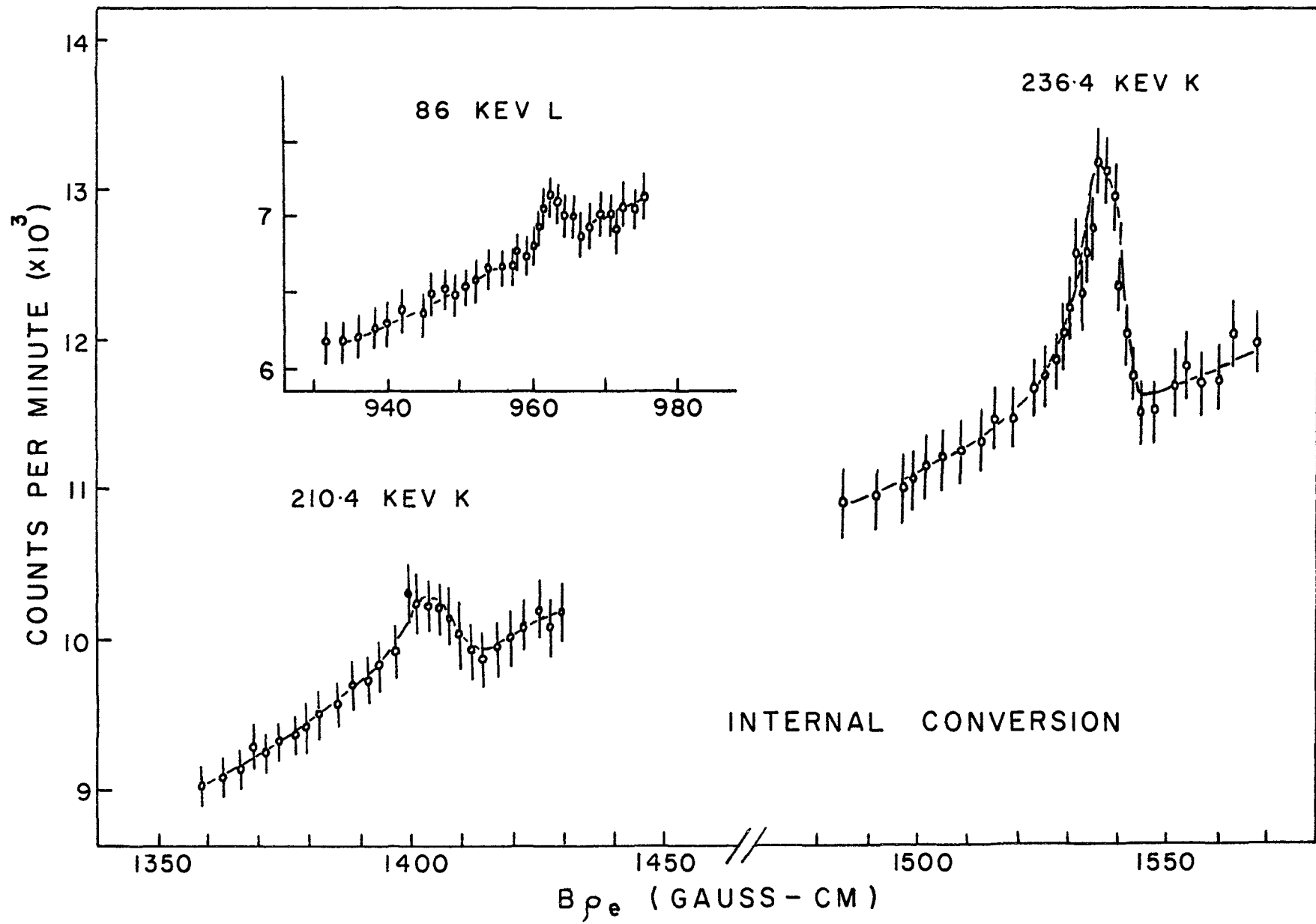


FIGURE 22

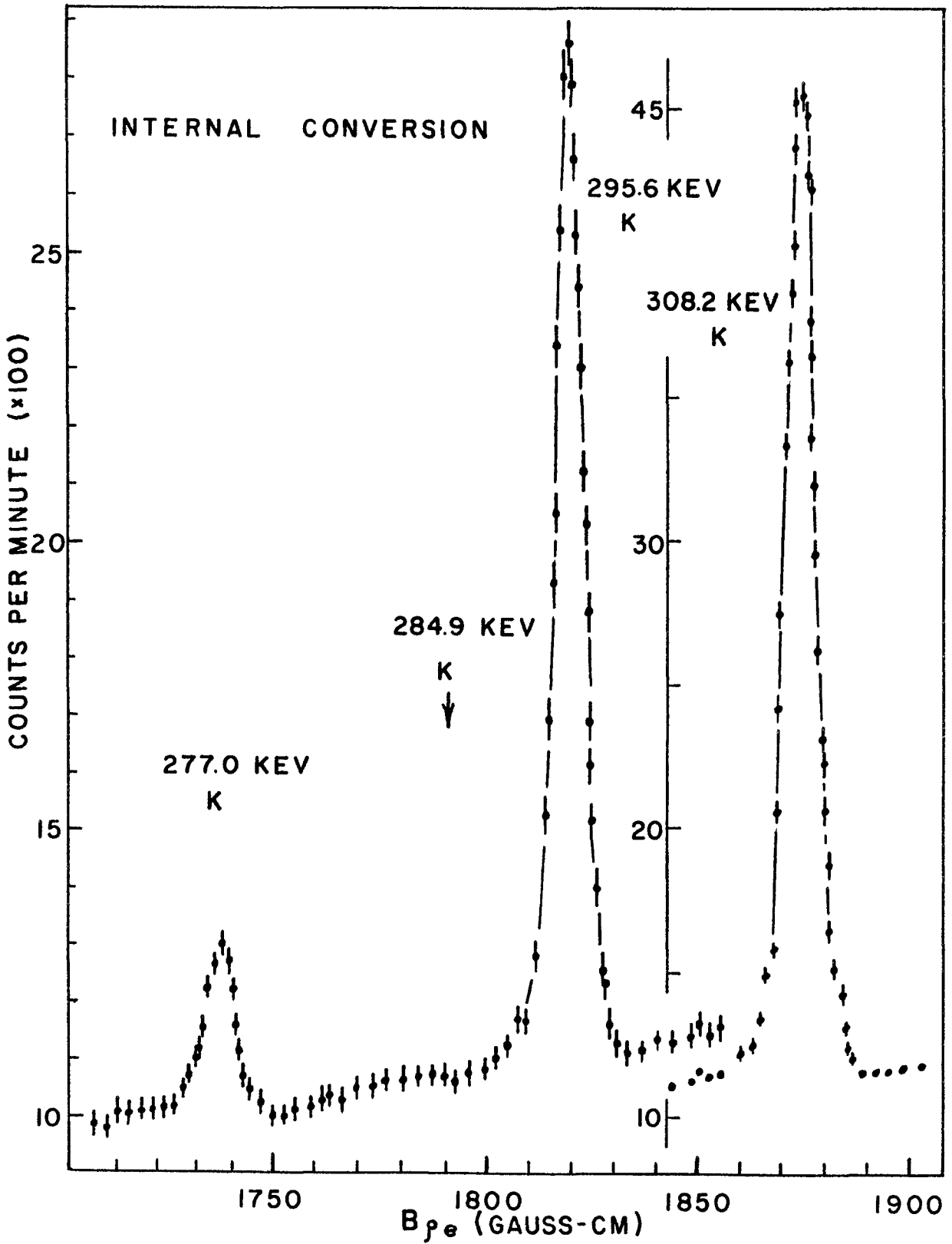
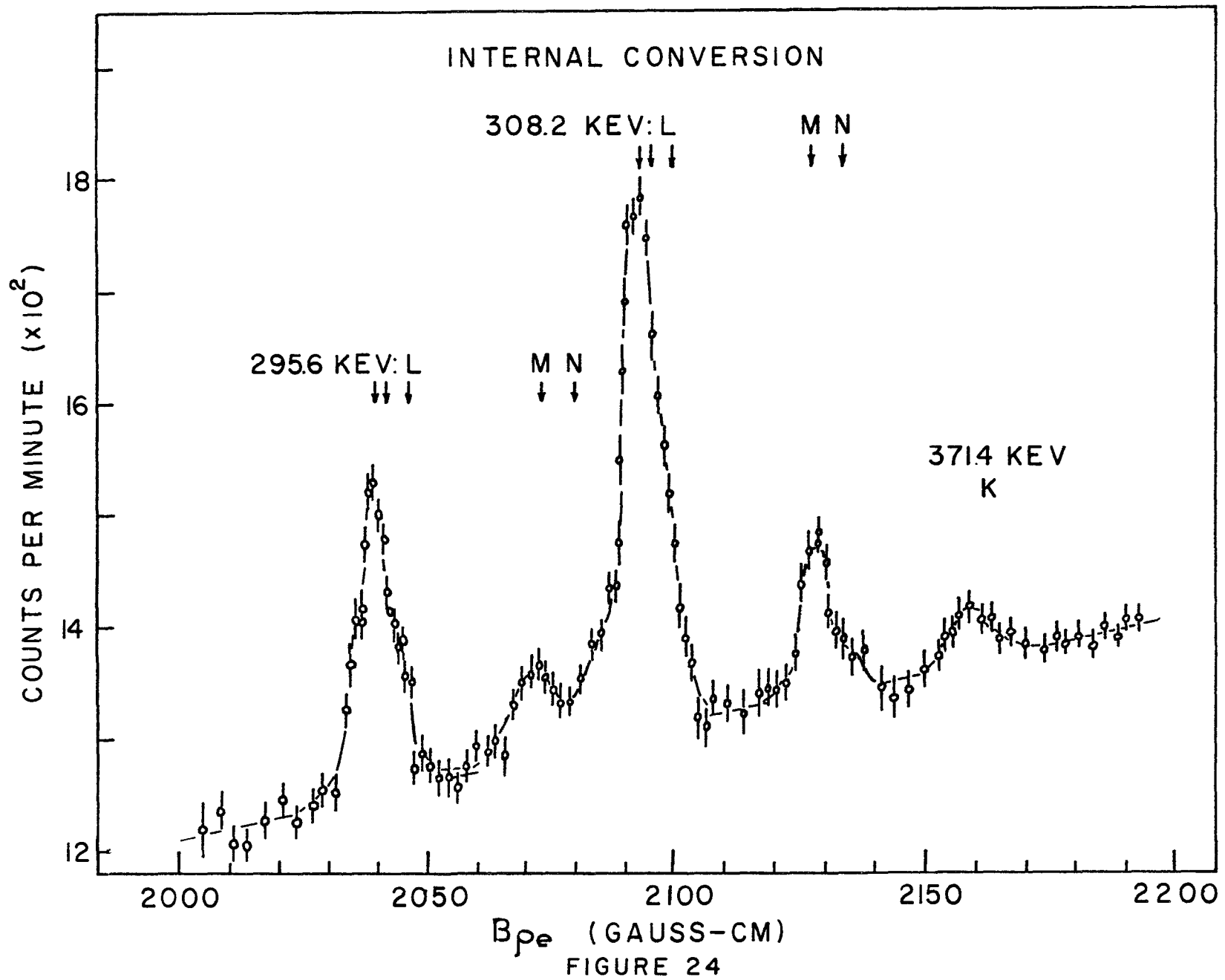


FIGURE 23



present a curved-crystal spectrometer measurement of the energy of a gamma-ray of 284.9 kev. The position of the K-peak of such a transition is shown on Figure 23. In spite of the fact that the sensitivity of the present method is much greater than theirs, no evidence for this transition has been found in either the internal or the external conversion spectra and it is believed that their original measurement is in error. Since Cranston et al. seem to have accepted the energy measurements of Hatch and Boehm as standards, it is likely that they have simply propagated the original error. Figure 24 presents the L- and M-lines associated with the 296- and 308 kev transitions and the K-peak of a 371.4 kev transition. The L-peaks associated with the latter radiation were observed but are not presented in the figure. Although the L-lines of the 277 kev transition were too weak to be observed, it is possible to set a lower limit on the K/L ratio for this radiation.

The data concerning the conversion electrons is summarized in Table IV. The conversion probabilities are relative to a value of 106×10^{-4} conversion electrons per disintegration for the K-conversion of the 308 kev transition. This measurement was obtained in the manner to be described in the following section.

(iv) The Beta Spectrum

The beta spectra of two different sources were measured and subjected to Fermi analysis. For each source, the number of electrons in the K-conversion peak of the 308 kev transition was carefully measured. Figure 25 presents the analysis of one of the spectra, while

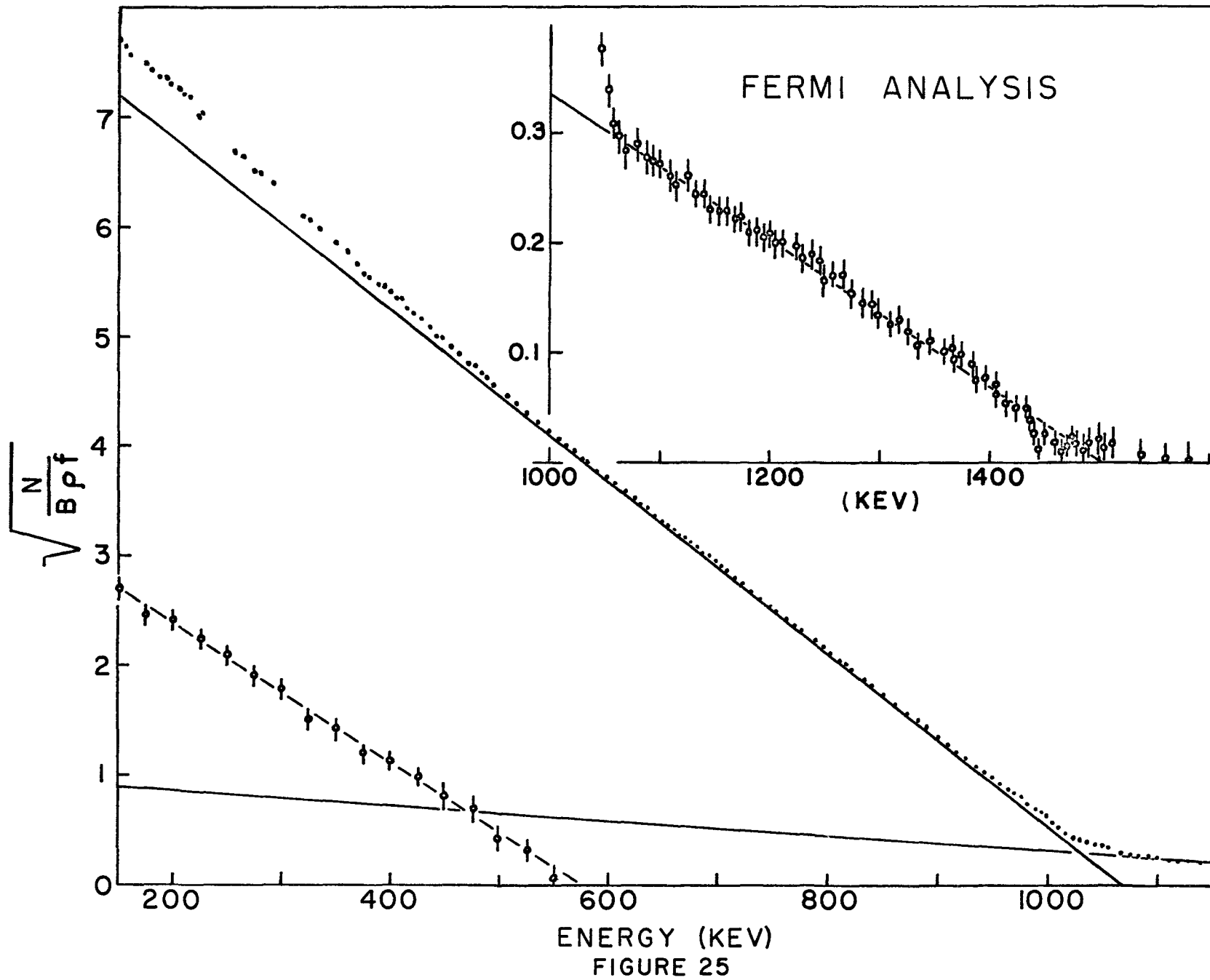


Table II presents the results of the analysis of these sources.

The 1500 kev group is believed, from the decay scheme, to be a composite of two spectra. In fact, in Source 2 it was possible to analyze the high energy group as two components, one with an endpoint of 1500 kev and an intensity of 1.4%, and the other with an endpoint of 1380 kev and an intensity of 0.7%. However, since both groups are very weak and not far separated in endpoints, the analysis is too subjective to be meaningful. If one accepts this group as simple, there is no difficulty in obtaining its intensity, except for the problem of obtaining sufficiently good statistics, since it is clear of interference from the strong 1065 kev group over a range of 450 kev.

The 1065 kev group is so strong that its intensity and endpoint are practically independent of the intensity of the high energy group, and so its endpoint has been chosen to define the energy available in the decay of Er^{171} . The disintegration energy of 1490 ± 2 kev has been determined by adding to the energy of this transition the 425 kev of energy due to cascading gamma-rays. This value is in good agreement with the one obtained in the Fermi analysis for the high energy beta group. The intensity of the 1065 kev beta group is only slightly sensitive to the fashion in which the Fermi analysis is made and can be made to vary by about 5% without doing violence to the data. This is not true for the beta group with endpoint at 575 kev. Not only is this group a composite of several weak beta groups, but its intensity and endpoint can be changed drastically by a small adjustment in the intensity of the 1065 kev group. The endpoint shown in Table II for

TABLE II

The Endpoints and Intensities of Beta Groups.

	Endpoint (kev)	Intensity (%)
1500 kev spectrum:	Source 1	1495 \pm 10
	Source 2	1490 \pm 10
	Mean Value	1492 \pm 7
1000 kev spectrum:	Source 1	1065 \pm 3
	Source 2	1065 \pm 3
	Mean Value	1065 \pm 2
Intensity from gamma-ray scale		92.5
575 kev spectrum:	Source 1	575*
	Source 2	575*
Disintegration energy 1065 + 425		1490 \pm 2
K-conversion probability of the 308 kev transition:		
	Source 1	1.01 \pm 0.06
	Source 2	1.11 \pm 0.06
	Mean Value	1.06 \pm 0.04

* Endpoint assigned from the decay scheme.

this group was arbitrarily chosen to agree with the endpoint of the strongest low energy beta group expected from the decay scheme. The measured intensity of this group (Table II) is about 30% greater than that predicted from the intensities of the gamma-rays presented in Table IV. Table II also includes the intensity of the 1065 keV group as derived from the transition intensities. In view of the limitations of the Fermi method of analysis, the beta intensities derived from the calculated transition intensities are regarded as more reliable and will, therefore, be used on the decay scheme. The only directly-measured beta group intensity is the 2.3% value for the high-energy group.

(v) The Direct Measurement of α_K of the 296- and 308 keV Transitions

In order to relate the beta- and gamma-ray intensity scales, the K-conversion coefficients of the 296- and 308 keV transitions were measured as described in Section 3.A(ii). Figure 26 shows the internal and external conversion lines obtained with both gold and erbium sources for one of the independent determinations made of these coefficients.

The results of these measurements and the values of α_K for the 308 keV transition obtained from the analysis of the beta spectrum are presented in Table III.

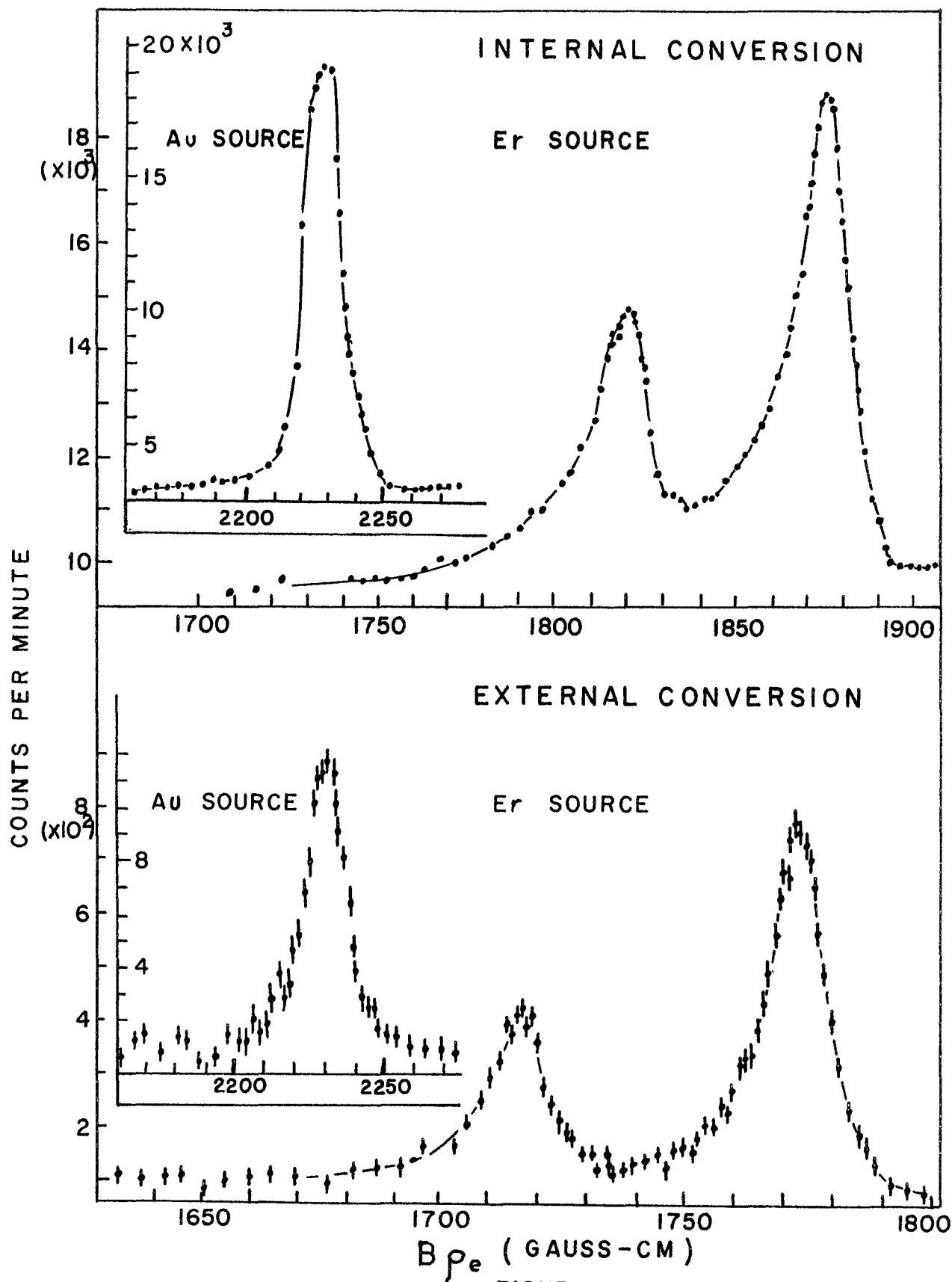


FIGURE 26

Table III
 α_K for the 296- and 308 kev Transitions

Method	296-kev Transition	308-kev Transition
Direct Method		
External Conversion in Au:	0.0199 0.0220	0.0172 0.0190
External Conversion in U:	0.0182	0.0150
Beta Spectrum Measurement		
Source No.1		0.0157
Source No.2		0.0174
Mean Value	0.0200 \pm 0.0011	0.0169 \pm 0.0008

The value of $\alpha_K = 0.0169$ for the 308 kev transition was now used to calculate the number of the 308 kev gamma-rays per disintegration from the number of K-conversion electrons per disintegration. The latter number was found from the beta spectrum, as described in Section (iv).

(vi) Summary of the Experimental Data

All the information obtained about the transitions in this decay is summarized in Tables IV and V. The former presents all the data obtained for the low energy transitions, while the latter presents the data dealing with the high energy transitions. For the high energy gamma-rays only energies and intensities were measured.

TABLE IV

Internal Conversion and Gamma-ray Data for the Low Energy Transitions

Energy keV	Gamma-ray Intensity $\times 10^2$	Conversion Electron Intensity $\times 10^4$			Conversion Coefficients and Ratios			Transition Intensity $\times 10^2$	Multi- polarity
		NK	NL	N_{M+N}	α_K	α_L	K/L		
86	-	-	0.9 ± 0.3	-	-	-	-	~ 0.1	
111.7 ± 0.1	33.8^*	2090 ± 80	502 ± 45	140 ± 10	0.62	0.15	4.2	51.1	M1
116.6 ± 0.2	2.7^*	86 ± 6	124 ± 15	-	0.23	0.33	0.69	4.8	E2
124.0 ± 0.2	19.8^*	368 ± 26	483 ± 42	128 ± 10	0.19	0.24	0.76	29.6	E2
166.4 ± 0.3	0.56 ± 0.13	8 ± 4	-	-	0.14	-	-	0.64	E2 E1+M2
210.4 ± 0.3	0.63 ± 0.06	3.6 ± 0.7	-	-	0.57	-	-	0.67	E1+M2
236.4 ± 0.7	0.51 ± 0.13	5.7 ± 0.2	-	-	0.11	-	-	0.57	E2+M1
277.0 ± 0.2	0.65 ± 0.05	9.0 ± 1.0	< 1.5	-	0.14	< 0.02	> 6	0.74	M1 E1+M2
295.6 ± 0.1	28.0 ± 0.6	56 ± 2	7.1 ± 0.5	1.9 ± 0.2	0.020	0.0025	7.9	28.7	E1
308.2 ± 0.1	63.1 ± 3.6	106 ± 4	14.4 ± 0.7	3.3 ± 0.7	0.0169	0.0023	7.4	64.4	E1
371.2 ± 0.4	~ 0.4	2 ± 1	1.0 ± 0.5	0.6 ± 0.3	0.05	0.02	2	~ 0.4	E3 ?

*calculated from decay scheme

TABLE V
High Energy Gamma-Rays

Energy (kev)	Intensity (%)	Energy Level De-excited	Possible Spin Assignment
404.0±0.8	.03±.013		
418.9±0.4	.09±.013		
543.7±1.0 557.1±1.0	0.04±0.02 0.08±0.02] H	≤ 3/2
572.7±0.5	0.07±0.02		
606.1±1.0 618.7±1.0	0.10±0.01 0.12±0.02] I	≤ 5/2
670.3±0.5 675.3±0.5	0.30±0.06 0.39±0.06] H	≤ 3/2
732.1±0.5 738.6±0.5	0.18±0.06 0.06±0.03] I	≥ 5/2
783.5±0.5 796.2±0.6	0.31±0.03 0.80±0.04] J	≤ 5/2
842 ± 2	0.04±0.02		
869 ± 2 882 ± 2	0.06±0.01 0.07±0.01] L	5/2 or 7/2
906 ± 1 910.5±1.0	0.88±0.13 0.25±0.06] J	> 3/2
962 ± 2	0.11±0.05		

In Table IV the first column gives the energies of the transitions as measured in this study. The errors quoted are the standard deviations of a mean determined from at least five independent peak measurements. The next column gives gamma-ray intensities, partly obtained from external conversion data and partly calculated from other information. The uncertainties shown on these intensities represent the experimental uncertainties in the relative measurements, and do not allow for any systematic error due to a possible error in the normalization factor (α_K for the 308 keV transition), or for the possible error in the measurement of the absolute number of 308 K-conversion electrons. The intensities of the 111.7-, 116.6- and 124.0 keV transitions were calculated from the decay scheme and will be discussed later.

The intensity of the 371.2 keV transition can hardly rate as a measurement since the K-line was masked in both gold (by the 296 keV M-conversion lines), and in uranium (by the 277 keV L-conversion lines). The value quoted in the table was obtained by estimating the height of the L-peak of the 277 keV radiation from the corresponding K-peak and subtracting this estimate from the composite "371-K + 277-L" peak in uranium.

The next three columns give the internal conversion intensities. Again, the error denotes the uncertainty in the actual relative measurement. In this case the scale was defined by the direct measurement of the 308 keV K-conversion probability. As previously pointed out, the 116.6 L-lines are superimposed on the 166.4 K-conversion line and so the uncertainty in the intensity measurement for the latter

is very large. Although the 277 keV L-lines were not observed, an upper limit could be established for their intensity. The gamma-ray and internal conversion intensities were added to give the transition intensity found in the next column. Columns 7, 8, and 9 present the conversion coefficients derived from the gamma-ray and internal conversion probabilities. It should be noted that, although the value of α_K quoted for the 296-keV transition in this table has been calculated in the same manner as all the other conversion coefficients in this table, the value presented is in very good agreement with the directly measured value (see Table IV).

The last column gives the probable multipolarity for each transition, based on the conversion coefficients and ratios presented in this table. For comparison, Table VI lists the theoretical coefficients for E1, E2, E3, M1 and M2 multipolarities corresponding to all the experimentally-derived quantities, together with the experimental value. In the case of the three low energy transitions of energies 111.7-, 116.6-, and 124.0 keV, the multipolarities have been assigned from the relative L-conversion-line intensities. The theoretical values for the ratios of $L_1:L_2:L_3$ at this energy ($k = 0.23 \text{ m}_0 c^2$) are as follows: E1 - 4.3:1:1.2; E2 - 1:5.3:4.8; E3 - 1:29:23; M1 - 80:7.1:1; M2 - 8.2:1:1.5. An inspection of Figure 21 shows that the 111.7 keV transition must be predominantly M1, while the other two are very similar and predominantly E2. A pure E2 assignment is required by the decay scheme. However, both K- and L-shell conversion coefficients are much lower than those predicted by theory. This matter will be discussed later.

TABLE VI
Theoretical and Experimental Conversion
Coefficients and Ratios

Gamma-Ray	Theoretical Values					Experimental Values	
	E1	E2	E3	M1	M2		
111.7	α_K :	0.207	0.72	2.40	1.90	14.2	0.62
	α_L :	0.034	0.97	24.0	<u>0.295</u>	4.0	0.15
	K/L:	6.09	0.804	0.100	<u>6.44</u>	3.55	4.2
116.6	α_K :	0.185	0.69	2.18	1.67	12.1	0.23
	α_L :	0.030	<u>0.78</u>	18.8	0.258	3.32	0.33
	K/L:	6.17	<u>0.89</u>	0.116	6.47	3.64	0.69
124.0	α_K :	0.158	0.59	1.95	1.42	10.0	0.19
	α_L :	0.0256	<u>0.605</u>	13.5	0.220	2.70	0.24
	K/L:	6.16	<u>0.976</u>	0.145	6.45	3.70	0.76
166.4	α_K :	<u>0.073</u> *	<u>0.262</u>	0.91	0.625	<u>3.50</u> *	0.14
210.4	α_K :	<u>0.040</u> *	0.137	0.45	0.32	<u>1.67</u> *	0.57
236.4	α_K :	<u>0.029</u> *	<u>0.100</u>	0.31	0.23	<u>1.05</u> *	0.11
277.0	α_K :	<u>0.020</u> *	0.065	0.193	<u>0.153</u>	<u>0.63</u> *	0.14
	K/L:	<u>7.0</u>	3.1	1.1	<u>7.3</u>	<u>5.0</u>	> 6
295.6	α_K :	<u>0.0167</u>	0.510	0.155	0.127	0.50	0.0200
	α_L :	<u>0.0025</u>	0.0167	0.130	0.0195	0.099	0.0025
	K/L:	<u>6.68</u>	3.05	1.19	6.52	5.05	7.9
308.2	α_K :	<u>0.0152</u>	0.0484	0.141	0.115	0.45	0.0168
	α_L :	<u>0.00217</u>	0.0147	0.109	0.0175	0.087	0.0023
	K/L:	<u>7.00</u>	3.28	1.29	6.57	5.17	7.4
371.	α_K :	0.0104	0.032	0.090	0.076	0.27	(0.047)
	α_L :	0.00155	0.0084	0.053	0.0115	0.053	(0.042)
	K/L:	6.71	<u>3.81</u>	<u>1.70</u>	6.6	5.09	1.1

* indicates a multipolarity mixture.

Underlining indicates the most probable multipolarities.

Table V presents the results for gamma-rays of energy greater than 400 kev. The striking feature of this table is the existence of doublets of separation 5 kev and 12 kev. The 12-kev doublets were completely resolved so that the relative intensities of each member of the pair are quite reliable. The 5-kev doublets were only partially resolved and so the relative intensities of these pairs are more insecure. The absolute intensities of these transitions should be quite reliable, since the intensity calibration curves from 300 kev upward were cross-checked many times and agree well with theory (see Appendix I). The energies quoted here represent in all cases the average of at least two measurements, one from external conversion data in gold and the other in uranium. The errors shown on the energy measurements are the standard deviation in the mean, and are probably somewhat optimistic.

Column 3 labels the levels de-excited by these radiations. Since the 5- and 12 kev separations are characteristic of the level separations in the ground state rotational band, the wave functions for each of these levels differ only in the rotational factor. Hence, the relative intensity within each doublet gives some indication as to the spin of the initial state. For example, the members of the 759-732 kev doublet represent transitions from a 738 kev level to a pair of levels of spin $1/2$ and $3/2$ and energies 0 and 5 kev, respectively. The fact that the low energy component is more intense than the high energy one suggests that the 738 kev level has a spin of $5/2$ or greater. This argument leads to the spin choices given in column 4. These cannot be given too much weight, but may provide some help in defining the decay scheme.

(B) Discussion of the Energy Levels in Thulium-171

(i) The Decay Scheme

The decay scheme based on the energy and intensity measurements and the multipole assignments of this work is shown on Figure 27. Although this decay scheme is quite similar to the one proposed by Cranston et al. (Figure 13), it will be found more instructive to present first the derivation of the present level scheme and then compare it with theirs.

All of the 30 gamma-rays observed fitted into 12 states. The energy fit is in all cases better than twice the standard deviation quoted on the energy measurements. The 12 energy levels are denoted by the letters A to L on the decay scheme and will be referred to by these letters. The levels A, B, C, and D form a ground state rotational band which is well documented by previous workers (Johansson (1957), Hatch and Boehm (1957), Cranston et al. (1958)) and will be accepted without any further justification. Similarly, the existence of a 2.6 micro-second meta-stable level at 425.1 keV (level E) is well established and needs no further consideration.

As previously noted, a number of doublets of either 5 or 12 keV spacing was observed in the external conversion spectrum. These are obviously transitions between energy levels above level E and the various levels of the ground state rotational band. On the basis of these doublets, five levels can be established (H, I, J, K, and L), all but one (level L) supported by four gamma-rays. Level L is only established through a doublet to levels C and D. Although level K is de-excited by two very weak transitions for which the doublet structure was not certain,

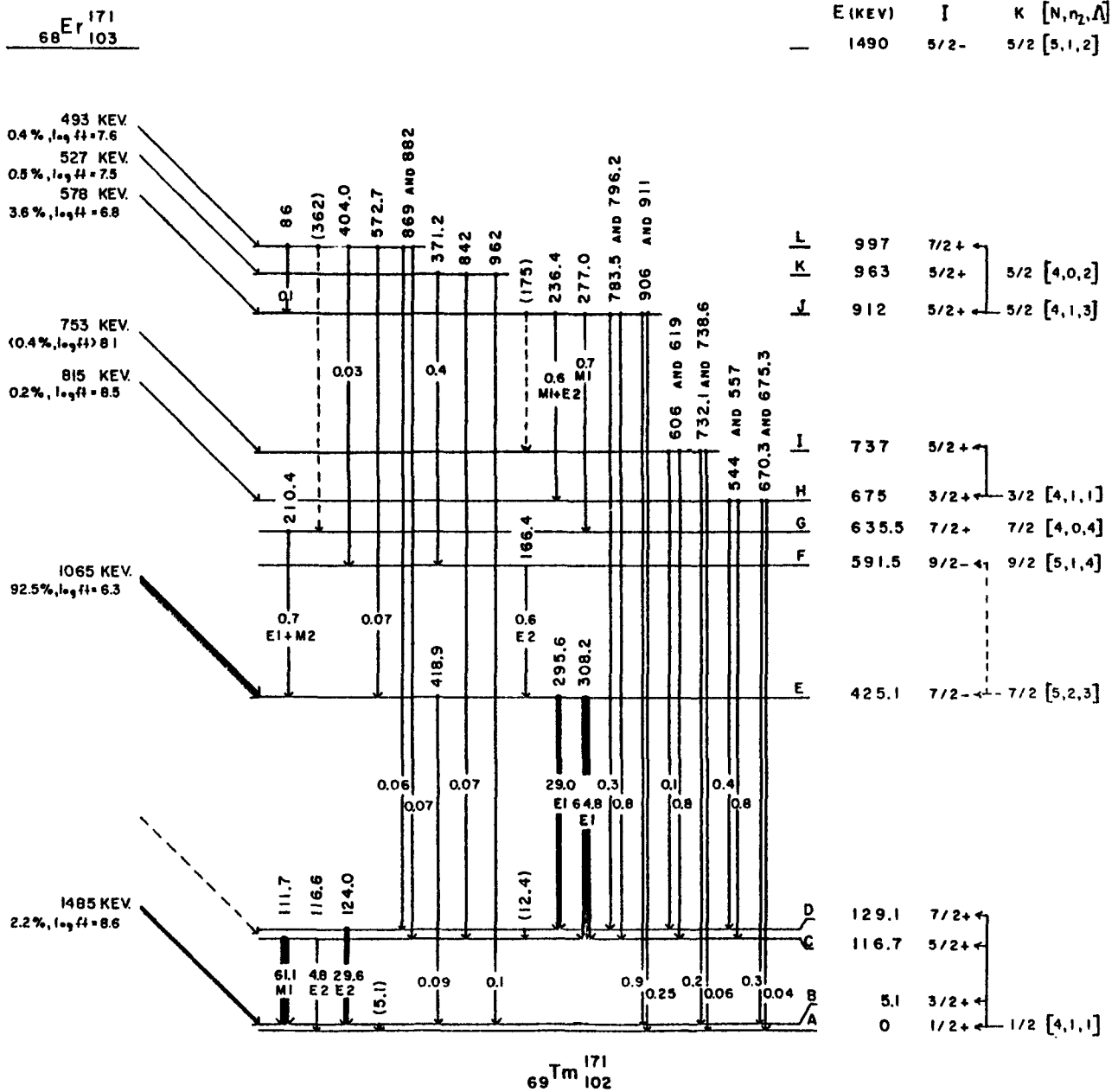


Figure 27

the energy difference of the two gamma-rays 962-842 keV, indicates that they are probably transitions to the ground state rotational band.

The remaining two levels, F and G, can be established by the energy fit. Level F is based on two cascading gamma-ray pairs. In the first place the 166.4 keV and the 371.2 keV transitions add to 537.6 keV which is equal to the energy difference between levels E and K (538 keV). In the second place, the 166.4 keV and 404 keV transitions sum to 570 keV, which is in reasonably good agreement with the energy difference between levels E and L (572). This establishes level F at 166.4 keV above level E. Level G is established by the 210-277 keV sequence. The sum of these energies is equal to the energy difference of 487 keV between the levels J and E. The position of this level is further confirmed by the coincidence work of Cranston et al. to be discussed below.

(ii) Coincidence Experiments of Cranston et al. as applied to the Present Decay Scheme

Since Cranston et al. had already carried out an exhaustive coincidence study, it was felt that further gamma-gamma coincidence experiments would be rather superfluous. This decay scheme is thus subject to the test of the coincidence results of Cranston et al. Since their published results are amply documented by graphs, it was possible to re-interpret, where necessary, their results in the light of the better energy and intensity measurements of this work. In general, the present decay scheme agrees with the results and interpretations of these workers (i.e., the position of the 12 keV doublets, the transitions below level F, and the position of the 236.4- and 86 keV

transitions). However, there is one coincidence experiment for which the present decay scheme demands a different interpretation.

The 210.4 keV transition was found to be in coincidence with gamma-rays of 285- and 372 keV. As stated in Section (iii) above, it is believed that the gamma-ray labelled 285 is really the 277 keV gamma-ray found in this study. If so, it would fit between levels G and J, as suggested by Cranston, since the present measurements require that the energy of the latter level be 912 keV rather than 921 keV, as given by them. The 372 keV gamma-ray, however, no longer fits between the levels suggested by Cranston (G and L), since level L has been lowered by 11 keV, and thus it must be relocated. An observation of the evidence for the 210-372 keV coincidences (Figure 5 and Table III of Cranston et al.) shows that the 372 keV transition is one sixth of the intensity of the 277 keV (alias 285 keV) transition. The 371.2 keV transition observed in this work, however, is about half as intense as the 277.0 keV transition. Moreover, if these authors used the energy of the 285 keV gamma-ray as standard, their energy measurement of 372 keV could be too high. In fact, if one uses the 113- and 210 keV peaks for energy calibration on the above-mentioned figure, the two coincidence peaks appear at ~ 277 keV and ~ 362 keV. It is therefore believed that the "372 keV" gamma-ray observed by Cranston et al. is really a 362 keV transition between levels G and L which is too weak to be observed in the high resolution spectrometer. The 371.2 keV gamma-ray is then a new transition not previously observed.

Three more of their coincidence experiments should be mentioned.

(1) The coincidence peak at 177 keV observed when gating in the interval 650-750 keV is probably caused by a weak 175 keV gamma-ray between levels J and I which was not observed in this work. (2) In the beta-gamma coincidence experiments, the peak attributed to the 177 keV transition may have been mainly due to the 166.4 keV transition observed in this work, since the 166.4 keV transition is at least five times as strong as the 177 keV gamma-ray. This error in assignment could again be due to the wrong energy assigned to the 277.0 keV gamma-ray. (3) Three gamma-rays are reported to be in delayed coincidence with the 308 keV gamma-ray: 210 keV, 285 keV (277 keV), and 372 keV. No delayed coincidences with either the 166 keV or 177 keV radiations are reported. However, it is stated that the coincidence counting rates were very low, so it is possible that the predicted coincidences were missed. A graphical presentation of this experiment is not shown in their publication.

It is clear from the above discussion that the coincidence experiments of Cranston et al. provide detailed confirmation of the level scheme as proposed in this work. The present levels GHIJ and L are identified with levels F-J in their decay scheme. For levels H, I, J, L, the experiments described here yield energy values about 10 keV lower than those obtained by Cranston et al. Levels F and K are necessary to explain new data obtained in the present work.

(iii) Beta- and Gamma-ray Intensities

A comparison of the intensities quoted in Table IV and those on the decay scheme in Figure 27 will reveal a slight difference. As explained previously, the intensities in Table IV were calculated from direct measurements of the number of the 308 K-conversion electrons per disintegration, and of the 308 kev K-conversion coefficient. Since the combined uncertainty in these two measurements amounts to $\sim 8\%$, it was felt that a slight renormalization based on the measured ground state beta-group intensity and the decay scheme would improve the accuracy of the transition intensities. Fortunately, the normalization required was very small, only 0.8%. According to these normalized values, the 1490 kev beta group (or the composite of the beta groups feeding the $3/2$, $5/2$ and $7/2$ levels of the ground state rotational band) has the value of 2.3% as obtained from the analysis of the beta spectrum (Section A(iv)), leaving 97.7% for the sum of the intensities of the other beta groups. The relative intensities of the lower energy beta groups were calculated from the gamma-ray intensity balance.

The gamma-ray intensities were calculated and normalized as discussed above, except for the 111.7-, 116.6- and 124.0 kev transitions. Since the gamma-ray intensity calibration curves were not reliable for gamma-ray energies below 200 kev, the intensities of these gamma-rays could not be calculated by the usual method. Instead, the decay scheme and the intensities of the other transitions were used to determine the number of gamma-rays necessary to provide an intensity balance for levels C and D. This determination was then used to predict the behaviour of the semi-

empirical intensity calibration curves at low energies (Appendix I).

(iv) The Internal Conversion Coefficients

From the decay scheme it is clear that the 111.7 keV transition must be either M1 or E2 or both. From the $L_1:L_2:L_3$ ratio it was found to be predominantly M1 in character. In the same way the 116.6- and 124.0 keV transitions have to be pure E2 in character. A comparison of the experimental values of α_K for these transitions with the corresponding theoretical ones will show that the experimental values are too low, with a discrepancy which is decreasing with increasing energy. This discrepancy cannot be explained. Obviously, it can arise from only two causes: (1) The number of K-conversion electrons detected here is less than 100 %, or (2) the theoretically-calculated conversion coefficients at these energies are not reliable. Although the second of these causes is the more attractive one from the experimental point of view, the possible causes of such an effect will not be explored, since it presents a difficult theoretical problem. In view of the fact that other workers have found anomalous conversion coefficients, such an explanation for this discrepancy may exist. On the other hand, an explanation based on the first of these causes, that of the loss of a fraction of the K-conversion electrons, also seems rather unlikely. It is difficult to see by what process the electrons would be lost from the electron beam other than by scattering from the detector crystal. In this case, however, the scattering must be a predominantly low energy effect and the energy

lost by the electrons to the detector crystal must be a very small fraction of their kinetic energy, since electrons with energies > 25 keV could be detected by raising the anode voltage of the photomultiplier. Since no increase in the counting rate on the 112 keV K-conversion peak was observed when the anode voltage on the photomultiplier was increased to make the detector sensitive to 25 keV electrons (a plateau of ~ 100 volts in length), the electrons not detected must have escaped with more than half of their kinetic energy. Intuitively, one feels that electrons must be being missed in the K-conversion detection process but at the moment the author cannot give an explanation. However, nothing in the decay scheme hinges on this matter.

The conversion coefficients measured for the 296.6 keV and the 308.2 keV transitions were found to be somewhat higher than expected from the theoretical values (Table VI) for pure transitions. This could be interpreted as an admixture of M2 multipolarity. However, it has been found that in the case of dipole transitions the deformed nuclei sometimes exhibit anomalous conversion coefficients, especially in the cases of retarded transitions (Asaro et al. (1960) and Nilsson and Rasmussen (1958)). However, in the light of the good agreement between the experimental and theoretical values for the L-conversion coefficients, it seems likely that these transitions are pure E1 with slightly anomalous K-conversion coefficients. Cranston et al. interpret the 308 keV transition as pure E1, and the 296 keV transition as an E1-M2 admixture. However, their conversion coefficient measurement of the 296 keV transition is based on the 308-296 keV relative intensity

measurement by Hatch and Boehm, which is in sharp disagreement with the relative intensity measured in the present work.

(v) Description of the energy levels in the Thulium-171 nucleus

As stated above, the first five levels in this nucleus are quite well established. Built on the ground state with the spin and parity of $1/2+$ is found a characteristic rotational band. From the energies of these levels and using Equation 2.5 with the correction term 2.6, Hatch and Boehm have calculated the following nuclear parameters: $a = -0.8563$, $\hbar^2/2\mathcal{J} = 11.631$ kev, $\Delta E_{(\text{vib})} = 0.02965 (2\mathcal{J}/\hbar^2)^2 \times (E_{(\text{rot})})^2$ kev. (The notation is defined in Chapter 2.) The fifth level in this sequence, $9/2+$, expected to occur at 343.9 kev, was proposed by Hatch and Boehm to accommodate the 210 kev transition (339 kev- 129 kev). However, this assignment for the 210 kev gamma-ray was rejected by Cranston et al. on the basis of their coincidence experiments. There is no doubt that such a level exists, but it is unlikely that it will be fed in this decay. The ground state of Tm^{171} is described by the notation of the Unified Model (defined in Section B.C.(ii)) as follows: $1/2+$, $1/2 [4,1,1]$. Level E, which has also been described by earlier workers, is a $7/2-$ level, at 425.1 kev. This is a hole state corresponding to a configuration of $7/2- 7/2 [5,2,3]^1 (1/2+ 1/2 [4,1,1])^2$. The half-life of this state was measured by Cranston et al. to be 2.6 micro-seconds.

A probable description of the remaining energy levels can be obtained using the experimental information about transition intensities

and multipolarities. Combining this information with the available single particle energy levels as obtained from Nilsson's diagram (Figure 28) for 69 protons and a nuclear deformation $\delta=0.28$ (Mottelson (1959)), it is possible to reach a self-consistent description of all the proposed levels. The levels F to L will now be described in turn, following the argument used by Cranston et al.

Considering the probable E2 character of the 166.4 keV gamma-ray and the fact that this is the only gamma-ray de-exciting this level, level F is believed to have negative parity. One such possible description for this level would be the $9/2^-$ member of the rotational band built on the $7/2^-$ level (E). The energy difference of 166.4 keV, however, is somewhat too large for the $7/2^-$ - $9/2^-$ rotational level difference (~ 110 keV), as calculated from the ground state nuclear parameters. Another possible description would be Nilsson's $9/2^-$ level denoted by quantum numbers $9/2^- [5,1,4]$. However, from Nilsson's diagram this $9/2^-$ level should be above a $7/2^+$ level which has been assigned to the next level in the scheme. A comparison with neighbouring nuclei will show that the $7/2^+$ and $9/2^-$ levels cross over at about Lu^{177} (Hatch et al. (1956a)). It seems, therefore, that the assignment of $9/2^-$ rotational level based on the $7/2^-$ hole state is a more attractive one, especially in the light of the E2 character of the 166.4 keV gamma-ray.

Level G is believed to be a $7/2^+$ particle level. It is de-excited to the $7/2^-$ level (E) by means of a $E1 + M2$ transition which would give it a positive parity. And since, according to the Nilsson scheme, the

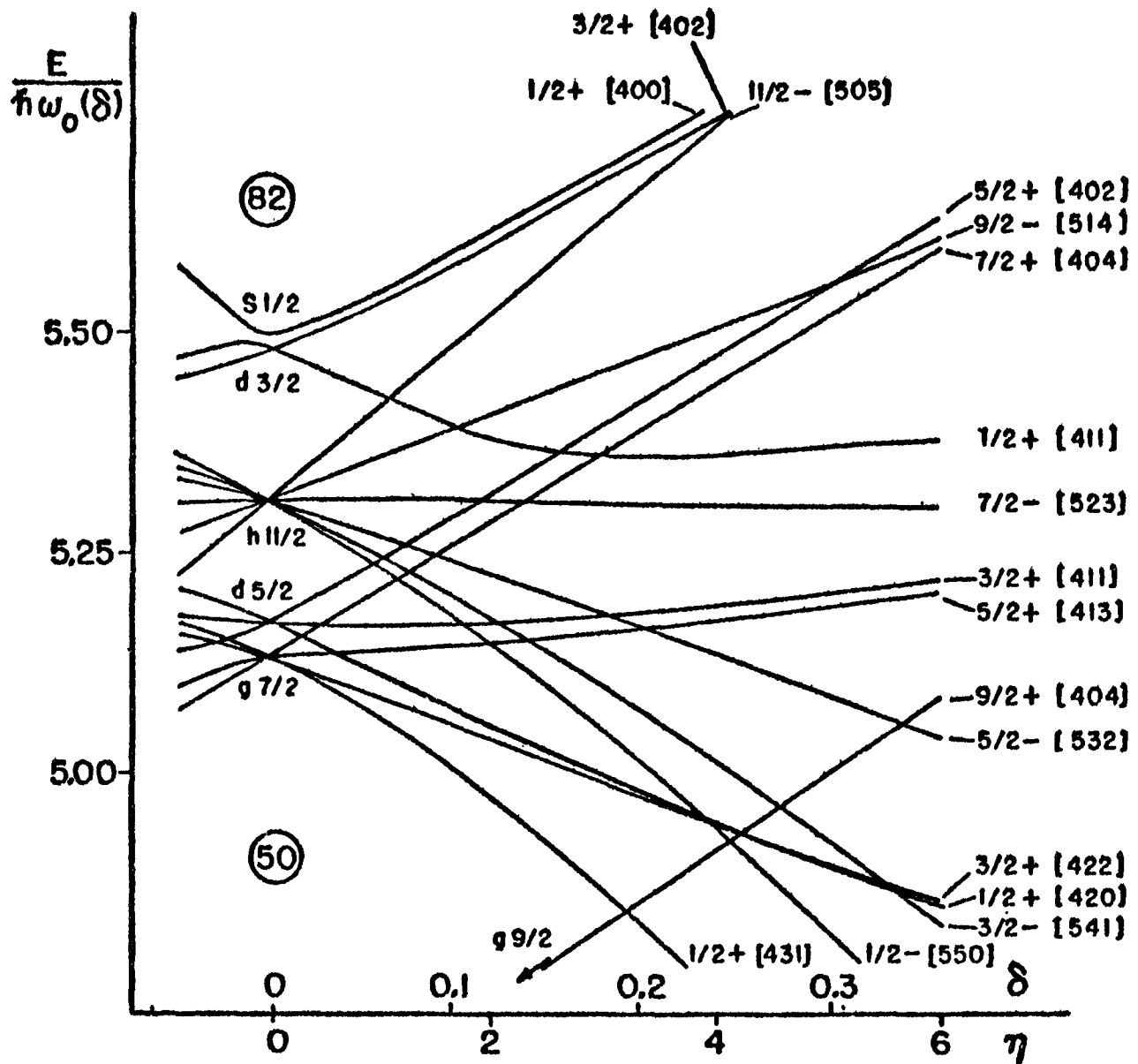


Figure 28.

first particle level above the $1/2+$ ground state is a $7/2+$ $7/2$ $[4,0,4]$ level, this assignment is given to level G. This is in agreement with the interpretation given by Cranston et al.

For the next two levels, H and I, the doublet structure will yield some information about the spins. According to Table V, level H probably has a spin $\leq 3/2$, while level I should have a spin $5/2$. In addition, the energy difference between the two levels ($737 - 675 = 62$ kev) is in good agreement with the energy difference expected between the two members of a rotational band with spins $3/2$ and $5/2$. The assumption is, of course, made here that the nuclear parameters in this rotational band are equal to the parameters in the nuclear ground state. A $3/2+$ hole state is available according to the Nilsson level scheme with quantum numbers $3/2$ $[4,1,1]$. These two levels are therefore described as the first two members of a rotational band based on the $3/2+$ $[4,1,1]$ hole state. This again agrees with the assignment of Cranston et al.

Levels J, K, and L can most conveniently be discussed together. Level J is the only one of the three where the doublet structure gives some indication as to the spin of the level. From Table V a tentative spin of $5/2$ ($\leq 5/2$ and $> 3/2$) can be assigned to this level. In addition, this level is de-excited to levels G, H and (I) with spins $7/2+$, $3/2+$, and $(5/2+)$, respectively. The existence of these transitions, together with the assigned multipolarities, agrees with the spin assignment of $5/2+$ to level J. Level K is believed also to be a +ve parity state with a spin neither very high nor very low. From the possible $E3$ characteristic of the 371.2 kev gamma-ray suggested in

Table IV, a spin of $3/2+$ or $5/2+$ might be suggested for this level. However, since there is no $3/2+$ level available for this region in the Nilsson diagram (i.e., accepting the $3/2+$ $3/2$ $[4,1,1]$ description for level H), but there are two $5/2+$ assignments possible, level K is also probably a $5/2+$ level. We thus have two $5/2+$ levels in this region which could be identified with the Nilsson levels $5/2+$ $5/2$ $[4,0,2]$ and $5/2+$ $5/2$ $[4,1,3]$, the former being a particle and the latter a hole state.

The third level in the triplet, level L, de-excites to a number of levels with spins $5/2+$ (J), $(7/2+$ (G)), $9/2-$ (F), $7/2-$ (E) $7/2+$ (D) and $5/2+$ (C). This indicates a reasonably high spin value for this level. A comparison of the energy level difference in a rotational band in this nucleus (85 kev, based on ground state parameters) with that of the energy difference between levels J and L, indicates that the L level may possibly be a $7/2+$ rotational level based on the $5/2+$ level J. The intensities of these gamma-rays indicate that no particular preference is given to any of these transitions with the possible exception of the 86 kev transition between levels L and J. Since the high energy transitions to the ground state rotational band based on a $K = 1/2$ particle level are about the same intensity as the 572.7 transition to the $7/2-$ hole state of considerably lower energy, one might guess that the level L is a hole level. This would agree with an assignment $5/2$ $[4,1,3]$ for levels J and L. At the same time, based on the same argument that a hole-to-hole transition is more likely than a hole-to-particle transition, the fact that a transition of about

$1/2$ the intensity of the L-E transition is found between levels L and F might suggest that the $9/2^-$ (F) level could be the first rotational level based on the $7/2^-$ hole level. Thus the levels J and L are interpreted as corresponding to the Nilsson level $5/2^+ 5/2 [4,1,3]$ and the first rotational level based on it, respectively, and level K as corresponding to the state $5/2^+ 5/2 [4,0,2]$. This interpretation of level K as a particle level would make it preferable to describe level F as a particle level rather than the $9/2^-$ rotational level of a hole nature. However, since the high energy transitions from the level K to the ground state rotational band are K-forbidden and the 371.2 keV gamma-ray could be an unhindered radiation of multipolarity $M2 + E3$, this may not be such a strong objection. Cranston *et al.* only find two levels here which they interpret as a rotational band based on a mixed level of the two Nilsson $5/2^+$ states. The description given above is in agreement with the multiplicities and intensities of all the gamma-rays with the exception of the relative intensities of the 236.4- and 277.0 keV radiations. The approximately equal intensities of the transitions from a hole level ($5/2 [4,1,4]$) to another hole level ($3/2 [4,1,1]$) and also to one described as a particle level ($7/2 [4,0,4]$) is difficult to explain. However, the transition between levels J-H is a hindered one violating the asymptotic selection rules, while the supposedly less likely transition J-G is an unhindered one.

On the decay scheme on Figure 27 the energy levels are described by the quantum numbers $I \pi K [N, n_z \Lambda]$ based on the conclusions reached

above. For the level F, two descriptions are given, since it is difficult to choose between them. Both the beta- and gamma-ray intensities agree with these descriptions. The beta groups to ground state rotational band members $3/2+$, $5/2+$, and $7/2+$, although first forbidden are, in addition, also forbidden by the K-selection rule (Equation 2.7); hence, the high $\log ft$ value for the 1485 keV beta group. The 1065 keV beta group is an allowed, hindered one, with a $\log ft$ value somewhat larger than expected for an allowed transition. The beta transition to the $9/2-$ level (F) would be a second forbidden one, and therefore it is not surprising that no transition to this level is observed. There is no beta transition either to level G; such a transition, if it exists, would be a first forbidden, hindered one, and a large hindrance factor would explain the very high $\log ft$ value. The transitions to levels H to L are all first forbidden, unhindered ones. The anomalously high $\log ft$ values for the beta transitions to levels H and I could be explained by the hole nature of these levels. The $\log ft$ values for the remaining three beta groups are consistent with values expected for the first forbidden, unhindered transitions, strengthening the arguments for the description of these levels.

In the above discussion the assumption is made that all the levels presented are either single particle levels, or rotational levels based on these. The collective motion levels of a vibrational nature have not been considered. Since no vibrational levels have been identified in odd A nuclei, and since no theoretical work has been done

to calculate the energies of the vibrational levels in these nuclei, no definite assignments can be made at present.

However, one may speculate on the presence of two vibrational levels. Based on the ground state of $K = 1/2$, one may have two γ -vibrations: one with $K = 3/2$ and the other with $K = 5/2$ (corresponding to $|\Omega - K| = 2$, respectively²). Level H may then be interpreted as the $K = 3/2$ γ -vibration based on the groundstate. In a sense this is a very attractive assignment, since levels H and I de-excite entirely to the ground state rotational band. In addition, this might explain the anomalously high $\log ft$ values for the first forbidden beta transitions to this level since Ω has to change from $5/2$ to $1/2$.

The second vibrational level with $K = 5/2$ might also be present and could be contributing to the behaviour of level J. Since there are two $5/2+$ single particle states close to each other ($5/2 [4,0,2]$ and $5/2 [4,1,3]$) plus a possible vibrational level $5/2+ 5/2 [4,1,1]$ ($\Omega = 1/2$), the three levels, J, K and L, might all contain components of each of these states. One might speculate that level J is a mixture of the $5/2+$ particle and of the vibrational state, and that level K is a hole state with slight particle admixture. Level L would still be a rotational level built on level J.

Although the addition of vibrational behaviour to the interpretation of this level scheme has certain advantages, no definite

²Sheline (1960) makes the statement that " $\Omega - K = 2$ ", which is believed to be in error. It should read " $|\Omega - K| = 2$."

assignments can be made at present since no quantitative basis exists for such assignments.

The ground state of Er^{171} is described as $5/2-5/2 [5,1,2]$ Nilsson level. The spin assignment of $5/2$ has recently been confirmed experimentally by Cabezas (1960) using atomic beam methods.

SUMMARY

On the basis of the experiments discussed in this thesis certain conclusions can be drawn about the decay of the neutron-activated erbium isotopes.

Er^{163} decay probably contains transitions not yet found. A further study of this isotope should prove informative. Er^{165} was found to decay by electron capture to the ground state of Ho^{165} .

A complicated energy level scheme has been proposed for the Tm^{171} nucleus. This scheme is interpreted in the light of the Unified Model. To each energy level is assigned a single-particle structure according to the deformed well single-particle model, as proposed by Nilsson. In addition, evidence for rotational and vibrational motion is found and, to a number of energy levels, collective motion properties are assigned.

The decay of Pm^{149} is found to consist of a single gamma-ray and two beta groups. The endpoints and the branching ratio are determined for the beta groups, and the energy, the conversion coefficients and ratios are measured for the 286 keV transition.

In addition, a set of semi-empirical curves for gold and uranium radiators is presented for the calculation of gamma-ray intensities from external conversion peak-height measurements. These curves are believed to be reliable for gamma-ray energies > 200 keV for gold, and > 300 keV for uranium radiators.

It is hoped that the decay scheme of Er^{171} proposed here will contribute to the understanding of the strongly deformed nuclei. It is also hoped that the intensity calibration study discussed in Appendix I will be found useful for measuring gamma-ray intensities with the high resolution beta-ray spectrometer.

APPENDIX I

GAMMA-RAY INTENSITIES FROM EXTERNAL CONVERSION MEASUREMENTS

Introduction

The determination of gamma-ray intensities using the external conversion method has many attractive features. With this method one can study a complex gamma-ray spectrum with a resolution comparable to that obtained in internal conversion. However, the translation of the external conversion peak heights or areas into gamma-ray intensities presents a rather difficult problem, since the behaviour of electrons in traversing matter is complex and difficult to deal with.

There are two approaches to this problem: (1) one can set up a semi-empirical expression for the gamma-ray intensities as a function of the photo-electric peak height. Since the instrumental transmission and the source-radiator geometry are unknown constants, this method can only be used to obtain relative gamma-ray intensities in the same source. This approach was suggested by Deutsch (1944), and is the one previously used in this laboratory (Johns and Nablo (1954), Nablo (1956)); (2) the second approach is that of Hultberg (1959) and is more theoretical. He has calculated the number of photo-electrons created by a gamma-source, taking into consideration the angular distribution of the photo-electrons, the physical size and shape of the source, and the source-radiator geometry. This calculation also depends, of course, on the photo-electron energy and the radiator material and thickness.

During the course of the work described in this thesis it was felt that a re-examination of this problem was warranted. After comparing the advantages and disadvantages of the two methods mentioned above, it was decided to continue using the first method. Although this approach permits one to make only relative measurements, it does not require reproducible source dimensions, or source-radiator geometry, thus allowing the worker to choose these variables to fit the problem at hand. The applicability of Hultberg's method is severely restricted by the fact that any change in these factors will mean a large amount of complicated computer calculation.

In this appendix a theoretical expression for the gamma-ray intensity as a function of the external conversion peak height will be derived and its validity tested with a series of experiments. It should be pointed out here that this investigation was undertaken with the main purpose of providing the experimenter with a set of reliable semi-empirical curves for the existing radiators, after a great deal of the data presented in Chapter 4 had been collected. The radiators tested are, therefore, not especially selected to test the theory and thus do not constitute the best possible set for this purpose.

(A) Theoretical Expressions

When a beam of gamma-rays passes through a thickness t of matter, a certain number of photo-electrons are created. If the thickness, t , is more than a few times the mean free path for electrons, the latter will undergo multiple scattering, and emerge from the stopping material with

almost isotropic distribution and somewhat retarded energy. In external conversion, where the photo-electrons are created throughout the entire volume of the radiator, the electrons will "diffuse" out of the radiator with a spread in their energies. For the sake of convenience, let this spread be given in units of momentum $\Delta B\rho$. Now a magnetic spectrometer will accept at one time a certain momentum band, Δp , that is, it will "see" only electrons having a momentum between p and $p + \Delta p$. Since Δp is a function of p , it is often more convenient to use $Rp \equiv \Delta p$ where R is the instrumental resolution ($R \equiv \Delta p/p$), and is a constant for a particular choice of source-baffle-detector geometry.

If $Rp \gg \Delta B\rho$, then the spectrometer will accept all the photo-electrons at the same time and the peak height of the photo-electric peak will be given by

$$n = kI_{\gamma} \sigma t \quad (\text{A.I.1})$$

where k is a constant of the spectrometer and the source radiator geometry, I_{γ} is the gamma-ray intensity, σ is the photo-electric cross section for the material, and t is the radiator thickness.

In the case where $Rp \ll \Delta B\rho$ the expression is again relatively simple because only a fraction $\Delta p/\Delta B\rho$ of the photo-electrons will be detected at one time. In this case

$$n = KI_{\gamma} \sigma t (Rp/\Delta B\rho) \quad (\text{A.I.2})$$

The above expression can be somewhat simplified. Since the stopping power I of a material can be defined as $I \equiv d(B\rho)/dt$, we can

set $\Delta B\rho = I \cdot t$. It will be convenient to define $C \equiv I\beta^3$ which will give $\Delta B\rho = Ct/\beta^3$. Equation (AI.2) then reduces to

$$n = kI_{\gamma} \left(R\rho\beta^3/C \right) \quad (\text{AI.2a})$$

The general case, however, is intermediate between the two extreme conditions described above. Deutsch has suggested a formula for the general case

$$n = kI_{\gamma} \left[1 + (Ct/R\rho\beta^3)^2 \right]^{-1/2} \quad (\text{AI.3})$$

which reduces to (AI.1) and (AI.2a) in the two limiting cases. This equation can be rewritten in the form

$$I_{\gamma} = K(n/p\beta^3) \left[C^2 + (R\rho\beta^3/t)^2 \right]^{1/2} \quad (\text{AI.4})$$

where $K = 1/kR$ is a constant whose value does not enter into the calculation of the relative gamma-ray intensities.

It is necessary to calculate the value of $C = I\beta^3$. White and Millington (1928) showed that C was approximately constant for $B\rho \gg 1400$ gauss-cm. Deutsch (1944) accepted these results and treated C as a constant in his calculations. This is a valid approximation at higher electron energies and with thin radiators, where the term $(R\rho\beta^3/t)^2 \gg C$, but at lower energies and with thicker radiators the slow variation of C with electron energy and radiator thickness should be considered. In the present work I has been calculated using the Landau formula as given by Chen and Warshaw (1951) who carried out a careful investigation of the stopping power of various materials for electrons. According to these authors the most probable energy loss T_0 by electrons

which have traversed a distance x in the material is

$$T_o = \frac{x}{\beta^2} \ln \frac{2x}{(1 - \beta^2) E_i^2 \exp(\beta^2 - 0.37)} \quad (\text{AI.5})$$

In this expression the energy is in units of $mc^2 = 0.51$ Mev, and distances are measured in units of $(2\pi r_o^2 n)^{-1}$ (r_o = the classical radius of the electron = 2.82×10^{-13} cm; $n = NdZ/A$ is the density of electrons in the stopping material of density d , atomic number Z and atomic weight A ; N is the Avogadro number), E_i is the mean ionization potential of the stopping material. Changing (AI.5) into a more convenient form and units gives

$$C = I\beta^3 = \left(\frac{\Delta B\rho}{t}\right)\beta^3 = 1.18 \frac{Z}{A} \left[\log t + \log \left(\frac{Z}{A}\right) - 2 \log E_i - \log(1 - \beta^2) - 0.434 \beta^2 + 8.35 \right] \quad (\text{AI.6})$$

where E_i is given in e.v. and t in mg/cm^2 .

Since both gold and uranium radiators were used, the material dependent constants in Equation (AI.6) were evaluated for both radiator types. In the case of the gold radiators this is a straightforward calculation, since only gold is present. For uranium radiators the problem is more difficult, since, in addition to uranium, the radiators also contain oxygen and carbon. It is now necessary to evaluate the number of electrons per nucleon ($\sum Z / \sum A$), and the mean ionization potential per atom in the mixed material. In Table A.1 U(rad.) gives the results for a radiator composed of 79% U, 16% O and 5% C by weight. The mean ionization potentials of Bakker and Segré (1951) were used.

TABLE A.I

Average Electron Densities and Mean Ionization Potentials
for Gold and Uranium Radiators

	Au	U	O	C	U(rad.)
Z/A	0.401	0.387	0.500	0.500	0.411
E_i (ev.)	730	881	93	76	238

Using the above values for gold and uranium radiators, the respective C's are given by the following equations:

$$C_{Au} = 0.473 (2.23 + \log t - \log(1 - \beta^2) - 0.434 \beta^2) \quad (AI.7a)$$

$$C_U = 0.485 (3.21 + \log t - \log(1 - \beta^2) - 0.434 \beta^2) \quad (AI.7b)$$

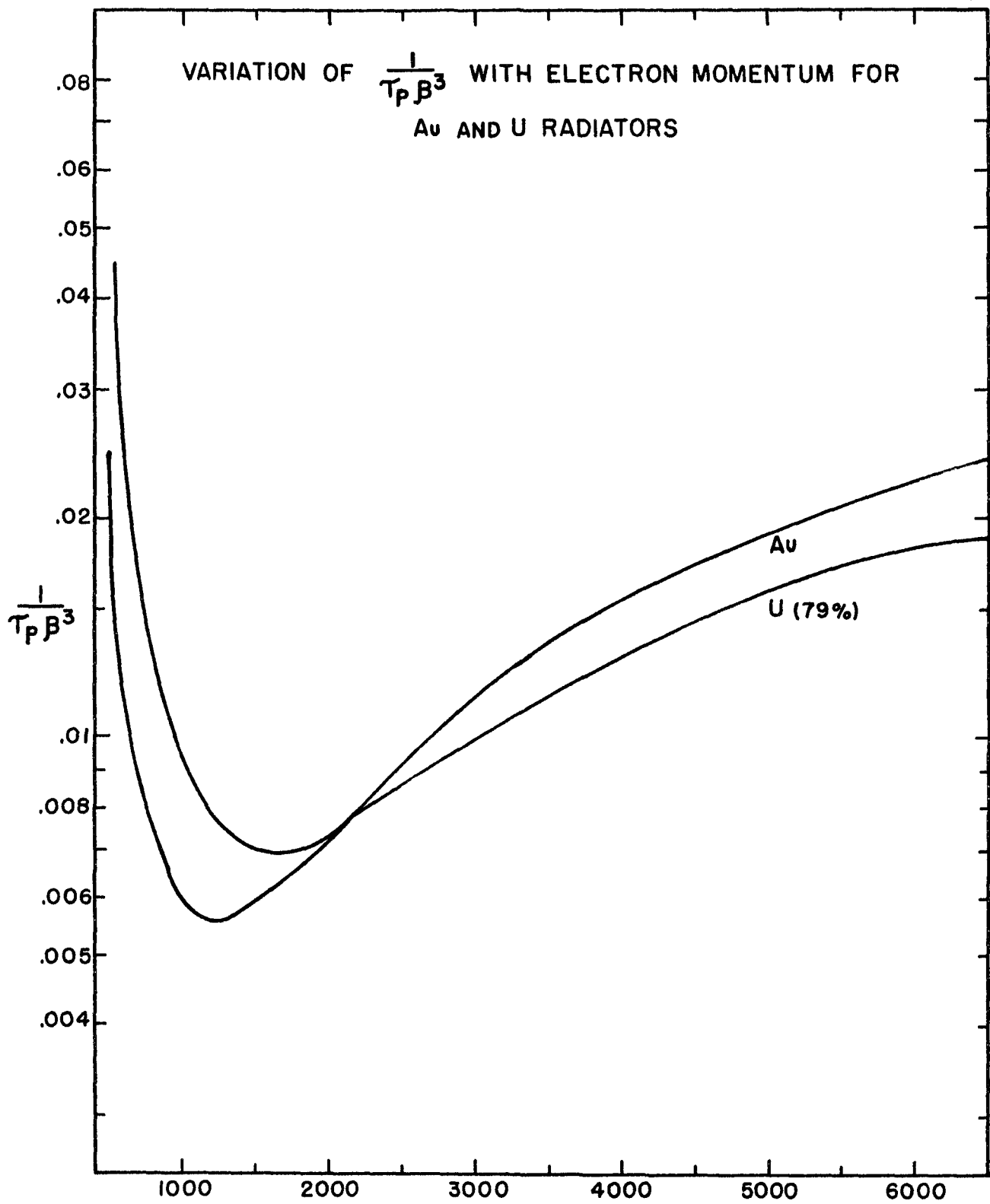
The problem of composition is also encountered in finding a proper t for the uranium radiators. In the equation for C (AI.7b), the thickness referred to is the total radiator thickness in mg/cm^2 . In Equations (AI.1) and AI.2), however, t refers to the thickness of uranium in the radiator, i.e., the amount of matter producing photo-electrons in the photo-peak. Since in both (AI.1) and (AI.2) \mathcal{J} and t appear together, it is possible to use one " t " throughout the expression (AI.4), if \mathcal{J} is replaced by $\mathcal{J}_{\text{eff}} = 0.79 \mathcal{J}_U$. The photo-electric cross-sections used were those published by Siegbahn (1955), the cross-section for gold being obtained by interpolation between platinum ($Z=78$) and lead ($Z=82$). The values for the total photo-electric absorption cross-sections were always

used with the assumption that the K-shell to total cross-section ratio remains constant. This is done because of the lack of reliable experimental data on K-shell photo-electric absorption cross-sections. However, the assumption is justified theoretically (Siegbahn (1955) Chap. 2).

With expressions A1.7a and 7b used to calculate C as a function of t and β , theoretical curves of $\frac{1}{\rho\beta^3}$ and $\sqrt{C^2 + \left(\frac{R\rho\beta^3}{t}\right)^2}$ as functions of $R\rho$, were prepared for various radiator materials and thicknesses. Families of such curves are presented in Figs. A.1 and A.2a and 2b.

(B) Experimental Tests of the Theory

The radiators used in these tests were the ones used in the Erbium-171 study. Altogether, three gold and four uranium radiators were tested. The gold radiators, which had been prepared by pressing together gold leaves 0.2 mg/cm^2 thick, had dimensions $0.9 \times 3.0 \text{ cm}^2$ and thicknesses 0.4 , 1.2 - and 4.4 mg/cm^2 . These thicknesses were calculated by counting the number of gold leaves and assuming that each leaf was 0.20 mg/cm^2 thick. The uranium radiators were prepared by the Zapon spreading technique referred to in Chapter 3. The radiators prepared by this process will contain uranium in the form of U_3O_8 with possibly an admixture of UO_3 and a certain amount of carbon as a bonding residue. It was estimated that the composition of the radiators used was 7% U, 16% O and 5% C by weight. Since the lines obtained with these radiators always had a resolution worse than the corresponding ones obtained with the gold radiators of equal thickness in mg/cm^2 , these radiators



B_{pe} (GAUSS-CM)

FIGURE A.1

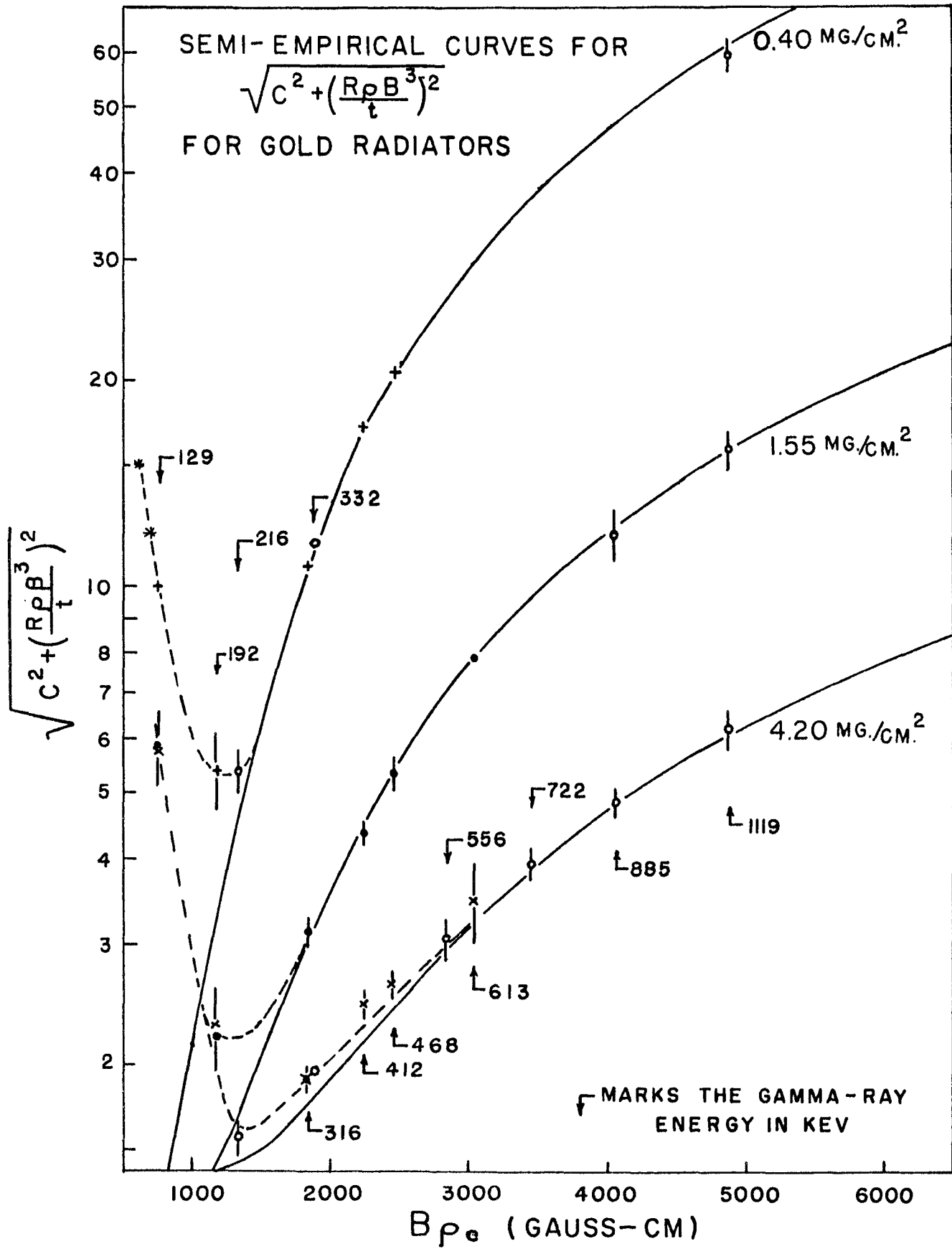
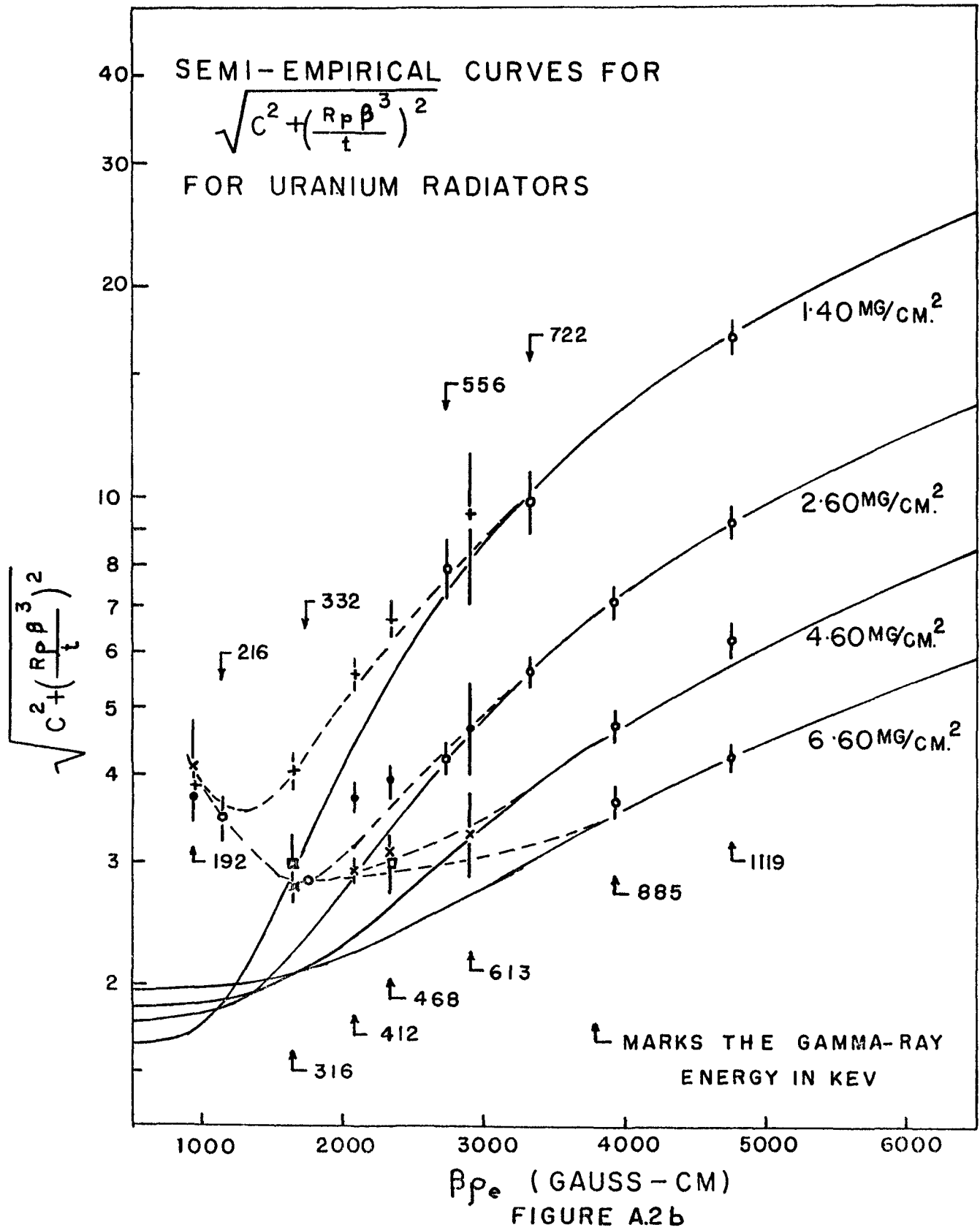


FIGURE A.2a



were made somewhat narrower in the hope of gaining in resolution. The thicknesses were determined by weighing the finished radiator and then subtracting the weight of the aluminium foil backing. The thinnest radiator, weighing 1.3 mg/cm^2 had dimensions $0.55 \times 3.0 \text{ cm}^2$, while the others weighing 2.6-, 4.8- and 7.2 mg/cm^2 , all measured $0.75 \times 3.0 \text{ cm}^2$. Since the width of the radiator is part of the instrumental geometry, it does not enter into the calculation of relative gamma-ray intensities.

Three somewhat overlapping sets of experiments were carried out. First, expression (AI.4) was tested for the high energy region. From the results of these experiments a check of the radiator thicknesses was also obtained. Second, the energy dependence of $\sqrt{C^2 + (Rp\beta^3/t)^2}$ term in the expression (AI.4) was checked. And third, a cross-check between the various radiators was obtained by measuring the intensities of a number of gamma-rays in several of the radiators. In all of these experiments the radiators were mounted in a standard geometry, and the baffle and detector settings kept constant.

In the first and third sets of experiments it was also necessary to maintain constant source-radiator, and radiator-detector-baffle geometries. The first was obtained by gluing the sources into the brass source holder which fitted into the steel cylinder in a unique way. The radiators were mounted on identical steel cylinders and centered on the focal plane of the instrument on the 50-cm radius. (Fig. 5 on page 43 shows the gamma-source holder.) The second condition, that of constant source-baffle-detector geometry, was not maintained, due to the variation of the widths of the radiators. In order to correct

for this, the variation of peak height with the radiator width was measured with a 4.5 mg/cm^2 uranium radiator which was cut down from 9 mm to 7.5 mm to 5.5 mm in width in successive stages. This experiment was carried out with the strong 1119 kev gamma-ray of Sc^{46} . Table A.II gives the results of these measurements.

TABLE A.II

The Variation of External Conversion Peak Height
with Radiator Width Using a 4.5 mg/cm^2 U Radiator

Radiator Width mm	Peak Height Counts/Minute	Resolution %	Correction Factor
9.0	6920 ± 30	0.65 ± 0.05	1.00
7.5	6600 ± 40	0.57 ± 0.05	1.05
5.5	5380 ± 40	0.56 ± 0.05	1.28

This variation in the external conversion peak height is attributed to two factors: to the change in the radiator volume, and to the change in the instrumental resolution R . Since the larger change in the resolution carried with it a very small change in the peak height, it seems that in fact the radiator volume contribution is the more important one. Although this measurement was carried out on one momentum setting, it is felt that the correction factors can be used at all electron energies. The only assumption made here is that the electrons undergo multiple scattering in the radiator and emerge with isotropic distribution. At the energies and

radiator thicknesses used, this is a valid assumption. In the following, all the peak heights obtained with the uranium radiators have been corrected for this effect. This correction cancels in the second set of experiments where two gamma-rays with related intensities were compared in the same radiator.

(i) Test of the Expression (AI.4) for the High Energy Region

The two equal intensity gamma-rays of Sc^{46} (885 and 1119 kev) were used to test the expression AI.4 at high electron momenta. The external conversion peak heights produced by these two gamma-rays in each of the radiators were measured. (In addition to the seven radiators described above, a 12 mg/cm^2 radiator previously used in this laboratory was tested. However, since this radiator is too thick to be used in the region in which the experiments were carried out, and since it was not used in the study of erbium, no further experiments were carried out with this radiator).

From Equation (AI.3) it is seen that these peak heights multiplied by $\frac{1}{\lambda} \sqrt{1 + (Ct/Rp\beta^3)^2}$ should be proportional to the radiator thickness. Figure A.3 shows a plot of $\frac{n}{\lambda} \sqrt{1 + (Ct/Rp\beta^3)^2}$ against t on a log-log scale. This straight line with slope 1 provides a check on three things: first, the fact that the plot is a straight line shows that at sufficiently high energies Equation AI.1 is a valid expression. In the range of this experiment the factor $\sqrt{1 + (Ct/Rp\beta^3)^2}$ made a significant contribution (i.e., more than a 5% correction) only in the case of the 4.8-, 7.2-, and 12 mg/cm^2 uranium radiators. Since

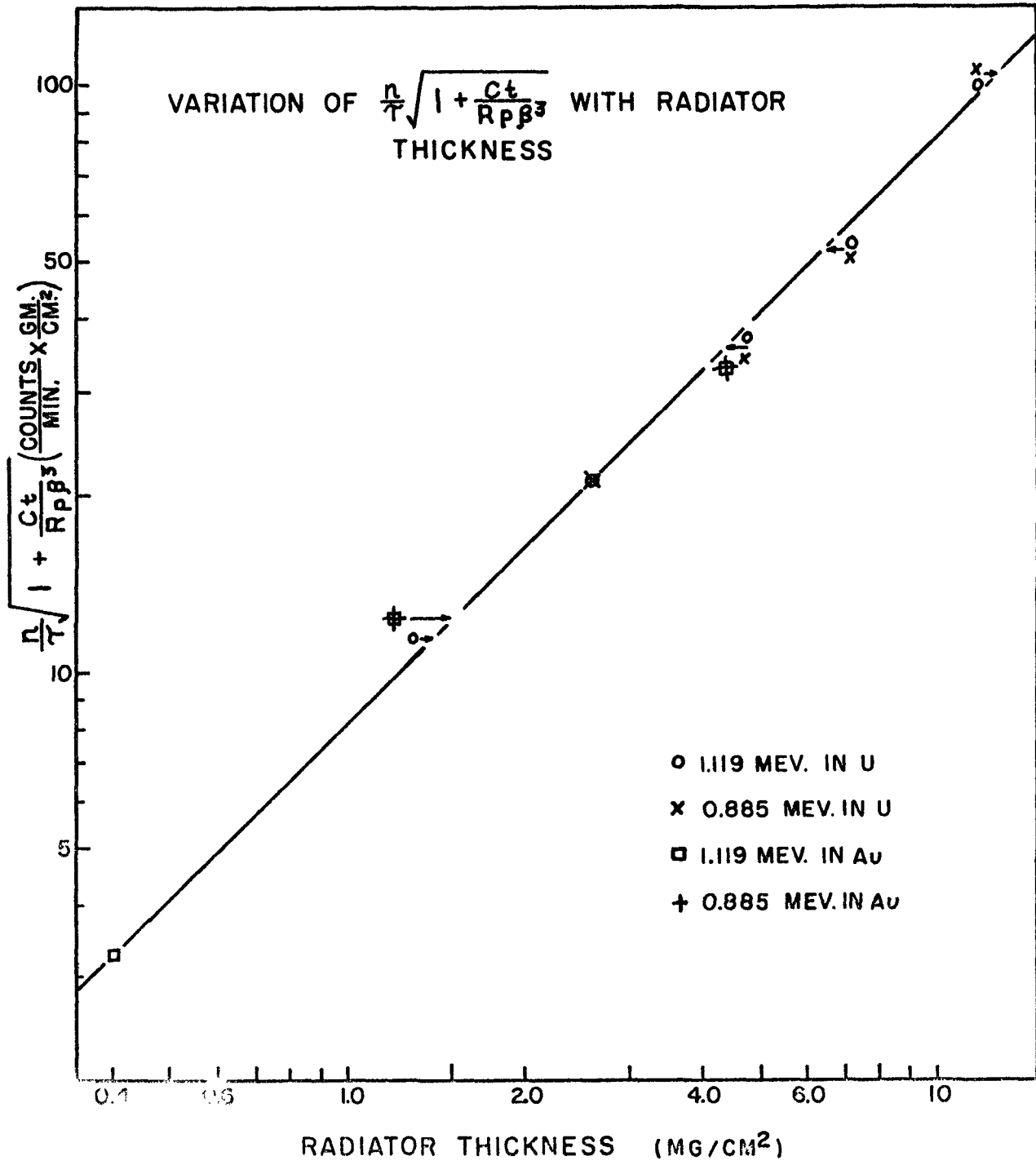


FIGURE A.3

at these energies, and for all of these radiators, $(Ct/R\mu\beta^2) < 1$, this experiment does not test the correctness of this factor. Second, the overlapping of the lines formed by the uranium and gold radiators indicates that the estimate of the carbon content of the uranium radiators was correct to within $\pm 3\%$. Third, it provides a check on the nominal radiator thicknesses. The scatter of the points about the straight line is attributed to errors in determining the thicknesses of the radiators. Inasmuch as a possible error of 10% could be assigned to these nominal values, it was decided to use Fig. A.3 to obtain more accurate measurements of the radiator thicknesses. From this figure, therefore, an adjusted thickness, which would put the experimental points on the straight line, was assigned to each radiator. This process was carried out with several other gamma-rays (613- and 468 kev lines of Ir^{192} , and the 412 kev line of Au^{198}) with similar

TABLE A.III

Radiator Thicknesses

Radiator	t_{Nominal}	$t_{\text{Corrected}}$
Uranium	1.3 mg/cm ²	1.40 mg/cm ²
	2.6	2.60
	4.8	4.40
	7.2	6.60
	12	12.5
Gold	0.4	0.40
	1.2	1.55
	4.4	4.20

results. Table A.III lists both the nominal and the corrected values for the thicknesses of the radiators. The corrections are small except for the 1.2 mg/cm^2 gold radiator. In this case it would appear that an error had been made in counting the number of gold leaves in the fabrication process. The corrected values for t were then accepted as the true radiator thicknesses in all subsequent work.

(ii) The Variation of the Photo-Electric Peak Height with Electron Momentum

The energy dependence of expression (A1.4) was checked by means of three pairs of gamma-rays with related intensities. These were

Sc ⁴⁶	885 kev - 1119 kev
In ¹¹⁴	556 kev - 722 kev
Hf ^{180m}	216 kev - 332 kev

These pairs are all cascading gamma-rays between rotational levels in even-even nuclei. In each case the gamma-ray intensities were corrected for the small difference in the gamma-ray absorption by the steel cylinder. This correction was very small, having a maximum value of 2% between the two Hf^{180m} gamma-rays. In addition, in the case of the Hf^{180m} lines, allowance was made for internal conversion, using the theoretical values for pure E2 transitions (Sliv (1956)). At the energies of the In¹¹⁴ and Sc⁴⁶ transitions internal conversion is negligible.

The experimental data obtained by these experiments, i.e., the external conversion peak heights measured, were used in the following manner. The intensity of the higher energy gamma-ray (γ_1) was calculated using the theoretical expression (A1.4) with the terms

$1/\rho\beta^3$ and $\sqrt{C^2 + (R\rho\beta^3/t)^2}$ read from the theoretical curves reproduced in Figs. A.1 and A.2a and 2b; from this I_γ the intensity of the lower energy gamma-ray of the pair (γ_2) was found, taking into account the proper corrections; and finally, from this calculated gamma-ray intensity, an empirical value of $\sqrt{C^2 + (R\rho\beta^3/t)^2}$ found for γ_2 . These data are plotted on Figs. AI.2a and AI.2b with open circles. In the case of Sc^{46} and In^{114} gamma-rays the intensity of γ_1 was calculated for each of the radiators and then the average value used as the "true" gamma-ray intensity. The experimental errors shown on these points are obtained by combining the standard deviation of the average intensity with the error in the corresponding peak height measurement. In the case of 5.5 hr. Hf^{180m} gamma-rays, it was not possible to combine the experiments with different radiators, since a different source was used in each experiment. Here the intensity of γ_1 represents just one measurement. The value of $\sqrt{C^2 + (R\rho\beta^3/t)^2}$ used for the intensity calculation is shown without an experimental error, while the calculated value of $\sqrt{C^2 + (R\rho\beta^3/t)^2}$ for the corresponding γ_2 is shown with an experimental error representing the uncertainties in both the peak height measurements. It should be noted that the values of $\sqrt{C^2 + (R\rho\beta^3/t)^2}$ assumed for γ_1 of Hf^{180m} in the 4.20 mg/cm^2 Au and the 2.60 mg/cm^2 U radiators do not lie on the theoretical curves. The reason for this will be explained below.

(iii) The Variation of the Photo-Electric Peak Height with Radiator Thickness

This set of experiments consisted of measuring the photo-electric peak heights of various gamma-rays in different radiators.

The following gamma-rays were used in this experiment: 129 keV Os¹⁹¹, 192 keV In¹¹⁴, 316 keV Ir¹⁹², 412 keV Au¹⁹⁸, 468 keV Ir¹⁹², and 613 keV Ir¹⁹². Here the intensity of the gamma-ray was calculated from the peak height measured in one radiator and then this I_γ used to find the values of $\sqrt{C^2 + (Rp\beta^3/t)^2}$ for the other radiators. The results of these experiments are shown with +, • and x. In each case the value of $\sqrt{C^2 + (Rp\beta^3/t)^2}$ used for the intensity calculation is shown without an experimental error. The uncertainty in that particular peak height measurement is considered as an experimental error in the measured intensity when determining the errors on the other points.

For the 316-, 412-, 468-, and 613 keV gamma-rays the intensities were calculated from the data obtained with either the 0.40 mg/cm² or 1.55 mg/cm² gold radiator. The thin gold radiators were chosen because for these the assumptions in the theory are more nearly fulfilled. The fact that the Hf^{180m} data follow the theoretical curves for thin gold radiators supports this view. The results of the experiments with the two low energy gamma-rays (129 keV and 192 keV) were interpreted together with the Hf^{180m} experiment.

An observation of Figs.A.2a and 2b will reveal that at low energies empirical curves (marked with dotted lines) have been obtained which deviate from the theoretical ones (marked with solid lines). The arguments used in arriving at these curves will now be presented. On the basis of the points at $B_{pe} = 2221-$, 2084-, and 1652 gauss-cm on Fig.A.2b empirical curves were drawn from $B_{pe} = 3000$ gauss-cm to $B_{pe} = 1650$ gauss cm. The Hf^{180m} data were then used to provide a

continuation to the curve for the 2.60 mg/cm^2 U radiator down to $B\rho_e = 1100$ gauss-cm. This extrapolated curve was now used to calculate the intensity of the 192 keV gamma-ray. The value obtained is considerably higher than the one calculated from the experiments with gold radiators using the theoretical values for $\sqrt{c^2 + (R\rho\beta^3/t)^2}$, although it should be pointed out that if one considers only the measurements in the three gold radiators a consistent intensity measurement using the theoretical values for the term $\sqrt{c^2 + (R\rho\beta^3/t)^2}$ may be obtained. At this point the empirical curves for the term $\sqrt{c^2 + (R\rho\beta^3/t)^2}$ seem to increase with decreasing electron momentum for both gold and uranium radiators. This behaviour is further borne out by the Er^{171} data. In order to account for all the transitions depopulating the 116.7 keV level, one would need $\sqrt{c^2 + (R\rho\beta^3/t)^2} = 14$ at $B\rho_e = 603$ (i.e., $E_e = 36.0$ keV) for the 0.40 mg/cm^2 gold radiator. The dotted line shows the estimated behaviour of the curve for the 0.40 mg/cm^2 gold radiator from $B\rho_e = 1180$ - to $B\rho_e = 600$ gauss-cm. The experimental points corresponding to the 129 keV gamma-ray are based on this extrapolation.

(C) Discussion

A comparison of the empirical curves with the theoretical ones reveals two points of interest. First, the empirical curves deviated from the theoretical ones at a higher electron momentum value in uranium than was the case with gold. Second, at the low energy end, the empirically-determined $\sqrt{c^2 + (R\rho\beta^3/t)^2}$ start to increase with decreasing electron momentum, while the theoretical ones decrease with

increasing electron momentum to a constant value. An explanation for the different behaviour of the two radiator types is probably to be found in their different compositions. This seems to indicate that, for mixed materials, the terms Z/A and E_i in the Landau formula (Eq. AI.5) are not given by simple average values. The second deviation is quite expected. The Landau formula (AI.5) which is used to calculate C is based on the assumption that the energy lost by the electron is small compared to its initial energy. This is no longer true for electron energies below 100 keV. Although the instrumental resolution during these experiments was 0.6%, the resolution of the 192 keV line in uranium radiators varied from 2% to $\sim 5\%$. This indicates that, in the thicker uranium radiator, a number of 76 keV electrons lost as much as 10% of their energy. Since at these energies $\sqrt{C^2 + (Rp\beta^3/t)^2} \approx C$, the theoretical curves can no longer be expected to be valid here.

As stated in the Introduction, this study was undertaken to provide the experimenter with a means of calculating reliable gamma-ray intensities from the external conversion experiments described in this thesis. It is felt that expression AI.4, together with the semi-empirical curves of Figs. A.2a and 2b, fulfil this purpose. It should be pointed out, however, that one is not justified in extrapolating the conclusion drawn from these experiments to areas which have not been tested.

Nevertheless, from the experience gained in this work, some recommendations can be made regarding a more extensive study of this

problem about the external conversion techniques in general. It has been found that at low energies ($E_e < 400$ kev) gold radiators give better peak heights than uranium radiators. It is probable that a radiator with still lower Z, tin for example, might be an improvement on gold at very low energies. In addition, the low binding energy of tin (29.18 kev) would make it possible to study gamma-rays, which cannot be converted in a high Z material such as gold, with external conversion. At high energies ($E_e > 400$ kev) the uranium radiators become much more efficient. The recommended radiators to be used at the various energy ranges are thus as follows: For $B\rho_e < 2000$ gauss-cm gold ($0.5 - 1.0$ mg/cm² thick) and possibly some low Z material; for $2000 < B\rho_e < 4000$ gold (thickness $2 - 4$ mg/cm²) and uranium (thickness $1 - 4$ mg/cm²); for $B\rho_e > 4000$ uranium (thickness > 5 mg/cm²) and as a second choice gold (thickness 5 mg/cm²). The optimum thickness to be used at these high electron energies ($E_e > 800$ kev) cannot be given, since no experiments were carried out with thick radiators and at these energies. The optimum size of the radiators used with an instrumental resolution of 0.6% (detector slits 4 mm wide and variable baffles open) seems to be 7 - 8 mm x 3.0 cm. Further experiments designed to extend this study both in the range of gamma-ray energy and for other radiator materials are being carried out by Miss Anne Staveley.

APPENDIX II

THE DECAY OF PROMETHIUM-149

Introduction

During the period of the work described in this thesis the decay of Pm^{149} was investigated jointly by Dr. M. E. Law and the author. This problem was suggested by Dr. M. W. Johns, at that time on sabbatical leave at the Clarendon Laboratories, Oxford University. The suggestion was made on the basis of a discrepancy between the published decay schemes and the one used by Chapman et al. (1960) at the Clarendon Laboratories in their nuclear alignment studies. Since it was felt that the instruments available in this laboratory were especially suited for this problem, a study of the Pm^{149} decay was undertaken. The results of this investigation are presented here in the form of the published article. Since this article was published some time ago, a few comments are in order at the present time.

The problem of the gamma-ray intensity measurements with the external conversion techniques has since been re-examined. In the light of the results presented in Appendix I, the statement on page 157 that the photo-electric yield factor f ($f = \frac{1}{4p\beta^2} \sqrt{c^2 + \left(\frac{Rp\beta^3}{t}\right)^2}$) is known to better than 5% is rather optimistic. A recalculation of α_K for the 286 keV transition using the new semi-empirical expression gives $\alpha_K = 0.061 \pm 0.006$. This value is somewhat lower than the

theoretical value for an M1 transition. However, it is now clear that at this electron momentum value ($Bp_e = 1500$) the semi-empirical expressions for the uranium radiators are not too reliable. From the Er^{171} measurements it can be seen that the conversion coefficient measurement using the uranium radiator is lower than the average value by about 10%, indicating that the exact behaviour of these curves at these energies is still not clear. This change in value of α_K does not, therefore, change any conclusions about the properties of the 286 keV gamma-ray. It will, however, change the calculated branching ratio from 2.9% to 3.5%.

Shortly after this article was submitted for publication Schmid and Burson (1960) reported their results of an investigation of this decay. The conclusions reached by Schmid and Burson about the 286 keV gamma-ray agree with the ones stated below. These authors also found some weak transitions, 548-, 582-, and 850 keV, in addition to the 286 keV transition. This is not in contradiction with the conclusions reported in the enclosed article, since an upper limit of 0.1% was set for any other radiation present. The gamma-rays reported by Schmid et al. are below this detection limit. However, these authors also measure the transition ratio to the 286 keV level in Sm^{149} to be 10%. This is considerably higher than the value of 3% reported here, and the value of 1.5% reported by Chapman et al. Since the 10% value was obtained from a Fermi analysis of the total beta spectrum, it is believed that the lower value of 3% is a more accurate one.

THE DECAY OF Pm^{149} ¹

AGDA ARTNA AND MARGARET E. LAW

ABSTRACT

The 52.8-hour activity of Pm^{149} has been investigated using a high resolution beta spectrometer, a lens type coincidence spectrometer, and a scintillation spectrometer in conjunction with a multichannel analyzer. The beta spectrum was found to consist of two groups with maximum energies of 1.072 ± 0.002 Mev and 0.786 ± 0.004 Mev, and intensities of $97.1 \pm 0.4\%$ and $2.9 \pm 0.4\%$ respectively. A gamma ray of energy 285.7 ± 0.3 keV was found to be in coincidence with the 0.786-Mev beta group. No other gamma rays with intensities greater than 0.1% were found. The *K* conversion coefficient for the 286-keV transition was measured to be 0.075 ± 0.008 . This together with the values of 6.5 ± 0.7 and 4 ± 1 obtained for the *K/L* and *L/M* conversion ratios respectively indicate that this transition is *M1* in character with less than 10% *E2* admixture.

INTRODUCTION

The 52-hour activity of Pm^{149} has been investigated previously by Rutledge, Cork, and Burson (1952), and by Kondaiah (1952). Rutledge *et al.* reported a strong 285-keV gamma ray in coincidence with a 1.05-Mev beta group, and a weak 1300-keV gamma ray. However, Kondaiah found that the decay consisted of a single beta group of end point 1.05 Mev leading to the ground state of Sm^{149} . More recently, Chapman, Grace, Gregory, and Sowter (1960) have carried out nuclear alignment studies on Pm^{149} . They also detected a 285-keV gamma ray associated with the 52-hour activity, but found it to be in coincidence with a weak beta group of end point 0.770 Mev. Since there is obvious disagreement between these three reports it was decided to investigate this decay scheme further.

Pm^{149} is the product of the 2-hour negatron decay of Nd^{149} . Neodymium oxide enriched to 82% in Nd^{148} was irradiated for 15 hours in the high flux reactor at Oak Ridge, and was received some 30 hours after removal from the reactor. The sample also contained 4% Nd^{146} and 7% Nd^{150} , producing the 11-day Nd^{147} and 27-hour Pm^{151} activities. In addition, a small amount of samarium was present, giving the 47-hour Sm^{153} activity.

EXPERIMENTAL

1. Gamma-ray Spectrum

The gamma-ray spectrum of the sample was investigated using a scintillation spectrometer consisting of a DuMont 6363 photomultiplier and a 3-in. NaI crystal, in conjunction with a RCL 256 channel analyzer. Figure 1 shows a typical spectrum taken 7 days after removal of the sample from the reactor. No higher energy radiations were seen with intensities greater than 10% of the 540-keV gamma ray.

¹Manuscript received August 8, 1960.

Contribution from the Department of Physics, McMaster University, Hamilton, Ontario.

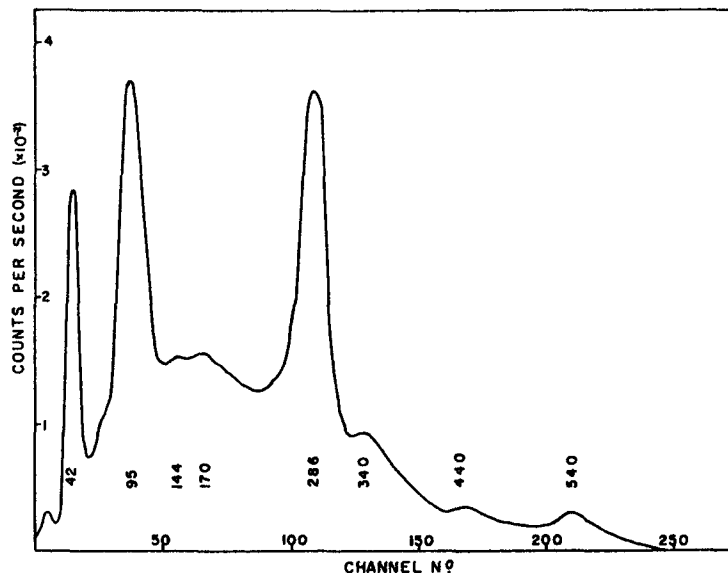


FIG. 1. Gamma-ray spectrum taken 7 days after removal of the sample from the reactor. The energies of the peaks are given in kev.

The spectrum was followed over a period of 20 days to obtain the half lives of the various peaks. The majority of these could be accounted for by the known gamma rays resulting from either Nd^{147} , Pm^{151} , or Sm^{153} decay. The 286-kev gamma ray was found to have a half life of 54 ± 2 hours and is therefore associated with the Pm^{149} decay. No other gamma rays were found to decay with this half life.

B. The 286-kev Transition

(i) Coincidence Experiments

The beta spectrum in coincidence with the 286-kev gamma ray was investigated with a double long-lens coincidence spectrometer of the Gerholm type (Gerholm 1955). One spectrometer (No. 1) was set on the 286-kev K conversion line and the beta spectrum scanned with the other (No. 2). A Bell, Graham, and Petch (1952) fast-slow coincidence circuit was used, set at 8 μsec resolving time. The sources were prepared by dissolving the neodymium oxide in nitric acid, and evaporating to dryness a small droplet of the solution on a backing of V.Y.N.S. film. The resulting sources were approximately 2 mm in diameter and 300 $\mu\text{g}/\text{cm}^2$ thick.

In all, three complete experiments were done. Each experiment lasted 4 days, during which time the beta spectrum was scanned approximately 20 times. Figure 2 shows the Fermi plot of the coincidence spectrum obtained from one of the experiments. The mean end point of the beta spectrum in coincidence with the 286-kev K line was found to be 0.788 ± 0.009 Mev.

From the singles counting rate in spectrometer No. 1, set on the 286-kev K peak, it was possible to obtain an accurate determination of the half life

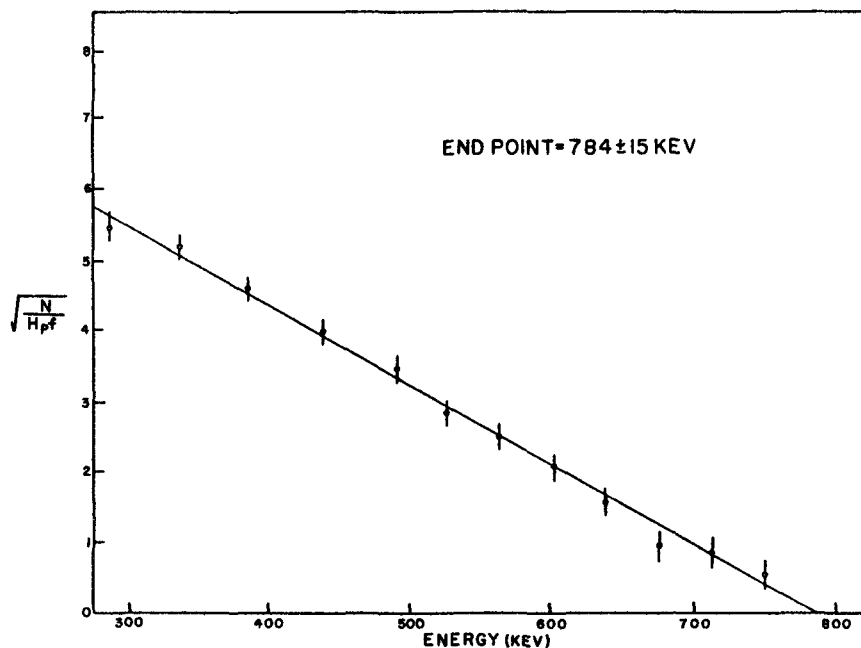


FIG. 2. Fermi plot of the beta spectrum in coincidence with the 286-keV K conversion line.

of the Pm^{149} activity. The counting rate obtained had to be corrected for the 27-hour Pm^{151} and the 11-day Nd^{147} contributions. The latter was measured after all the shorter-lived activities had died, while the former was estimated from the intensity of the gamma rays associated with Pm^{151} as measured with the scintillation spectrometer. Neither correction amounted to more than 5% of the total. In addition, it was estimated from the internal conversion spectrum that $1.5 \pm 1.0\%$ of the activity was due to 47-hour Sm^{153} . However, because of the similar half lives of Sm^{153} and Pm^{149} , the half-life plot was insensitive to this small amount of impurity, and over a period of 4 days the correction for this was negligible compared to the statistical errors. The resulting half life of Pm^{149} is 52.8 ± 0.3 hours.

(ii) *External and Internal Conversion Experiments*

The internal and external conversion lines of the 286-keV transition were studied using a 50-cm Siegbahn type beta-ray spectrometer (Johns *et al.* 1953). Line sources for this instrument were prepared as described above (*B (i)*), the source backing in this case being aluminum-coated mylar. These sources were 2.5 cm long and had varying widths and thicknesses depending on the resolution and counting rates desired.

The K internal conversion coefficient, α_K , was measured directly by comparing the number of K conversion electrons with the gamma-ray intensity from the same source. The number of gamma rays was obtained from the external conversion peak according to the equation $N_\gamma = N_{p.e.} \times f \times k$ where

$N_{p.e.}$ is the photoelectron peak height, f is the photoelectric yield for a given gamma-ray energy and for a given radiator material and thickness (this factor has been discussed by Johns *et al.* 1954), and k is a factor depending on the source radiator geometry. α_K is then given by

$$\alpha_K = N_{eK}/N_\gamma = N_{eK}/N_{p.e.} \times f \times k.$$

The source radiator geometry factor, k , was measured by repeating the experiment in the same geometry with the 412-keV Au^{198} transition, for which $\alpha_K = 0.028$ (Wapstra *et al.* 1958). Figure 3 shows the internal and external conversion peaks for both these transitions. The gold source consisted of 0.5×2.5 cm² rectangle of gold-coated mylar ($30 \mu\text{g}/\text{cm}^2$ Au). The promethium source of the same dimensions had an approximate thickness of $500 \mu\text{g}/\text{cm}^2$. The continuum underlying the external conversion peaks is mainly due to

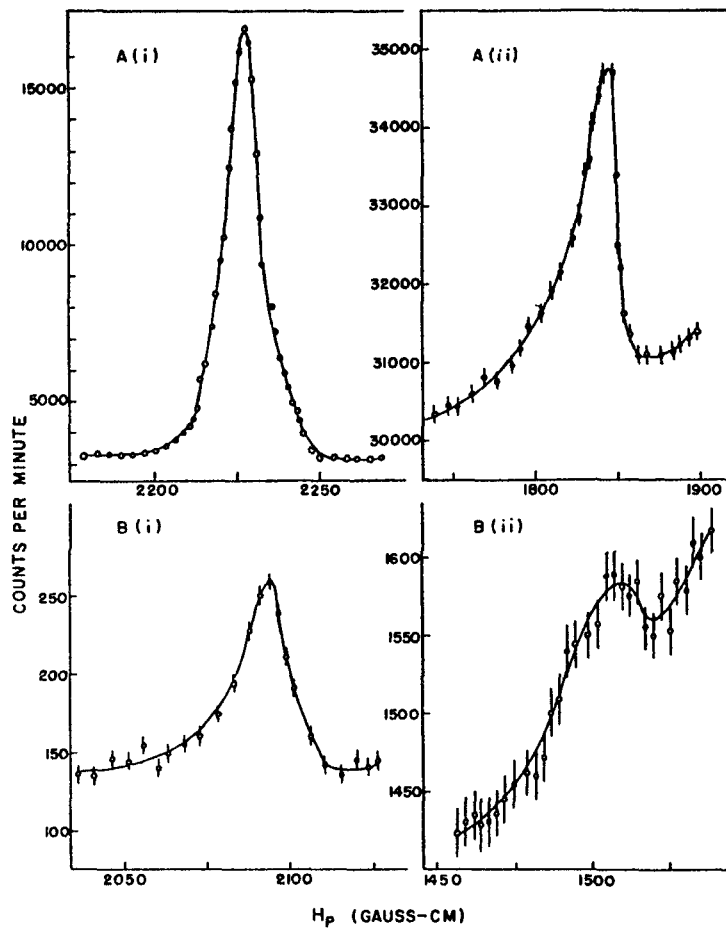


FIG. 3. The internal (A) and external (B) conversion lines of the 412-keV gamma ray of Au^{198} (i) and the 286-keV gamma ray of Pm^{149} (ii).

high energy betas which have penetrated the radiator backing used as the beta stopper. In the case of the promethium peak, some of the continuum is also due to Compton electrons accompanying the higher energy gamma rays of Pm^{151} . In order to check the reproducibility of the geometry, the experiment was carried out with two different radiators of 2.2 mg/cm^2 and 2.9 mg/cm^2 uranium. The K conversion coefficient was found to be 0.075 ± 0.008 , the error being mainly due to the uncertainty in the 286-keV external conversion peak height. The photoelectric yield factor for this instrument, f , is known to better than $\pm 5\%$.

The internal conversion lines were studied using a $0.2 \times 2.5 \text{ cm}^2$ beta source, approximately $50 \text{ } \mu\text{g/cm}^2$ thick. The spectrometer resolution under these conditions was 0.5% . Figure 4 shows the K , L , and M peaks. The K/L and

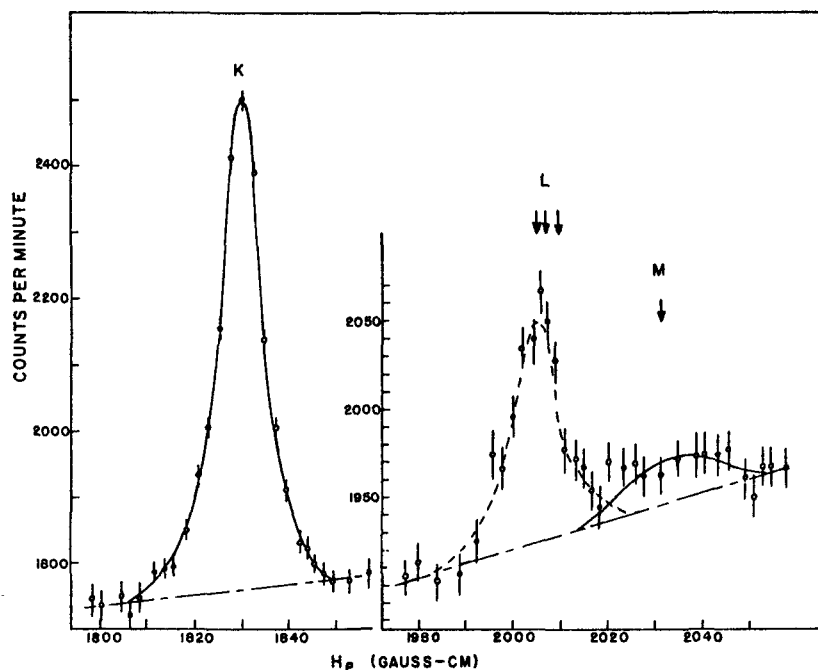


FIG. 4. Internal conversion peaks of the 286-keV transition. Superimposed on the L peaks is the normalized outline of the K peak.

L/M ratios obtained from these were 6.5 ± 0.7 and 4.0 ± 1.0 respectively. In addition, from a comparison of the profiles of the K and L lines it could be concluded that the L peak consisted mainly of the L_1 component. An upper limit of 0.1 could be set for the $(L_1 + L_2/L_3)$ ratio.

The energy of the transition as measured in both external and internal conversion experiments is $285.7 \pm 0.3 \text{ keV}$. The standards used for this measurement were the thorium F line and the 411.77-keV gamma ray of Au^{198} for internal conversion, and the 316.46 line of Ir^{192} , and the 411.77 line of Au^{198} for external conversion.

C. Beta-ray Spectrum

The beta continuum was scanned with the high resolution spectrometer. The end point of the spectrum as obtained from a Fermi plot is 1.073 ± 0.002 Mev. Subtracting from this the energy of the gamma ray, the end point of the second group is 0.786 ± 0.002 Mev. Since only one gamma ray was found to belong to this decay the beta spectrum was assumed to consist of only these two groups.

The method of Fermi analysis normally used to obtain branching ratios could not be used here because of the presence of impurities, in particular Sm^{153} , which have end points similar to that of the inner group. This type of analysis is very sensitive to such small corrections. Instead, the intensity of the 0.786-Mev beta group (b_1) was calculated in terms of the number of conversion electrons (N_{eK}), and either the number of betas in the ground state transition ($N_{\beta 0}$), or the total number of betas ($N_{\beta T}$), according to the equations

$$b_1 = N_{eK}(1 + \alpha_T) / \alpha_K N_{\beta 0} + N_{eK}(1 + \alpha_T), \quad (\text{i})$$

$$b_1 = N_{eK}(1 + \alpha_T) / \alpha_K N_{\beta T}. \quad (\text{ii})$$

Figure 5 shows a Fermi plot of the total spectrum. The number of ground state betas could be found by reconstructing the spectrum as shown in the insert (curve B). The second curve in the insert (curve A) shows the total beta spectrum after the Nd^{147} , Pm^{151} , and Sm^{153} contributions had been

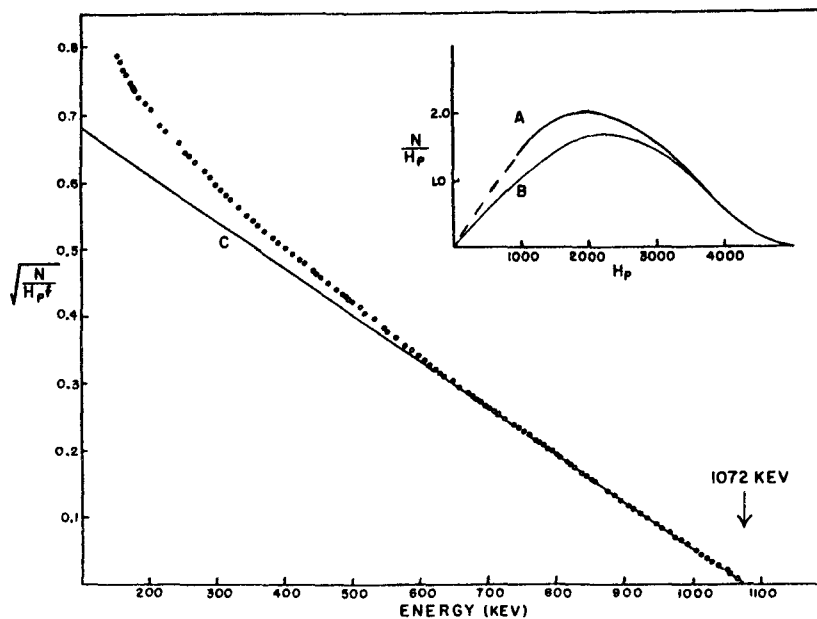


FIG. 5. Fermi plot of the total beta spectrum. The insert shows the total beta spectrum (A), and the spectrum of the high energy beta group (B) reconstructed from the straight line of the Fermi plot (C).

subtracted. Since curve B is an ideal spectrum with no source thickness effects, equation (i) gives an upper limit for b_1 . The spectrum was scanned three times. The mean value of b_1 obtained from equation (i) was 0.033 ± 0.004 , and from equation (ii) 0.028 ± 0.003 . A similar analysis of the singles spectrum measured in spectrometer No. 2 of the coincidence spectrometer gave results in agreement with these.

In addition, the relative intensity b_1 could also be calculated from the data of the coincidence experiments, using the following equation:

$$b_1 = A_{\text{coinc}(2)} / A_{\text{total}(2)} \times (1 + \alpha_T) / \alpha_K \cdot w(1)$$

where $A_{\text{coinc}(2)}$ is the area under the beta continuum in coincidence with the 286-keV K peak; $A_{\text{total}(2)}$ is the area under the total beta continuum, and $w(1)$ is the transmission of spectrometer No. 1 set on the 286-keV K peak. Using values of $\alpha_T = 0.089 \pm 0.009$, $\alpha_K = 0.075 \pm 0.008$, and $w(1) = 0.017 \pm 0.002$, a mean value of 0.029 ± 0.006 was obtained for b_1 .

From these results the intensities of the 1.072-MeV and 0.786-MeV beta groups were found to be $97.1 \pm 0.4\%$ and $2.9 \pm 0.4\%$ respectively, leading to $\log ft$ values of 7.1 and 8.1.

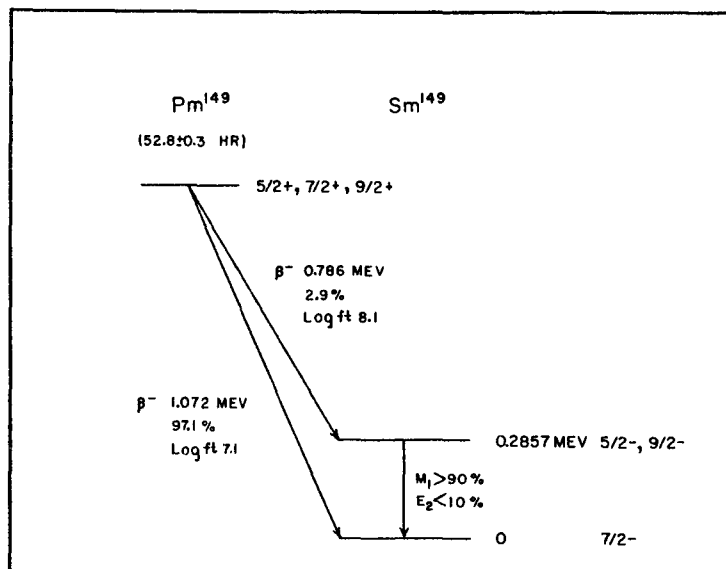
SUMMARY

Table I compares the measured values of the conversion coefficients and ratios for the 286-keV transition with the theoretical predictions for several multipolarities. From these results it was deduced that the gamma ray is $>90\%$ $M1$ with possible $E2$ admixture.

TABLE I
Conversion data for the 286-keV transition

	Theoretical conversion coefficients and ratios ($k = 0.56$, $Z = 62$)					Experimental values
	$E1$	$E2$	$E3$	$M1$	$M2$	
α_K	0.014	0.050	0.16	0.078	0.33	0.075 ± 0.008
α_L	0.0018	0.011	0.084	0.010	0.058	0.011 ± 0.002
$K:L$	7.8	4.4	2.1	7.9	5.7	6.5 ± 0.7
$L_1:L_2:L_3$	11:1:1	2:1.5:1	1:2.5:1.5	77:5:1	17:1.7:1	$L_1 \gg L_2 + L_3$
$L:M$	3.0	2.8	2.8	2.8	3.0	4 ± 1

Figure 6 shows the proposed decay scheme for Pm^{149} , which is essentially in agreement with that of Chapman *et al.* (1960). The only discrepancy is in the branching ratio of the beta groups. The value of $1.8 \pm 0.3\%$ obtained by Chapman *et al.* for the relative intensity of the inner group, is lower than the value measured in this work. The spin of the ground state of Sm^{149} is known to be $7/2$ (Bogle and Scovil 1952). From the $M1$ character of the 286-keV transition it can be deduced that the excited state has negative parity with spin $5/2$, $7/2$, or $9/2$. Chapman *et al.* (1960) have ruled out the $7/2$ possibility from their alignment studies. There is no evidence from Coulomb excitation experiments (Heydenburg and Temmer 1955) for collective motion in this nucleus. It would therefore seem most likely that the 286-keV

FIG. 6. The decay scheme of Pm^{149} .

level is due to particle excitation with spin $5/2^-$. The $\log ft$ values and the allowed shapes of the two beta spectra (Figs. 2 and 5) indicate that these are both first forbidden non-unique. This leads to a positive parity for the ground state of Pm^{149} . The possible spin assignments are $5/2$, and $7/2$ if the spin of the 286-kev level is $5/2$, and $7/2$, or $9/2$ if the excited level has spin $9/2$. The shell model prediction for the spin of Pm^{149} is $5/2$. However, recent unpublished work at Berkeley (quoted by Chapman *et al.* 1960) has shown that the spin is $7/2$.

In comparing this decay scheme with those of neighboring odd neutron nuclei one might expect a level at approximately 100 kev. Sm^{147}_{86} , Gd^{151}_{87} , and Sm^{153}_{89} have levels at 121 kev, 108 kev, and 66 kev respectively. Since no evidence was found for a gamma ray of this energy with intensity comparable to that of the 286-kev transition, this level, if it exists in Sm^{149} , must be very weakly fed.

ACKNOWLEDGMENTS

The sources used in this experiment were obtained through the courtesy of the United States Atomic Energy Commission and the Oak Ridge National Laboratory.

We are indebted to the Canadian National Research Council and the Ontario Research Foundation for financial assistance in the form of research grants. One of the authors (M.E.L.) was a recipient of a National Research Council Fellowship during this work.

We should also like to thank Professors M. W. Johns and M. A. Preston of this laboratory for helpful discussions, and Chapman *et al.* of Oxford for sending details of their work prior to publication. Finally the assistance of R. Goodman and D. MacArthur in recording data is gratefully acknowledged.

REFERENCES

- BELL, R. E., GRAHAM, R. L., and PETCH, H. E. 1952. *Can. J. Phys.* **30**, 35.
BOGLE, G. S. and SCOVIL, H. E. D. 1952. *Proc. Phys. Soc. A*, **65**, 368.
CHAPMAN, C. J. S., GRACE, M. A., GREGORY, J. M., and SOWTER, D. V. 1960. *Proc. Roy. Soc.* To be published.
GERHOLM, T. R. 1955. *Rev. Sci. Instr.* **26**, 1069.
HEYDENBURG, N. P. and TEMMER, G. M. 1955. *Phys. Rev.* **100**, 150.
JOHNS, M. W., WATERMAN, H., MACASKILL, D., and COX, C. D. 1953. *Can. J. Phys.* **31**, 225.
JOHNS, M. W. and NABLO, S. V. 1954. *Phys. Rev.* **96**, 1599.
KONDAIAH, F. 1952. *Phys. Rev.* **81**, 1056.
RUTLEDGE, W. C., CORK, J. M., and BURSON, S. B. 1952. *Phys. Rev.* **86**, 775.
WAPSTRA, A. H., NIJGH, G. J., SALOMONS-GROBBEN, N., and ORNSTEIN, L. TH. M. 1958. *Nuclear Phys.* **9**, 538.

REFERENCES

- Alaga, G., (1957); Nuclear Phys. 4, 625.
- Asaro, F., Stephens, F.S., Hollander, J.M., Perlman, I., (1960);
Phys. Rev. 117, 492.
- Bakker, C.J., Segré, E., (1951); Phys. Rev. 81, 489.
- Bell, R.E., Graham, R.L., Petch, H.E., (1952); Can. J. Phys. 30, 35.
- Bethe, H.A., Backer, R.F., (1932); Rev. Mod. Phys. 8, 82.
- Bisi, A., Terran, S., Zappa, L., (1956); Nuovo Cimento 4, 758.
- Blatt, J.M., Weisskopf, V.F., (1952); "Theoretical Nuclear Physics"
John Wiley and Sons, Inc., New York.
- Bohr, A., (1952); Dan. Mat. Fys. Medd. 26, No. 14.
- Bohr, A., Mottelson, B.R., (1953); Dan. Mat. Fys. Medd. 27, No. 16.
- Bohr, A., Mottelson, B.R., (1955); Dan. Mat. Fys. Medd. 30, No. 1.
- Bohr, N., (1936); Naturwissenschaften 24, 241.
Nature 137, 344, 351.
- Brink, D.M., (1960); Progr. in Nuclear Phys. 8, 97.
- Brueckner, K.A., (1955); Phys. Rev. 97, 1353.
- Burgy, M.T., Krohn, V.E., Rovey, T.B., Ringo, G.K., Telegdi, V.L. (1958);
Phys. Rev. 110, 1214.; Phys. Rev. Letters 1, 324.
- Eutement, F.D.S., (1950); Proc. Phys. Soc. (London) 63A, 775.
- Eutement, F.D.S., (1951); Proc. Phys. Soc. (London) 64A, 395.
- Cabezas, A.Y., (1960); UCRL Report No. 9346.
- Chapman, C.J.S., Grace, H.A., Gregory, J.H., Sowter, C.V., (1950);
Proc. Roy. Soc. 259A, 377.
- Charpak, G., Suzor, F., (1959); J. phys. radium 20, 513.

- Chen, J.J.L., Warshaw, S.D., (1951); Phys. Rev. 84, 355.
- Clark, M.A., Robson, J.M., Nathans, R., (1958); Phys. Rev. Letters 1, 100.
- Cranston, Jr., F.P., Bunker, M.E., Starner, J.W., (1958); Phys. Rev. 110, 1427.
- Davisson, C.M., Evans, R.D., (1952); Rev. Mod. Phys. 24, 79.
- Davydov, L.S., Fillipov, G.F., (1958); Nucl. Phys. 8, 237.
- Deutsch, M., Elliott, L.G., Evans, R.D., (1944); Rev. Sci. Instr. 15, 178.
- Dodson, R.W., Graves, A.C., Helmholtz, L., Hufford, D.L., Potter, R.M., Povelites, J.G., (1952); "Miscellaneous Physical and Chemical Techniques of the Los Alamos Project", ed. by Graves and Froman, McGraw Hill.
- Eden, R.J., (1957); Progr. in Nuclear Phys. 6, 26.
- Feenberg, E., Trigg, G., (1950); Rev. Mod. Phys. 22, 399.
- Feenberg, E., (1955); "Shell Theory of the Nucleus" Princeton University Press.
- Fermi, E., (1934); Z. Physik 88, 161.
- Fowler, R.H., (1930); Proc. Roy. Soc. (London) A 129, 1.
- Frauenfelder, H., Bobone, R., von Goeler, E., Levine, N., Lewis, H.R., Peacock, R.N., Rossi, A., DePasquali, G., (1957); Phys. Rev. 106, 386.
- Gerholm, T.R., (1955); Rev. Sci. Instr. 26, 1069.
- Goldhaber, M., Grodzins, L., Sunyar, A.W., (1958); Phys. Rev. 109, 1015.
- Gorodinskii, G.M., Murin, A.N., Pokrovskii, V.N., Preobrazhenskii, B.K., (1957); Izvest. Akad. Nauk SSSR, Ser. Fiz. 21, 1004.
- Grigorev, O.I., Kusnetsov, B.S., Shimanskaya, N.S., Yutlandov, I.Ya. (1958); Izvest. Akad. Nauk SSSR, Ser. Fiz. 22, 850.
- Habib, E.E., (1961); Ph. D. Thesis, McMaster University.
- Hall, H., (1936); Rev. Mod. Phys. 8, 358.

- Handley, T.H., Olson, E.L., (1953); Phys. Rev. 92, 1260.
- Harmatz, B., Handley, T.H., Mihelich, J.W., (1959); Phys. Rev. 114, 1082.
- Hatch, E.N., Boehm, F., (1956); Bull. Am. Phys. Soc. 1 No. 8, 390.
- Hatch, E.N., Boehm, F., Marmier, P., DuMond, J.W.M., (1956a); Phys. Rev. 104, 745.
- Hatch, E.N., Boehm, F., (1957); Phys. Rev. 108, 113.
- Haxel, O., Jensen, J.H.D., Suess, H.E., (1948); Naturwissenschaften 35, 376.
- Haxel, O., Jensen, J.H.D., Suess, H.E., (1950); Z. Physik 128, 295.
- Heitler, W., (1944); "Quantum Theory of Radiation", Oxford University Press.
- Hill, D.L., Wheeler, J.A., (1953); Phys. Rev. 89, 1102.
- Hultberg, S., (1959); Arkiv Fysik 15, 307.
- Johansson, S.A.E., (1957); Phys. Rev. 105, 189.
- Johns, M.W., Waterman, H., MacAskill, D., Cox, C.D., (1953); Can. J. Phys. 31, 225.
- Johns, M.W., Nablo, S.V., (1954); Phys. Rev. 96, 1599.
- Keller, H.B., Cork, J.M., (1951); Phys. Rev. 84, 1079.
- Ketelle, B.H., Peacock, W.C., (1948); Phys. Rev. 73, 1269A.
- Kundu, D.N., Service, J.P., Pool, M.L., Boyd, G.E., (1952); Phys. Rev. 87, 203B.
- Kurie, F., Richardson, J., Paxton, H., (1936); Phys. Rev. 49, 368.
- Lee, T.D., Yang, C.N., (1956); Phys. Rev. 104, 254.
- Lee-Whiting, G.E., Taylor, E.A., (1957); Can. J. Phys. 35, 1.
- Lindstrom, G., (1951); Phys. Rev. 83, 465.
- Lindstrom, G., Hedgran, A., Alburger, D.E., (1953); Phys. Rev. 89, 1303.

- Mayer, M.G., (1948); Phys. Rev. 74, 235.
- Mayer, M.G., (1949); Phys. Rev. 75, 1969.
- Mayer, M.G., Jensen, J.H.D., (1955); "Elementary Theory of Nuclear Shell Structure," John Wiley and Sons, New York.
- Miller, S.E., (1942); Electronics 14, 27.
- Mottelson, B.R., Nilsson, S.G., (1959); Dan. Mat. Fys. Skrifter 1, No.8.
- Muller, D.E., Hoyt, H.C., Klein, D.J., DuMond, J.W.M., (1952); Phys. Rev. 88, 775.
- Nablo, S.V., (1956); Ph. D. Thesis, McMaster University.
- National Bureau of Standards, U.S. Dept. of Commerce (1952); "Tables for the Analysis of Beta Spectra"
- Nilsson, S.G., (1955); Dan. Mat. Fys. Medd. 29, No. 16.
- Nilsson, S.G., Rasmussen, J.O., (1958); Nuclear Phys. 5, 617.
- Parker, W., DeCroes, M., Sevier, Jr. K., (1960); Nuclear Inst. and Methods 7, 22.
- Rainwater, J., (1951); Phys. Rev. 79, 432.
- Reines, F., Cowan Jr., C.L., (1953); Phys. Rev. 92, 830.
- Rose, M.E., (1958); "Internal Conversion Coefficients", North Holland Publ. Co., Amsterdam.
- Schmid, L.S., Burson, S.B., (1960); Phys. Rev. 120, 158.
- Sheline, R.K., (1960); Rev. Mod. Phys. 32, 1.
- Siegbahn, K., Svartholm, N., (1946); Nature 157, 872.
- Siegbahn, K., (1955); "Beta- and Gamma-Ray Spectroscopy", North Holland Publ. Co., Amsterdam.
- Sliv, L.A., Band, I.M., (1956); "Coefficients of Internal Conversion of Gamma Radiation", The Academy of Sciences of the U.S.S.R.
- Wapstra, A.H., Nijch, G.J., Salomons-Grobhen, N., Ornstein, L.Th.M., (1958); Nuclear Phys. 9, 538.
- White, P., Millington, G., (1928); Proc. Roy. Soc. A120, 701.

Wolfson, J.L., (1961); Can. J. Phys. 39, 773.

Wu, C.S., Ambler, E., Hayward, R.W., Hoppes, D.D., Hudson, R.D.,
(1957); Phys. Rev. 105, 1413.